The SAGE-Spec Spitzer Legacy program: The life-cycle of dust and gas in the Large Magellanic Cloud. Point source classification I.

Paul M. Woods[1⋆], J. M. Oliveira[2], F. Kemper[1], J. Th. van Loon[2], B. A. Sargent[3], M. Matsuura[4,5], R. Szczerba[6], K. Volk[3], A. A. Zijlstra[1], G. C. Sloan[7], E. Lagadec[8,1], I. McDonald[1], O. Jones[1], V. Gorjian[9], K. E. Kraemer[10], C. Gielen[11], M. Meixner[3], R. D. Blum[12], M. Sewiło[3], D. Riebel[13], B. Shiao[3], C.-H. R. Chen[14], M. L. Boyer[3], R. Indebetouw[14,15], V. Antoniou[16], J.-P. Bernard[17], M. Cohen[18], C. Dijkstra[19], M. Galametz[20], F. Galliano[20], Karl D. Gordon[3], J. Harris[20], S. Hony[20], J. L. Hora[21], A. Kawamura[22], B. Lawton[3], J. M. Leisenring[14], S. Madden[20], M. Marengo[16,21], C. McGuire[1], A. J. Mulia[23], B. O'Halloran[24], K. Olsen[17], R. Paladini[25], D. Paradis[25], W. T. Reach[25], D. Rubin[20], K. Sandstrom[26,18], I. Soszyński[27], A. K. Speck[23], S. Srinivasan[28,13], A. G. G. M. Tielens[29], E. van Aarle[11], S. D. Van Dyk[25], H. Van Winckel[11], Uma P. Vijh[30], B. Whitney[31], A. N. Wilkins[7]

[1] *Jodrell Bank Centre for Astrophysics, Alan Turing Building, School of Physics and Astronomy, The University of Manchester, Oxford Road, Manchester, M13 9PL, UK.*
[2] *School of Physical & Geographical Sciences, Lennard-Jones Laboratories, Keele University, Staffordshire, ST5 5BG, UK*
[3] *Space Telescope Science Institute, 3700 San Martin Drive, Baltimore, MD 21218*
[4] *Institute of Origins, Department of Physics and Astronomy, University College London, Gower Street, London, WC1E 6BT, UK*
[5] *Institute of Origins, Mullard Space Science Laboratory, University College London, Holmbury St. Mary, Dorking, Surrey, RH5 6NT, UK*
[6] *N. Copernicus Astronomical Center, Rabianska 8, 87-100 Torun, Poland*
[7] *Department of Astronomy, Cornell University, Ithaca, NY 14853*
[8] *European Southern Observatory, Karl-Schwarzschild-Straße 2, D-85748 Garching bei München, Germany*
[9] *JPL/Caltech, MS 169-506, 4800 Oak grove Dr., Pasadena, CA 91109*
[10] *US Air Force Research Laboratory, Space Vehicles Directorate, 29 Randolph Road, Hanscom AFB, MA 01731*
[11] *Instituut voor Sterrenkunde, Katholieke Universiteit Leuven, Celestijnenlaan 200D, 3001 Leuven, Belgium*
[12] *NOAO, 950 North Cherry Avenue, Tucson, AZ 85719*
[13] *Department of Physics and Astronomy, Johns Hopkins University, Homewood Campus, Baltimore, MD 21218*
[14] *Department of Astronomy, University of Virginia, P.O. Box 400325, Charlottesville, VA 22904*
[15] *National Radio Astronomy Observatory, 520 Edgemont Road, Charlottesville, VA 22903*
[16] *Department of Physics & Astronomy, Iowa State University, Ames, IA 50011, USA*
[17] *Centre d'Étude Spatiale des Rayonnements, 9 Av. du Colonel Roche, BP 44346, 31028 Toulouse Cédex 4, France*
[18] *Radio Astronomy Laboratory, University of California at Berkeley, 601 Campbell Hall, Berkeley, CA 94720-3411*
[19] *Passiebloemweg 31, 1338 TT Almere, The Netherlands*
[20] *Laboratoire AIM, CEA/DSM - CNRS - Université Paris Diderot DAPNIA/Service d'Astrophysique Bât. 709, CEA-Saclay F-91191 Gif-sur-Yvette Cédex, France*
[20] *Steward Observatory, University of Arizona, 933 North Cherry Avenue, Tucson, AZ 85721*
[21] *Harvard-Smithsonian Center for Astrophysics, 60 Garden Street, MS 65, Cambridge, MA 02138-1516*
[22] *Department of Astrophysics, Nagoya University, Chikusa-Ku, Nagoya 464-01, Japan*
[23] *Physics & Astronomy Department, University of Missouri, Columbia, MO 65211*
[24] *Astrophysics Group, Imperial College London, Blackett Laboratory, Prince Consort Road, London, SW7 2AZ,UK*
[25] *Spitzer Science Center, California Institute of Technology, MS 220-6, Pasadena, CA 91125*
[26] *Max Planck Institut für Astronomie, D-69117 Heidelberg, Germany*
[27] *Warsaw University Observatory, Al. Ujazdowskie 4, 00-478 Warszawa, Poland*
[28] *Institut d'Astrophysique de Paris, 98 bis, Boulevard Arago, Paris 75014, France*
[29] *Leiden Observatory, P.O. Box 9513, NL-2300 RA Leiden, The Netherlands*
[30] *Ritter Astrophysical Research Center, University of Toledo, Toledo OH 43606*
[31] *Space Science Institute, 4750 Walnut Street, Suite 205, Boulder, CO 80301*

Mon. Not. R. Astron. Soc. **000**, 2–34 (2010) Printed 30 September 2010 (MN LATEX style file v2.2)

ABSTRACT

We present the classification of 197 point sources observed with the *Infrared Spectrograph* in the *SAGE-Spec* Legacy program on the *Spitzer Space Telescope*. We introduce a decision-tree method of object classification based on infrared spectral features, continuum and spectral energy distribution shape, bolometric luminosity, cluster membership, and variability information, which is used to classify the *SAGE-Spec* sample of point sources. The decision tree has a broad application to mid-infrared spectroscopic surveys, where supporting photometry and variability information are available. We use these classifications to make deductions about the stellar populations of the Large Magellanic Cloud and the success of photometric classification methods. We find 90 asymptotic giant branch (AGB) stars, 29 young stellar objects, 23 post-AGB objects, 19 red supergiants, eight stellar photospheres, seven background galaxies, seven planetary nebulae, two HII regions and 12 other objects, seven of which remain unclassified.

Key words: galaxies: individual (LMC) — infrared: galaxies — infrared: stars — Magellanic Clouds — surveys — techniques: spectroscopic.

1 INTRODUCTION

The *SAGE-LMC* program (Meixner et al. 2006), the vanguard of the *Surveying the Agents of Galaxy Evolution* (*SAGE*) collaboration, is a *Spitzer Space Telescope* Legacy Program which took a photometric inventory of the Large Magellanic Cloud (LMC) using the *Infrared Array Camera* (IRAC; Fazio et al. 2004) and *Multi-Band Imaging Photometer for Spitzer* (MIPS; Rieke et al. 2004) instruments on board the *Spitzer Space Telescope* (Werner et al. 2004). Observations were taken over two epochs separated by three months. The survey detected some 6.5 million point sources at 3.6, 4.5, 5.8, 8.0 μm (IRAC) and 24, 70, 160 μm (MIPS). To follow up on the *SAGE-LMC* program, the *SAGE-Spec* project (Kemper et al. 2010), obtained 196 staring-mode pointings using *Spitzer*'s *Infrared Spectrograph* (IRS; Houck et al. 2004) (5.2-38 μm) of positions selected from the *SAGE-LMC* catalog. In addition, several other *Spitzer* programs have targeted objects in the LMC with the IRS; see Table 4 of Kemper et al. (2010) for an overview of these.

Characterization of the point sources observed in the *SAGE-LMC* survey, *SAGE-Spec* survey, and IRS data archive, builds an inventory of dusty sources and their interrelation in the LMC. One of the major science outputs of *SAGE-Spec* will be to relate the *SAGE-LMC* photometry to the spectral characteristics for different types of objects in the LMC, and ultimately, to classify all the photometric point sources in the LMC. This paper makes the first steps towards this goal. We discuss the method of classification into various source types in §2. In §3 we have executed the classification method on the point sources observed in the *SAGE-Spec* program. This classification, combined with the photometric classification of the 250 brightest infrared sources in the LMC (Kastner et al. 2008; Buchanan et al. 2009) and a large sample of LMC young stellar objects (Seale et al. 2009), is used to further characterize the stellar content of the LMC (§4), and compare it with existing classifications.

Eventually, our classification will be extended to cover all archival IRS observations of point sources within the *SAGE-LMC* footprint (Woods et al., in prep., Paper II). The classification of each of these additional ∼750 sources will be part of the data delivery of the *SAGE-Spec* legacy project to the *Spitzer Science Center* and the community[1]. The classification will be used to benchmark a colour-classification scheme that will be applied to all ∼6.5 million point sources in the *SAGE-LMC* survey (Marengo et al., in prep).

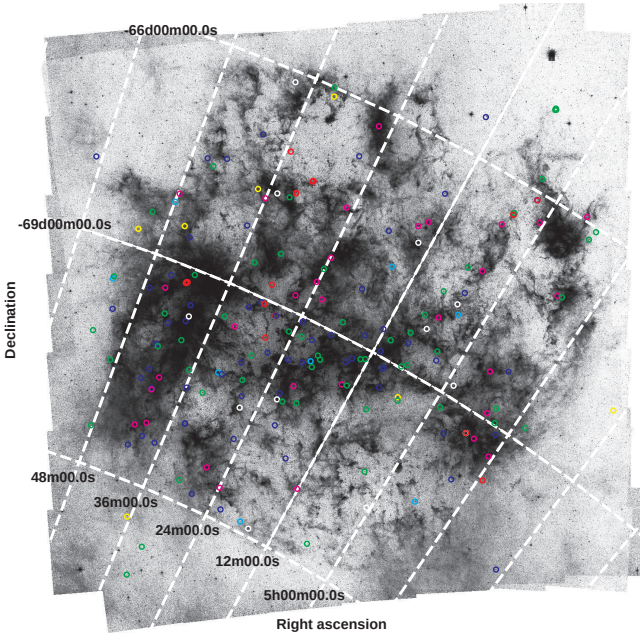

Figure 1. The *SAGE-Spec* sources distributed on the sky, overlaid upon a *SAGE-LMC* 8 μm map. The colour of the points represent our classifications: YSO & HII (magenta), STAR (cyan), O-AGB, O-PAGB & O-PN (blue), C-AGB, C-PAGB, C-PN (green), RSG (red), GAL (yellow), OTHER & UNK (white). See text for class definitions.

* E-mail: Paul.Woods@manchester.ac.uk

[1] http://ssc.spitzer.caltech.edu/legacy/sagespechistory.html

Table 1. Classification groups

Code	Object type
YSO-1 to YSO-4	Young stellar object
STAR	Stellar photosphere
C-AGB	C-rich AGB star
O-AGB	O-rich AGB star
RSG	Red supergiant
C-PAGB	C-rich post-AGB star
O-PAGB	O-rich post-AGB star
C-PN	C-rich planetary nebula
O-PN	O-rich planetary nebula
HII	HII region
GAL	Galaxy
OTHER	Object of known type
UNK	Object of unknown type

2 THE CLASSIFICATION METHOD

A full description of the *SAGE-Spec* project and the techniques used in the reduction of the IRS data utilised in this work can be found in Kemper et al. (2010) and the documentation accompanying the *SAGE-Spec* database deliveries to the *Spitzer* Science Center. The 197 objects in the *SAGE-Spec* sample (observed with 196 IRS staring mode pointings; see Kemper et al. 2010) are classified using the *Spitzer* IRS spectrum for each object; the *U*, *B*, *V*, *I*, *J*, *H*, *K*, IRAC and MIPS photometry; a calculation of bolometric luminosity; variability information; cluster membership and other information found in the literature. The *UBVI* photometry comes from the Magellanic Clouds Photometric Survey (MCPS; Zaritsky et al. 2004); JHK_s/K' photometry comes from both the Two Micron All Sky Survey catalog (2MASS; Skrutskie et al. 2006) and the Infrared Survey Facility (IRSF) survey (Kato et al. 2007); IRAC and MIPS photometric data were taken from the *SAGE-LMC* database (Meixner et al. 2006). The *SAGE-Spec* sample was matched to Optical Gravitational Lensing Experiment (OGLE-III) catalogs of variable stars (Soszyński et al. 2008, 2009a,b) and to the Massive Compact Halo Objects (MACHO) database (Alcock et al. 1998; Fraser et al. 2005; Fraser, Hawley & Cook 2008) to obtain periods. Bolometric luminosities were calculated over the range of available photometric points (typically U-band to IRAC 8 μm or MIPS 24 μm) and compared with published values (e.g., Srinivasan et al. 2009). A literature search was also performed for each object to retrieve other information useful in the purposes of classification, including (but not limited to) determination of the stellar type, luminosity, the age of nascent cluster (if the star was found to be a member of a cluster of stars), Hα detections, etc. Appendix A provides a brief summary of this survey for each object. Many of the objects in the sample were newly-discovered in the *SAGE-LMC* survey, and hence have not been well-studied in the literature. We also matched our source list to recent lists of YSO candidates, viz. Whitney et al. (2008), Gruendl & Chu (2009), Seale et al. (2009).

We adopt the following categories for the source classification. Low and intermediate mass ($M < 8\,M_\odot$) post-Main Sequence stars are classified by chemistry (O- or C-rich) and by evolutionary stage (Asymptotic Giant Branch; post-Asymptotic Giant Branch; and Planetary Nebula), hence our groupings `O-AGB, O-PAGB, O-PN, C-AGB, C-PAGB, C-PN`. More massive red supergiants have a class of their own, `RSG`. Young stellar objects can be identified (`YSO`). Stars showing a stellar photosphere, but no additional dust or gas features are classified as `STAR`. We also distinguish galaxies (`GAL`), and HII regions (`HII`). We have the classification `OTHER` for objects of *known type* which do not fit into another category (e.g., R Coronae Borealis stars). These objects are usually identified by searching the astronomical literature for pertinent information and similar spectra. A literature search was performed for all *SAGE-Spec* objects, and is summarised in Appendix A. Finally, we use `UNK` for objects which cannot be classified (unknown objects) due to low signal-to-noise data, or unidentifiable spectral features. Table 1 summarises the classification groups. The following sections discuss the description of the individual categories, along with the classification criteria.

2.1 Young stellar objects

A robust sub-classification of young stellar objects by evolutionary stage or mass involves complex SED-fitting of multiband photometry so that some distinction between classes can be made (e.g., Whitney et al. 2008). Given that such an in-depth treatment would be out of place in this work, we classify YSO spectra phenomenologically into four groups (see below and our further comments in §3).

The spectra of YSOs are characterised by oxygen-rich dust features superimposed onto a cold dust continuum, and often exhibit strong silicate features at 10 μm and in the 18–20 μm region, either in emission or absorption (e.g., Furlan et al. 2006, 2008). In Galactic sources silicate absorption superimposed on a very red continuum is indicative of embedded protostellar objects (e.g., Furlan et al. 2008). These objects are traditionally classified as Class I sources (based on their IR spectral index; Lada 1987) and more recently as Stage I sources (based on their modelled mass-accretion rates; Robitaille et al. 2006).The 10-μm feature can also be self-absorbed at critical optical depths.

Ice absorption features are another common feature in spectra of embedded YSOs. The IRS spectra can show prominent ice features at 5−7 μm and 15.2 μm that are attributed to a mixture of H_2O, NH_3, CH_3OH, HCOOH, H_2CO and CO_2 ices respectively (e.g., Oliveira et al. 2009). At shorter wavelengths, ice features of water and CO are found in the 3–5-μm range (e.g., Shimonishi et al. 2010; Oliveira et al. 2009; Shimonishi et al. 2008). Also common in the spectra of many YSOs are emission features attributed to polycyclic aromatic hydrocarbons (PAHs). The infrared YSO spectra show a superposition of ice, dust and PAH features that can be difficult to disentangle.

At later stages, the envelopes of the YSOs become less dense and hotter, their continua are bluer, and eventually emission from the circumstellar disc dominates the SED and silicate emission becomes conspicuous. Such objects are usually classified as Class II (Lada 1987) or Stage II objects (Robitaille et al. 2006). Amongst such objects are Herbig Ae/Be (HAeBe) stars. These intermediate-mass (2–8 $M_\odot$) YSOs have hot (>7 000 K; Cox 2000) central stars which are able to illuminate PAH molecules in their environs, and thus often show a mixture of PAH emission

and silicate dust emission in their mid-infrared spectra (Keller et al. 2008; Acke et al. 2010). Spectroscopically it can often be challenging to distinguish these more evolved YSOs with dusty discs from post-AGB stars in the IR. One could resolve this degeneracy with complementary data, perhaps looking for signs of accretion (pre-Main Sequence) or chemical enrichment (post-AGB) in optical observations, or correlating positions with known star-forming clusters or molecular clouds. Several groups have spectroscopically identified YSOs in the LMC (e.g., van Loon et al. 2005c; Oliveira et al. 2006; Shimonishi et al. 2008; Oliveira et al. 2009; Seale et al. 2009; Shimonishi et al. 2010).

2.2 Stellar photospheres

Most Main Sequence and sub-giant stars show no significant emission in excess over that from the stellar photosphere alone and present largely featureless IRS spectra ("naked stars"). Stars of spectral class K or earlier present infrared spectra similar to 10 000-K blackbodies, because the hotter spectra are on the Rayleigh-Jeans tail, and the H^- ion dominates the opacity in the cooler spectra (e.g., Engelke 1992). For A-type and earlier-type stars hydrogen absorption lines are usually present, and are noticeable in spectra with good signal-to-noise, even at the low resolution of the spectra presented here. When the spectrum is plotted in Rayleigh-Jeans units ($\lambda^2 F_\nu$ vs. λ), a true Rayleigh-Jeans tail will appear as a horizontal line (Cohen, Walker & Witteborn 1992).

Stars with only a small infrared excess with no obvious dust features may also be classified as naked stars. These correspond to the "type F" sources of Volk & Cohen (1989) in the Infrared Astronomical Satellite (IRAS) Low Resolution Spectrometer (LRS) spectra. Stars with molecular absorption features but no overt dust features have been classified as AGB stars.

Naked stars in the *SAGE-Spec* survey may include foreground Main Sequence stars, Cepheid variables and other luminous stars in the LMC. These different types of stars can be distinguished on the basis of their short wavelength colours, but often cannot be readily distinguished based on the IRS spectrum alone. Interested readers are referred to Heras et al. (2002) for a classification of stellar photospheres.

2.3 Stars on the Asymptotic Giant Branch

AGB stars are characterised by an infrared excess at wavelengths longer than a few microns due to circumstellar dust or a combination of molecular absorption features and photometric variability. The dust and molecular features reveal the particular chemistry of the star.

Carbon-rich AGB stars have undergone a series of thermal pulses which dredge carbon produced by the triple alpha sequence from the interior to the photosphere (Iben & Renzini 1983). When carbon atoms outnumber oxygen atoms, the formation of CO ties up all of the oxygen, resulting in carbon-rich molecules and dust grains. CO, C_3, C_2H_2, and HCN can produce strong absorption features (∼4–8.5 and 13.5–14 μm, e.g., Jørgensen, Hron & Loidl 2000; Matsuura et al. 2006). Dust is usually present, and amorphous carbon and graphite dominate the composition (e.g., Martin & Rogers 1987). The emission from amorphous carbon is featureless, but trace elements like SiC produce features at ∼11.3 μm, either in emission or absorption (e.g., Treffers & Cohen 1974; Gruendl et al. 2008; Speck et al. 2009). MgS dust produces a broad emission feature at ∼30 μm (22–38 μm; Goebel & Moseley 1985; Hony, Waters & Tielens 2002; Zijlstra et al. 2006; Sloan et al. 2006; Lagadec et al. 2007).

As long as the C/O ratio remains below unity, silicates are the dominant dust component in the spectra of AGB stars, with features at 10 and 18 μm, either in emission or absorption (e.g., Gillett, Low & Stein 1968; Woolf & Ney 1969; Merrill & Stein 1976). Silicate self-absorption at 10 μm indicates an extreme or optically thick O-rich AGB star (e.g., Sylvester et al. 1999; Trams et al. 1999). A molecular absorption at 8 μm due to the fundamental vibrational mode of SiO is an indication of oxygen-rich chemistry, and is often manifested as a slight inflection in the spectrum. Water absorption or emission can cause a broad feature in the region 6.4–7.0 μm. Alumina or spinel has a feature at 13–14 μm which can be seen in emission or absorption. A continuous, featureless mid-IR excess can be caused by metallic iron dust (McDonald et al. 2010).

AGB stars of both chemistries can be variable, and often have regular, well-defined periods from 100 days to over 1 000 days for extreme carbon and OH/IR stars (e.g., Wood et al. 1992; Whitelock et al. 2003). The "classical" luminosity limit for AGB stars based on the core-mass–luminosity relationship is given as $M_{\rm bol} = -7.1$ mag (Wood et al. 1983; Smith et al. 1995), although evolutionary calculations including hot-bottom burning allow for AGB stars as bright as $M_{\rm bol} = -8.0$ mag (Wagenhuber & Groenewegen 1998; Herwig 2005; Poelarends et al. 2008).

2.4 Red supergiants

Red supergiants (RSGs) are in general more luminous than AGB stars, although there is some overlap in the range $-7.1 \gtrsim M_{\rm bol} \gtrsim -8.0$ mag (Wood et al. 1983, 1992; van Loon et al. 2005a; Groenewegen et al. 2009). We consider a suitable O-rich star to be an RSG if its bolometric magnitude is greater than the classical AGB luminosity limit of $M_{\rm bol} = -7.1$, or if it resides in a cluster too young for a low-mass star to have reached the AGB. They exhibit a similar dust chemistry to O-rich AGB stars, although to our knowledge no supergiant has been associated with silicate absorption.

Red supergiants which reside in clusters can then be distinguished from O-rich AGB stars providing the age of the cluster can be determined. Ages of red supergiants vary from ∼3–30 million years (Schaller et al. 1992) since they are more massive than AGB stars (>8 $M_\odot$) and thus evolve more rapidly. An 8 $M_\odot$ star will spend ≈55 Myr on the Main Sequence.

Red supergiants show no large-amplitude brightness variations, and have previously been distinguished from O-rich AGB stars by means of period-magnitude diagrams or amplitude of light-curve (Wood et al. 1992). They are generally classified as irregular or semi-regular pulsating variables.

2.5 Post-AGB stars

As the AGB mass-loss phase ceases, the circumstellar dust shell continues to move outwards, thus gradually exposing the central star. This generally results in a double-peaked SED with one peak due to stellar emission and the other due to circumstellar dust (e.g., Van Winckel 2003). This double-peaked shape means that post-AGB stars can be readily distinguished from AGB stars by means of colour. Some post-AGB stars have SEDs with strong near-infrared emission, pointing to the presence of hot dust in the system. Some of these particular stars reside in a binary system, which has led to the formation of a stable dusty circumbinary disc (Waters, Trams & Waelkens 1992; De Ruyter et al. 2006; Gielen et al. 2008; Van Winckel 2007; Van Winckel et al. 2009).

Carbon-rich chemistry produces a dust-dominated continuum with a variety of possible emission features, from PAHs, or MgS at 30 μm, or the unidentified "21-μm feature" (Kwok, Volk & Hrivnak 1989; Hrivnak, Volk & Kwok 2009). Oxygen-rich post-AGB objects typically exhibit silicate emission features, but with a strong contribution from crystalline grains, which produce narrower features at 11, 16, 20, 23, 28, and 33 μm (Gielen et al. 2008, 2009). This high degree of crystallinity and the presence of large grains indicates a circumbinary dusty disc (e.g., AFGL4106; van Loon et al. 1999; Molster et al. 1999). Some sources show mixed chemistry with both carbon-rich and oxygen-rich molecules and dust, such as the Red Rectangle (HD 44179; Waters et al. 1998) and IRAS 16279-4757 (Matsuura et al. 2004).

2.5.1 RV Tauri-type stars

RV Tauri stars are a particular class of post-AGB stars (Jura 1986) which show a distinct variability pattern – alternating deep and shallow minima – due to pulsations, since they cross the Population II Cepheid instability strip. Typically they have (minimum-to-minimum) periods of 20–68 days (Soszyński et al. 2008). They exhibit photospheric depletion in refractory elements which is consistent with the presence of a dusty circumstellar disc. This depletion phenomenon is commonly observed in binary post-AGB stars with discs, which led Van Winckel et al. (1999) and Gielen et al. (2009) to suggest that these depleted RV Tauri stars must also be binary stars surrounded by such discs. Presently it is not possible to distinguish between a regular oxygen-rich post-AGB object and a pulsating one (RV Tau) via mid-infrared spectra; one must in addition obtain a lightcurve from several years' observations. Various catalogues exist which make this determination straightforward, e.g., MACHO (Alcock et al. 1998) and OGLE-III (Soszyński et al. 2008). Time-variable U−B or B−V colours could point to pulsating behaviour, although this could also be due to other factors (e.g., variable reddening due to the circumstellar disc).

2.6 Planetary nebulae

The material around the hot central stars of planetary nebulae is readily ionized, and thus their spectra show evidence of forbidden line emission from excited atomic species. Commonly-observed lines in the *Spitzer* IRS bandwidth are [ArII] (6.99 μm), [ArIII] (8.99 μm), [SIII] (18.71 and 33.48 μm) , [SIV] (10.51 μm), [SiII] (34.81 μm), [NeII] (12.81 μm), [NeIII] (15.56 μm), [NeV] (14.32 and 24.30 μm), [NeVI] (7.64 μm) and [OIV] (25.91 μm), where the latter three "high excitation" lines are indicative of highly-ionizing photon fields. The radiation field in PNe also readily excites PAH emission. Stanghellini et al. (2007) showed that the presence of carbon-rich dust (i.e., SiC, MgS or PAHs) in the *Spitzer* IRS spectrum correlated with carbon-rich planetary nebulae, and so we can make a distinction between `C-PN` and `O-PN`. In PNe the dust continuum first rises towards longer wavelengths, but then turns over ($\lambda \approx 30\,\mu$m for young PNe) due to a lack of large amounts of cold dust in the regions around PNe (Bernard-Salas et al. 2008, 2009).

2.7 HII regions

HII regions form around young hot stars and appear very similar to planetary nebulae in their mid-infrared spectra. They show the same range of forbidden line emission, with the exception of the higher-excitation lines [NeV] and [OIV], due to the less strongly-exciting radiation field in HII regions. Another differentiating feature is that the dust continuum at longer wavelengths ($\lambda \gtrsim 30\,\mu$m) continues to rise and falls at wavelengths far outside of the *Spitzer* IRS range since HII regions are typically embedded in Giant Molecular Clouds. Buchanan et al. (2006) find that HII regions in their sample are more luminous than PNe, having an infrared (1–100 μm) luminosity of $0.2–5\times10^5$ $L_\odot$.

It should be noted that since *Spitzer* IRS observations in the LMC are likely only sensitive to more massive YSOs, there is a continuum of properties from embedded YSO to ultra-compact HII region to classical HII region, and at the distance of the LMC this may also become confused by spatial resolution issues. The IRS has an angular resolution of the order of arcseconds, which at the distance of the LMC would mean a resolution of 0.5 pc at best. Therefore (ultra)compact HII regions would not be resolved (cf. Churchwell 2002). Thus there may be some ambiguity between different classes here, especially when, for instance, weak silicate absorption is veiled by PAH emission. For this reason, we classify (ultra)compact HII regions as YSOs (see discussion in §3) and classify featureless spectra with low-excitation forbidden line emission as HII regions.

2.8 Galaxies

Quiescent galaxies are usually elliptical and have very low rates of star formation. Thus their infrared spectra appear to be similar to the spectrum of a K and M star combined, since these star classes are what dominate the stellar population in these galaxies. Active galaxies are presently star-forming, and thus show emission lines from [NeII] and frequently [NeIII]. Those active galaxies with active galactic nuclei (AGN) will show [NeV] emission. Active galaxies also show PAH emission. These narrow features are red-shifted in spectra of galaxies, allowing a good determination of distance. Broader features (e.g., silicate emission at 10 μm) are also red-shifted, but a precise determination of redshift is more difficult. Mid-infrared spectra of galaxies are discussed

in more detail in Hao et al. (2007), for example. The galaxies in our sample are unresolved, and treated as point sources.

2.9 Other types of object

Less-common objects were not given their own classes, but examples are described below and plotted under the catch-all of "`OTHER`" in Figs. 14 and 15. Their classifications are given common astronomical abbreviations in Table 3.2.

2.9.1 R Coronae Borealis stars

R Coronae Borealis stars (R CrB) are hydrogen-deficient supergiants which are irregularly variable. Thought to be formed by the merger of two white dwarf stars or by a final helium-shell flash, they go through episodic dimming due to the formation of what is proposed to be carbon dust in their atmospheres (Clayton 1996, 2002). In the mid-infrared they appear featureless, and they exhibit a red SED akin to an evolved star (e.g., Lambert et al. 2001; Kraemer et al. 2005).

2.9.2 B supergiants

B supergiants (BSGs) are early-type dusty stars which usually present a flat spectrum with weak silicate features (Buchanan et al. 2009). They also show a deeply double-peaked SED with a blue stellar peak and a red dust peak thought to be due to a dusty circumstellar disc or torus, (e.g., Bolatto et al. 2007; Bonanos et al. 2009, 2010).

2.9.3 Wolf-Rayet stars

Wolf-Rayet (WR) stars are evolved massive stars surrounded by a thick, dusty envelope. Characterised by strong emission lines such as HeII, [NeII], [NeIII], [SIV] and [OIV], they also show a red SED due to warm circumstellar dust. WR stars show dust emission from three sources: 1) self-produced carbon dust, only detected in late-type WC stars as a 7.7 μm-type feature, attributable to a C–C stretch mode of carbonaceous-type grains and consistent with a lack of C–H stretch or bend modes given that their stellar winds are H-deficient (Chiar, Peeters & Tielens 2002; Cherchneff et al. 2000); 2) wind collisions between a WR wind and a colliding O/B star wind (Tuthill, Monnier & Danchi 1999) and 3) swept-up interstellar dust. With the low spectral resolution of *Spitzer*, it will be hard to identify one of these three mechanisms.

2.10 Unknown objects

Objects that we have not been able to classify with a high confidence are classified as "Unknown" (`UNK`). Generally the cause of this is low signal-to-noise data, where spectra have been too noisy to show distinct features, or where a mis-pointing of the telescope has meant that our intended target was missed and no target was located in the slit.

2.11 Usage of the classification tree

2.11.1 Operation

Our classification methodology is shown in the form of a decision tree (Fig. 2). The tree aims to classify objects into different categories via means of Yes/No selections. Not all of the decisions rely solely on the appearance of the infrared spectrum in question, but where possible this has been the main discriminant. Such a rigorous method of classification lends itself to the classification of large samples of (spectroscopic) infrared data. Thus this tree could readily be applied to data from the *Infrared Astronomical Satellite* (IRAS) and *Infrared Space Observatory* (ISO) satellites, and with a few adaptations could also be applied to AKARI, *Herschel Space Observatory* (*Herschel*) and *James Webb Space Telescope* (JWST) data, for example. It also lends itself to automation, given that the requisite information on variability and cluster membership, for example, can be gathered. The classification tree is designed to be simple to use; however, some of the decision boxes may require slightly more explanation than that provided in the caption to Fig. 2.

"Featureless cont. with PAHs or atomic emission lines?" partially filters out the spectra without dust or molecular features, given the aforementioned (§2.1) issues with diffuse PAH and atomic features in the spectrum. Spectra captured by this filter will generally comprise of a rising continuum at longer wavelengths with several atomic emission lines or PAH features, and this indicates that the emitting object is a planetary nebula or HII region. Other featureless spectra are collected by the "Dust features?" box.

"Solely molecular features?" is intended to filter spectra with dust and molecular features from spectra with just molecular features. Ideally, this filter captures embedded YSOs with evident ice absorption features but no (or weak) silicate features, and also evolved stars (C-AGB/O-AGB/RSG) which do not appear significantly dusty.

"Falling spectrum over range ∼20–32 μm?" is intended to distinguish between YSOs and evolved oxygen-rich objects. Generally, if a spectrum falls after the 20 μm silicate feature the emitting object is an evolved star, with only moderate amounts of cold dust (van Loon et al. 2010). However, if a spectrum rises or remains level it is more often than not a young object. The particular range of ∼20–32 μm was chosen to exclude $\lambda > 32\,\mu$m to avoid any far-IR rise due to contaminating sources in the IRS Long-Low slit. If spectral data in the region 20–32 μm is missing, one should use the 24 μm photometry as a replacement.

"Double-peaked SED" (in two locations) is used to separate post-AGB objects. Here the crucial distinction to make is between an SED with a stellar component which has a large infrared excess, and an SED with a stellar and a dust peak with a minimum between them. An illustration is given in Fig. 3.

"Other" (in two locations) is a catch-all for unusual or uncommon objects. The classification of the objects which fall into this category is then performed by referring to the astronomical literature (e.g., with the help of SIMBAD[2]) or by comparing spectra of similar, known objects. If an object cannot reliably be classified in this way, or if the suggested

[2] `http://simbad.u-strasbg.fr/simbad/`

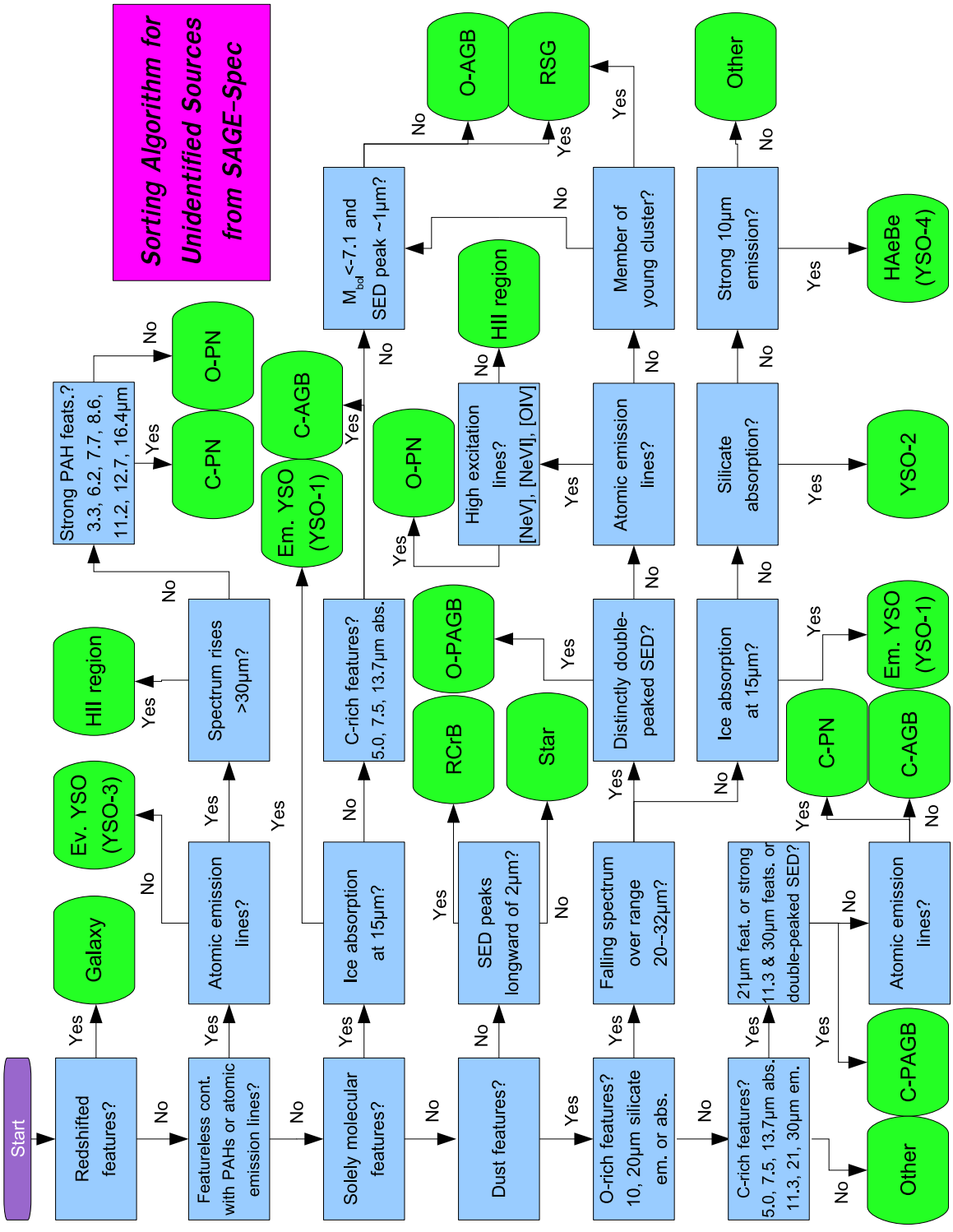

Figure 2. The decision tree for the classification of the *SAGE-Spec* sample. For the purposes of the classification tree, the word "spectrum" is used to indicate a plot of flux intensity (F_ν) against wavelength (λ) showing the higher dispersion data from the spectrograph, and this is different to "SED", which is used to mean a plot of $\log(\lambda F_\lambda)$ (or νF_ν) against $\log(\lambda)$ which includes all available photometry, as well as the spectral data. Abbreviations used in this figure: 'cont.' for continuum, 'ev.' for evolved, 'em.' for embedded, and 'feat(s).' for features. See §2.11.1 for more details.

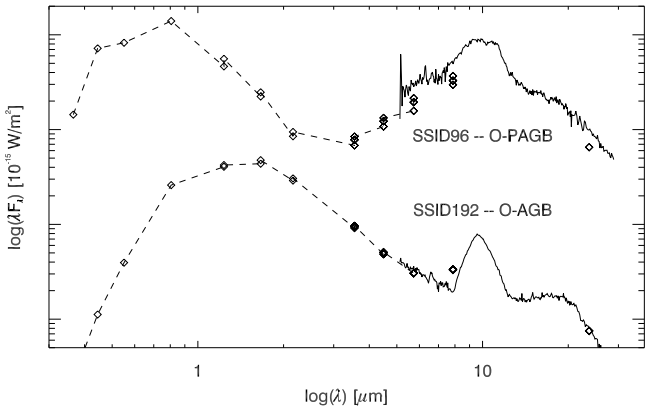

Figure 3. An illustration of a double-peaked SED (post-AGB) compared to a stellar peak with a large dust excess (AGB). See text.

classification is not in accord with the *Spitzer* IRS spectrum, it is deemed 'unknown' and classified as `UNK`.

2.11.2 Caveats and data issues

The decision tree in Fig. 2 is a useful formalisation of a difficult task. As a simplification of a complex problem, it is, however, open to error, and this error can be minimised by being aware of the following:

Spectral identification error. The largest source of error is incorrect identification of spectral features. The correct identification of features is crucial, and the error reduces only with experience in looking at spectra or very careful inspection of the spectra. One particular class of object which may prove difficult to spot is low-redshift galaxies ($z \gtrsim 0.02$). The potential shift in wavelength of distinguishing dust features such as PAH emission and silicate emission features due to different physical effects alone (e.g., ionization of PAHs, differing dust grain shapes) may mask the redshift of the emitting object.

Low signal-to-noise data/mispointings. Noise can often masquerade as real features in low-contrast spectra. For instance, the spectrum for SSID42 could potentially show PAH features redshifted to z∼1.57. However, given the low levels of flux and the lack of an obvious point source in 8 μm images, it seems that this spectrum is solely noise. Spectra can also be contaminated by nearby objects thereby altering the continuum shape and spectral features. *Spitzer*'s IRS instrument has two low-resolution modules named Short-Low (SL) and Long-Low (LL), each of which has two orders, SL1, SL2 and LL1, LL2. Each slit of SL has an aperture of $3\farcs6\times57''$ (with a $22''$ separation). The two LL slits are $10\farcs6\times168''$ apertures. With such a large difference in apertures between SL and LL it is possible that SL and LL may observe different objects. This was determined to be the case for one observation, where supergiant GV 60 (SSID16), the intended target, was observed with SL, whereas LL picked up emission from a nearby Wolf-Rayet star, LHα120-N 82 (alternatively named Brey 3a or IRAS 04537-6922) (SSID17). Thus not only is it possible to add serendipitous detections to the sample, but it is also possible that contamination may affect the observed spectrum, especially in LL. A more full discussion of these two objects can be found in van Loon et al. (2010, object #4). Furthermore, issues in data reduction can introduce spurious features. For *Spitzer* IRS data an obvious place for this to occur is at the joins between modules. For instance, the join between SL1 and LL2 falls at ∼14 μm, which can complicate the continuum determination to the blue of the ice feature due to CO_2 ice. Similarly, the join between SL1 and SL2 at ∼8 μm could affect the recognition of an SiO feature in a stellar spectrum.

Foreground objects. We take no account of foreground objects in the decision tree (Fig. 2). Since the only place where we take distance into account in the tree is indirectly through the luminosity discriminant between oxygen-rich AGB stars and red supergiants, source classification is not particularly affected by distance. It may be that the `RSG` category is contaminated by foreground oxygen-rich red giant branch and asymptotic giant branch stars, however these objects should be distinguishable by means of colour, variability or radial velocity measurements.

Limited data. In the case where spectral coverage is limited (e.g., Long-Low data is not available) or other information is lacking, the decision tree may fail to end in a firm classification. In this case the classification must be limited to the classes remaining along the branch of the tree where the failure occurred.

2.11.3 Quality control

IRAC 8 μm images were examined for all 196 pointings in order to flag the presence of nearby objects and the *Spitzer* Basic Calibrated Data (BCDs) were thoroughly examined for multiple sources, cosmic-ray hits and diffuse emission not localised to the point source. A full discussion of the errors associated with the observations and the steps taken to correct them can be found in the *SAGE-Spec* data delivery document (Woods et al. 2010). PAH emission is seen frequently in the spectra, but arises in many cases due to the presence of diffuse ISM along the line of sight to our intended target. Similarly, spectra can include background emission lines at 15.6, 18.7, 33.5, 34.8 and 36.0 μm, arising from diffuse gas in the LMC. These are due to [NeIII], [SIII], [SIII], [SiII] and [NeIII] lines respectively, and are not always subtracted effectively due to non-uniform variation across the slit. As such, the design of the classification tree (Fig. 2) is devised so as not to use the presence of PAH emission as an indication of a carbon-rich nature, except in the case of carbon-rich PNe (Stanghellini et al. 2007).

3 *SAGE-Spec* POINT SOURCE CLASSIFICATION

3.1 Calculation of $M_{\rm bol}$

Bolometric magnitudes were calculated for all *SAGE-Spec* sources using the method described by Sloan et al. (2008). We adopt a distance to the LMC in our calculations of 50 kpc (e.g., Schaefer 2008; Keller & Wood 2006; Feast 1999), and thus a distance modulus of 18.5 mag (e.g., Alves 2004). The Sloan et al. (2008) technique involves an integration of the IRS spectrum and photometry points, fitting a 3 600 K Planck Function to the optical photometry, and adding a Rayleigh-Jeans tail to the long-wavelength data. For redder

Table 4. Classification groups and tally

Type	Count	Type	Count
C-AGB	50	GAL	7
O-AGB	40	OTHER	5
YSO	29	C-PAGB	5
RSG	19	O-PN	4
O-PAGB*	18	C-PN	3
(*inc. RV Tau)	(9)	HII	2
STAR	8	UNK	7

sources with large amounts of cold dust, this will mean that the bolometric magnitude we derive will be a lower limit. For stellar photospheres, low dust-excess oxygen-rich AGB stars and red supergiants, we also calculate the bolometric magnitude by fitting a MARCS stellar atmosphere model (Gustafsson et al. 1975, 2008) to the SED. This method provided a better fit to the optical and near-IR photometry which cover the peak of the energy distribution of these objects. Such a method has been previously used by McDonald et al. (2009), Boyer et al. (2010) and McDonald et al. (2010, submitted), and we refer the reader to those papers for details of the MARCS models, and for an evaluation of errors. In general, the agreement between the Sloan et al. (2008) method and McDonald et al. (2009) method was good to within 0.1 mag. We prefer the McDonald et al. (2009) method values for the abovementioned three categories. As a further check, we compared the luminosities derived for AGB stars with those calculated by Srinivasan et al. (2009) for their sample of LMC AGB stars. Again, agreement was reasonably good, although the values of Srinivasan et al. (2009) were generally 0.15 mag brighter across the board. This is likely due to the use of a different zero-point flux. Results of our calculations are shown in Table 2.

Fig. 4 shows histograms of bolometric magnitudes for AGB stars, post-AGB stars, RSGs and YSOs. Most C-AGB stars have a bolometric magnitude of ∼-5 mag, whilst O-AGB stars have two peaks, the one at higher magnitude possibly due to O-AGBs currently undergoing Hot Bottom Burning (Boothroyd & Sackmann 1992). C-PAGB stars show a peak in bolometric magnitude which coincides with that for C-AGB stars.

3.2 Classification results

The results of the classification process are summarised in Table 3.2, along with *SAGE-Spec* identifier (SSID), coordinates and alternate designations for the sample objects, and class counts are tallied in Table 4.

3.2.1 YSOs

The 30 YSO spectra in the *SAGE-Spec* sample broadly fall into two categories: those with a rising F_ν spectrum toward longer wavelengths, and those with a flat or declining spectrum (Fig.5). The first group is significantly larger, with 23 YSOs falling into this group. Many of these objects are still enveloped in dust, and the varying slopes of their continua are evidence of dust at a range of temperatures. The remaining seven objects represent more evolved YSOs with silicate features in emission superimposed on a hotter dust continuum. Additional care needs to be taken when identifying objects belonging to the latter group, as some oxygen-rich evolved stars also exhibit silicate emission (see §2.3).

We use mid-IR spectral features to classify the 30 YSOs in distinct groups:

(i) YSOs with ices (Fig. 5, `YSO-1`)
(ii) YSOs with silicate absorption (Fig. 5, `YSO-2`)
(iii) YSOs with PAH emission (Fig. 5, `YSO-3`)
(iv) YSOs with silicate emission (Fig. 5, `YSO-4`).

The classification of the spectra into the first three of these groups is hierarchical, in the sense that a YSO is classified in Group 1 if its spectrum has ice absorption features, irrespective of the presence of silicate and/or PAH features; most (but not all) YSOs in this group exhibit silicate absorption and PAH emission. The spectra of objects in Group 2 show no evidence for ice features but exhibit silicate features in absorption, while the spectra of YSOs in group 3 have PAH emission without ice or overt dust features. This phenomenological classification approach is similar to that employed by Seale et al. (2009). The icy objects in Group 1 are the YSOs described in Oliveira et al. (2009) while the other YSOs are newly identified in this work: three in Group 2, six in Group 3 and eleven in Group 4.

Groups 1–3 roughly represent an evolutionary sequence for massive YSOs: from sources deeply embedded in the cold molecular material that exhibit strong ice and dust absorption features in their mid-IR spectra (e.g., Boogert et al. 2008), to (ultra-)compact HII sources, whose spectra are dominated by PAH and fine structure line emission, where the central object becomes hotter and the dusty envelope becomes progressively more tenuous (e.g., Churchwell 2002). As discussed previously and extensively in Seale et al. (2009) and Oliveira et al. (2009), the issue of spatial resolution at the distance of the LMC needs to be considered carefully when trying to diagnose the evolutionary state of a YSO. The IRS slits are wide enough that emission originating from regions external to the YSO envelope can contaminate the observed spectrum (i.e., as is likely the case for objects that sit near to HII regions). This is likely to be the explanation for the difference in appearance between our Group 1 YSOs, for example, and the Galactic Class I YSOs discussed by Furlan et al. (2008). Many of their icy YSOs do not show PAH features, whereas our sample do, and this is likely due to the coverage of the IRS slits, which cover a larger region in the LMC than they do in the Galaxy. It is also possible that the observed spectrum originates from a small compact cluster not from a single source.

Group 4 represents a more evolved state of lower mass YSOs, likely HAeBe stars. This stage is reached once the accretion rate from the cold envelope is depressed, as most of the dusty material is now found in a circumstellar disc. The shape of the SED for these objects is also sensitive to other factors like disc inclination angle. The silicate emission features in such objects can exhibit signatures of dust processing (e.g., crystallization or modification of the grain size distribution), as dust grains are subjected to higher temperatures. PAH emission is also common in Galactic HAeBe stars (e.g., Keller et al. 2008). From the sample of 11 objects in Group 4, four objects show silicate emission superimposed on a rising continuum. Furlan et al. (2008) observed objects

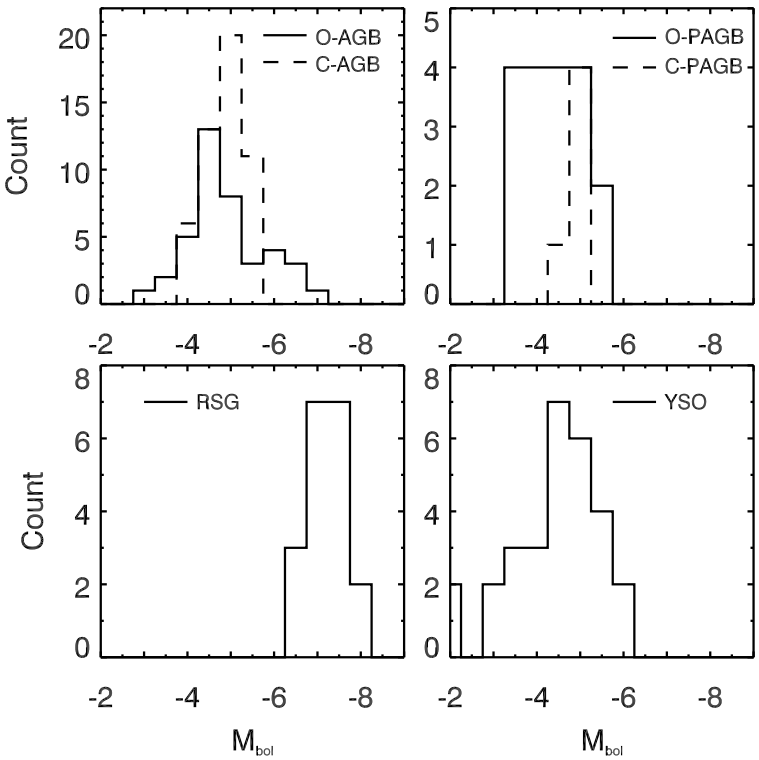

Figure 4. Luminosity functions for AGB stars, post-AGB stars, RSGs and YSOs.

with similar spectral properties in the Galaxy and suggested that such objects are likely examples of a transition between Class I and Class II YSOs, already with a significant contribution from a dusty disc but still embedded in a relatively low-density envelope. The remaining 7 LMC YSOs in this group have a flat or downward sloping continuum and thus are likely the LMC analogs of Galactic Class II sources (Furlan et al. 2006).

3.2.2 Stellar photospheres

Two of the eight of the sample classified as `STAR` have an SED peak between 1–2 μm and calculation of *J-H* and *H-K* shows that they are likely foreground K giants. These are SSID19 and 195. The remaining six have significantly cooler effective temperatures of $\approx$3 400–3 600 K. This, combined with their *J-H* and *H-K* values, would indicate that SSID32, 76, 81, 88, 133 and 188 are M4 or M5 giants. SSID81 and 188 are both classified by Kontizas et al. (2001) as carbon stars, but we see no indication of carbon-rich molecular or dust features in the IRS spectra. SSID88 and 133 show PAH features from foreground emission; SSID88 is not visible in *SAGE-LMC* 8 μm images, and SSID133 is a faint point-source.

3.2.3 Carbon-rich AGB stars

The sample of carbon star spectra ranges from almost-photospheric with mild acetylene absorption to extremely red objects (EROs; according to the definition of Gruendl et al. 2008). The colour criteria for EROs, that they have extremely red mid-IR colours ([4.5]$-$[8.0]>4.0), and that they all fall in a narrow range of brightness (7.0<[8.0]<8.5), are met by three of the sample, SSID65, 125 and 190. All three have a strong MgS features at $\sim$30 μm (Fig. 6). These criteria are also met by two carbon-rich post-AGB objects, SSID84 and 196. We identify four objects which we dub very red objects (VROs) which are not quite as extreme in colours as EROs. They meet the criteria, 2.0<[4.5]$-$[8.0]<4.0 and 6.0$\leqslant$[8.0]$\leqslant$7.0, and have very pronounced SiC features. These objects are SSID9, 18, 140 and 167. Figure 6 shows the seven VRO and ERO spectra. All seven VROs and EROs would be classed as "extreme AGB" stars by Blum et al. (2006), Srinivasan et al. (2009) and others, who use the criteria J$-$[3.6]$\geqslant$3.1, [3.6]$\leqslant$10.5.

In general, we note that the C_2H_2 bands appear stronger in the dusty LMC C-rich AGB stars than in Galactic analogs, such as AFGL 3068 and IRC+10216 (Justtanont et al. 1998, 2000). This has been noticed and discussed in much depth previously (e.g., van Loon et al. 1999; Matsuura et al. 2002, 2005; van Loon 2006; Sloan et al. 2006; Speck et al. 2006; Zijlstra et al. 2006; van Loon et al. 2008). This tendency also appears to be present for the less dusty objects in our sample, although in those cases it is more difficult to distinguish between the photospheric and circumstellar molecular bands. In these less-dusty objects, the 11.3 μm feature appears weaker than in typical C-rich Galactic AGB stars (e.g, Zijlstra et al. 2006). The EROs show clear instances of SiC absorption, and these features are stronger than in any known Galactic object. As near-infrared colours are similar in both samples, this does not appear to be solely a total optical depth effect. The 30 μm feature strength varies widely from object to object, in some cases being very weak

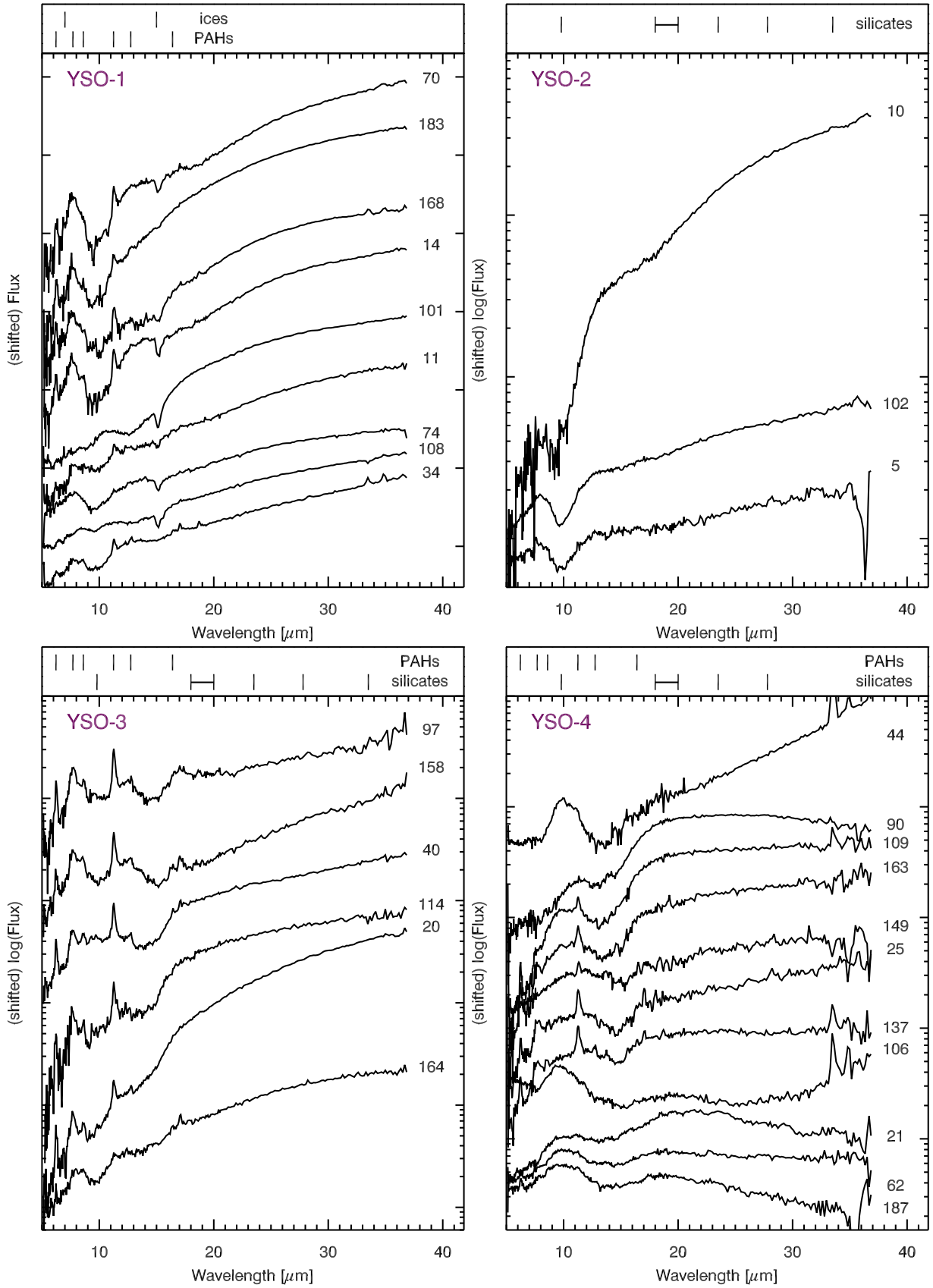

Figure 5. *SAGE-Spec* YSO spectra, sorted into four groups. These (except for those in group `YSO-1`) and subsequent spectra in Figs. 6–13 are presented as $\log(F_\nu)$ versus λ for display purposes. Group 1 contains YSOs with ices, Group 2 has YSOs with silicate absorption (but no ices), Group 3 has YSOs with PAH emission (but no ices or overt silicate absorption) and Group 4 contains YSOs with silicate emission. Numeric labels refer to SSID (see Table 3.2).

Table 2. Bolometric magnitudes for *SAGE-Spec* sources. Effective temperatures derived from fitting the SED of small-dust-excess oxygen-rich stars are given in parentheses. Typical errors are ±100 K.

SSID	$M_{\rm bol}$	SSID ($T_{\rm eff}$)	$M_{\rm bol}$	SSID ($T_{\rm eff}$)	$M_{\rm bol}$	SSID ($T_{\rm eff}$)	$M_{\rm bol}$	SSID ($T_{\rm eff}$)	$M_{\rm bol}$	SSID	$M_{\rm bol}$
C-AGB		156	-4.67	197 (3 106 K)	-4.78	168	-4.66	37 (3 985 K)	-6.66	42	-1.82
51	-5.70	41	-4.66	148 (3 010 K)	-4.63	187	-4.50	35 (3 986 K)	-6.29	184	-1.54
31	-5.70	132	-4.56	13 (3 269 K)	-4.53	11	-4.36	O-PAGB		138	-1.04
87	-5.61	103	-4.54	63 (2 980 K)	-4.49	90	-4.36	162	-5.60	OTHER	
30	-5.54	3	-4.51	67 (3 143 K)	-4.47	109	-4.34	177	-5.31	17 (W-R)	-5.44
167	-5.52	49	-4.49	96	-4.47	164	-4.33	56	-5.02	50 (BSG)	-5.35
33	-5.52	141	-4.46	77 (3 122 K)	-4.44	5	-4.26	115	-4.93	69 (BSG)	-5.04
18	-5.47	47	-4.42	110 (2 886 K)	-4.43	21	-4.23	118	-4.86	94 (RCrB)	-4.60
48	-5.45	60	-4.39	1 (3 524 K)	-4.43	106	-4.21	131	-4.85	26 (RCrB)	-3.55
145	-5.41	80	-4.37	152 (2 925 K)	-4.38	97	-3.83	73	-4.75	C-PAGB	
190	-5.35	179	-4.23	59 (5 437 K)	-4.38	114	-3.63	161	-4.74	150	-5.05
105	-5.30	46	-4.17	72 (3 085 K)	-4.36	163	-3.32	192	-4.28	196	-5.00
86	-5.25	57	-4.05	91	-4.71	137	-3.30	111	-4.26	52	-4.89
119	-5.25	53	-4.04	89 (3 542 K)	-4.33	158	-2.98	85	-4.18	84	-4.88
12	-5.22	191	-3.91	166 (3 660 K)	-4.20	44	-2.91	29	-4.03	64	-4.50
136	-5.11	43	-3.83	99 (3 538 K)	-4.16	149	-2.10	157	-3.95	O-PN	
120	-5.10	O-AGB		124 (2 561 K)	-4.02	25	-1.77	107	-3.94	186	-4.10
189	-5.09	121	-7.04	54	-3.98	RSG		75	-3.72	100	-2.29
15	-5.06	165 (2 561 K)	-6.68	182	-3.85	27 (4 140 K)	-8.19	95	-3.55	174	-2.22
125	-5.06	82 (3 183 K)	-6.43	8 (2 561 K)	-3.74	117 (3 977 K)	-7.91	28	-3.43	153	-1.33
139	-5.04	180	-6.50	79	-3.68	135 (3 638 K)	-7.68	113	-3.31	C-PN	
45	-4.94	142 (3 686 K)	-6.01	185	-3.08	16 (3 159 K)	-7.57	STAR		92	-4.85
9	-4.93	61 (2 987 K)	-5.97	YSO		116 (3 781 K)	-7.52	19 (5 250 K)	-7.56	144	-4.66
7	-4.89	38	-6.17	101	-6.13	171 (4 487 K)	-7.47	195 (4 892 K)	-6.97	175	-4.17
126	-4.88	173 (3 139 K)	-5.91	20	-5.85	147 (3 652 K)	-7.43	81 (3 514 K)	-5.01	HII	
55	-4.86	6	-5.54	108	-5.63	122 (3 871 K)	-7.42	133 (3 187 K)	-4.98	104	-6.23
83	-4.85	178 (3 512 K)	-5.68	34	-5.51	134 (4 188 K)	-7.32	32 (3 471 K)	-4.71	71	-1.58
140	-4.82	68 (3 500 K)	-5.34	102	-5.42	169 (4 008 K)	-7.17	76 (3 439 K)	-4.67	UNK	
23	-4.80	130 (2 561 K)	-5.25	183	-5.33	170 (3 851 K)	-7.10	88 (3 575 K)	-4.31	78	-5.04
65	-4.78	143 (3 284 K)	-5.22	62	-5.03	129 (3 985 K)	-7.09	188 (3 588 K)	-4.27	155	-4.18
66	-4.78	58 (3 552 K)	-5.13	40	-5.01	123 (3 844 K)	-7.03	GAL		146	-3.73
194	-4.78	93	-5.10	10	-4.86	128 (4 041 K)	-6.99	154	-3.14	39	-2.09
181	-4.73	176 (2 587 K)	-4.99	74	-4.86	172 (3 524 K)	-6.84	193	-2.64	112	-1.14
98	-4.71	22 (3 965 K)	-4.97	70	-4.82	127 (4 078 K)	-6.84	151	-2.58	24	—
36	-4.67	159 (3 536 K)	-4.79	14	-4.77	4 (3 693 K)	-6.68	2	-2.14	160	—

even when the SED indicates a large total dust optical depth (cf., Leisenring, Kemper & Sloan 2008; Lagadec et al. 2007). The cause of this wide variation is not known; in the Galactic objects one does not see such a wide range of 30 μm feature strengths in the dustier objects (Hony et al. 2002).

3.2.4 Oxygen-rich AGB stars

Again, a single segregation can be made in this group which results in two populous subgroups. Several `O-AGB`s (SSID13, 58, 68, 124, 142, 173, 178) appear as stellar photospheres with an inflection at 8 μm due to SiO and have little if any IR excess. The remaining objects in this group exhibit dust emission, most notably 10 μm silicate features. In some cases this is weak (SSID1, 59, 89, 143, 176) but in other cases (see Fig. 7) both 10 and 20 μm features are pronounced or self-absorbed. Curiously, SSID6 shows a strong and broad 10 μm feature but no discernible sign of a 20 μm feature.

SSID91, 180 and 96 show silicate features which peak short of 10 μm; the shape of feature suggests that the silicates are largely amorphous in form. In these three objects there is relatively little IR excess. SSID96, along with SSID82, is considered in more detail in Sargent et al. (2010), and modelling shows the presence of a CO_2 gas feature at 15 μm. SSID79, 93, 182 and 38 show more developed 10 μm features, with an increasing prominence of the 11 μm crystalline silicate feature and the 20 μm feature, indicating an enhanced dust production and evolutionary stage. SSID93 and 182 also show weak 16 and 19 μm features, probably due to forsterite. SSID54 appears to be a highly evolved star, showing evidence of a molecular sphere with broad line emission, in particular, H_2O at 6.7 μm, and a significant amount of dust, indicated by the flattening of the silicate peaks due to the onset of silicate self-absorption. Finally, SSID121 (IRAS05298−6957) is a very highly-evolved star with an initial mass of 4 $M_\odot$, a large dust excess, silicate in absorption, a high mass-loss rate, and 1612 MHz OH maser emission (Wood et al. 1992; Trams et al. 1999; van Loon et al. 2001, 2010). Its spectrum appears very similar to those of very embedded oxygen-rich dust sources in the LMC shown in Fig. 10 of Sloan et al. (2008). Narrow absorption features superimposed on the broad amorphous silicate absorption would indicate the presence of enstatite in the dust. This sequence of increasing evolution and dust production for O-AGBs has been discussed previously in the context of Galactic stars by Sloan & Price (1995) and

Landscape table to go here.

Table 3.

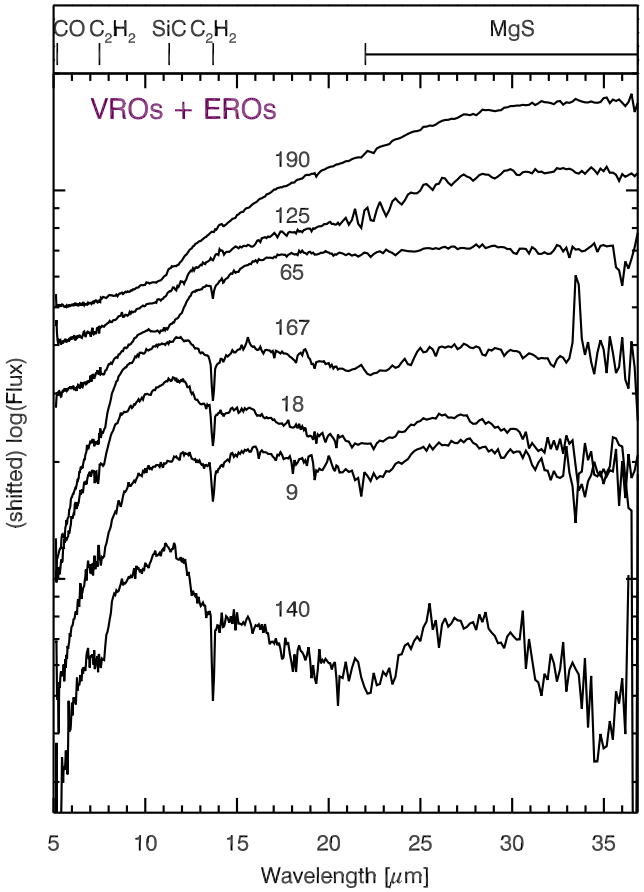

Figure 6. Spectra of the VRO and ERO carbon-rich AGB stars.

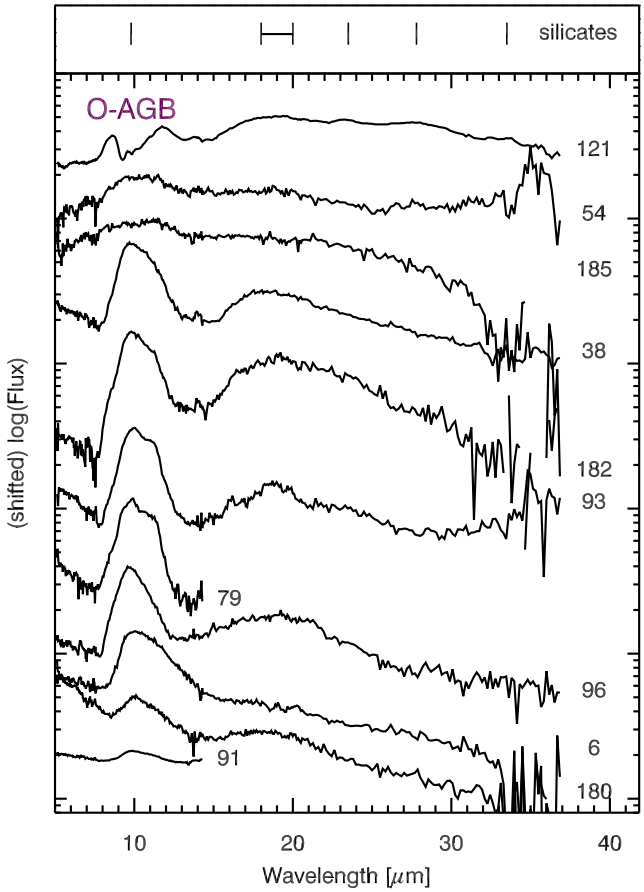

Figure 7. Spectra of the heavily dust-enshrouded oxygen-rich AGB stars.

Speck et al. (2000), among others. O-AGBs with the lowest mass-loss rates produce Al-bearing dust, whilst those with higher mass-loss rates produce Mg- and Fe-bearing amorphous silicates (Sloan et al. 2003), which produce the features that we see here. Also, O-AGBs with a lesser dust excess exhibit stronger amorphous silicate features compared to crystalline (Sylvester et al. 1999), and as mass-loss rates increase, crystalline features become more dominant due to the optically thicker dust shell (Kemper et al. 2001), also seen in our sample. There is no clear example in these spectra of the narrow 13 μm feature often seen in Galactic O-AGBs (Sloan, Levan & Little-Marenin 1996).

3.2.5 Red supergiants

The RSG spectra show a range of oxygen-rich dust features (Fig. 8). Five of the sources (SSID35, 37, 117, 127, and 134) appear to be nearly dust-free, although the spectral coverage stops at 14 μm. Others have particularly weak or absent 20 μm features, a phenomenon that has not been noted in Galactic samples. The sources include examples of classic silicate features at 10 μm (SSID16, 27, 147), amorphous alumina (SSID4, 128), as well as both (SSID116, 123); in several cases, the signal-to-noise ratio was insufficient to pin down the type of dust present, other than its oxygen-rich nature. At least six objects have PAH emission features, although these could potentially be interstellar in the case of SSID16 and 171, where *SAGE-LMC* maps show some faint and diffuse 8 μm emission. Only one source (SSID16) shows emission from a fine-structure line ([NeII] at 12.81 μm), which is consistent with the small number of RSGs with ionized lines seen previously in the LMC (Buchanan et al. 2006, 2009; van Loon et al. 2010). The RSGs in those samples tend to have much stronger 10 μm features, probably due to one of their selection criteria of an MSX 8 μm detection (Kastner et al. 2008).

3.2.6 Oxygen-rich post-AGB stars

Half of the O-PAGB sample of 18 objects is composed of RV Tau type stars (SSID29, 73, 85, 95, 107, 131, 157, 161, 192), identified by obtaining periods from the literature, which appear almost identical to the other O-PAGB spectra (SSID28, 56, 75, 111, 113, 115, 118, 162, 177). However, the lightcurves (Soszyński et al. 2008) of these objects distinguish the pulsating RV Tau stars from other oxygen-rich post-AGB stars. SSID73, 131 and 161 are investigated in detail in Gielen et al. (2009). Of the spectra of the nine non-RV Tau objects, three show very square, blocky features indicative of a high degree of crystalline silicates (SSID56, 75, 177), whilst all nine show some degree of crystallinity. It should be noted that the far-infrared rise in the spectrum of SSID95 is likely to be due to an encroaching red source in the LL slit, and that the spectrum of SSID28 is likely contaminated by emission from nearby MSX LMC 1271. SSID161

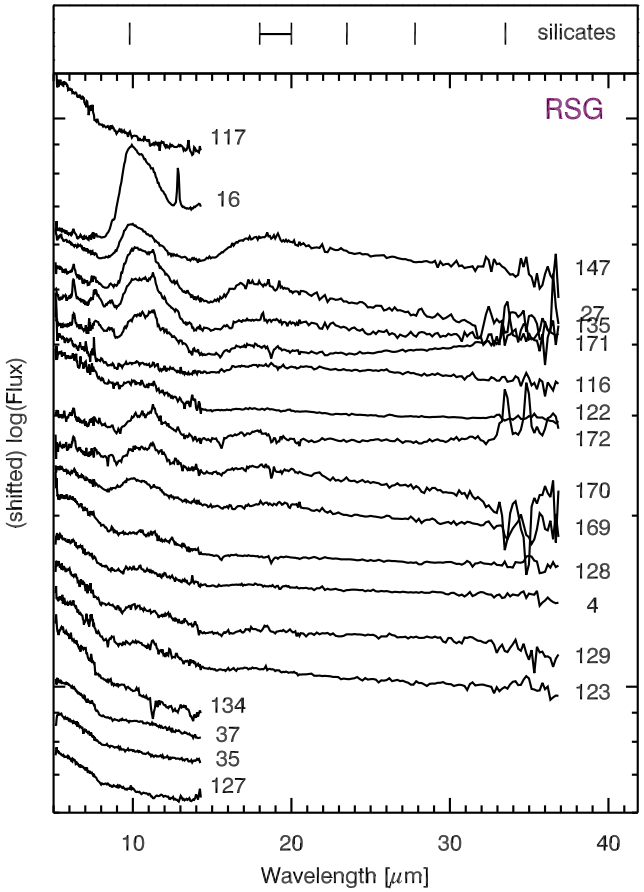

Figure 8. Spectra of the RSGs contained in the *SAGE-Spec* sample.

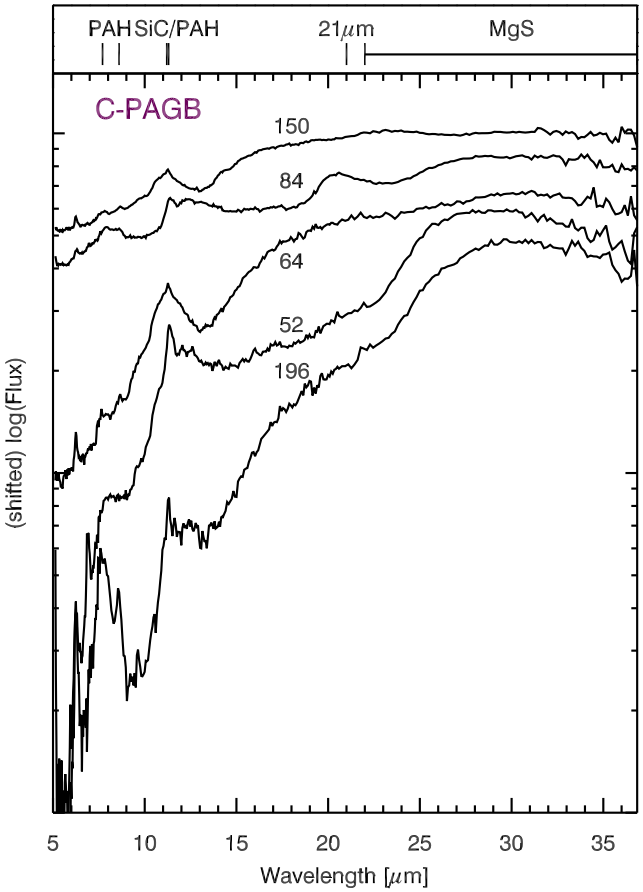

Figure 9. Spectra of two C-PAGB objects with very triangular SiC features, as well as SSID84, which has a pronounced 21 μm feature.

is an unusual object in that it does not show 10 μm silicate emission. It does show PAH emission, which arises along the line-of-sight, and this may mask a weak 10 μm feature. It has been classified as an RV Tau by Soszyński et al. (2009a) and by us. In this case LL was unfortunately not observed.

3.2.7 Carbon-rich post-AGB stars

This small group of five objects proves to be very interesting (Fig. 9). All five spectra show a prominent MgS feature at 30 μm, whilst SSID84 additionally shows a 21 μm feature, only found in post-AGB carbon-rich objects (Hrivnak et al. 2009). SSID64 and 150 appear very similar to each other, with a very sharp SiC feature at 11.3 μm that appears triangular and could be somewhat self-absorbed. These triangular features are also seen in PNe (e.g., Bernard-Salas et al. 2009), where they are attributed to a superposed PAH band. The 11.2 μm PAH band is dominated by neutral PAHs, whilst the other mid-IR PAH bands arise from ionized PAHs.

3.2.8 Oxygen-rich planetary nebulae

The four oxygen-rich PNe (SSID100, 153, 174 and 186) show either very weak or absent PAH emission (Fig. 10). Weak PAH emission in these cases was determined to come from diffuse emission regions along the line-of-sight, through analysis of the *SAGE-LMC* 8 μm images. Two of the sample (SSID174 and 186) show strong [NeV] lines at 14.3 and 24.5 μm and [OIV] lines at 25.9 μm. The spectrum of SSID174 contains a high-excitation [NeVI] line. SSID153 shows only a weak [ArII] line since Long-Low data are not available.

3.2.9 Carbon-rich planetary nebulae

The three carbon-rich PNe in the *SAGE-Spec* sample (SSID92, 144 and 175) show reasonably strong PAH emission, along with [NeIII], [SIII] and [SIV] lines. SSID175 also shows a strong [OIV] line (Fig. 10).

3.2.10 HII regions

Only two objects are classified as HII regions, SSID71 and 104, although due to spatial resolution issues (§2.7) some HII regions may be confused with evolved YSOs (`YSO-3`s). They both show a [SIII] line and a continuum which rises with wavelength. The weak PAH features appear to be due to nebulous material along the line of sight to the objects, apparent in *SAGE-LMC* 8 um images of the regions concerned.

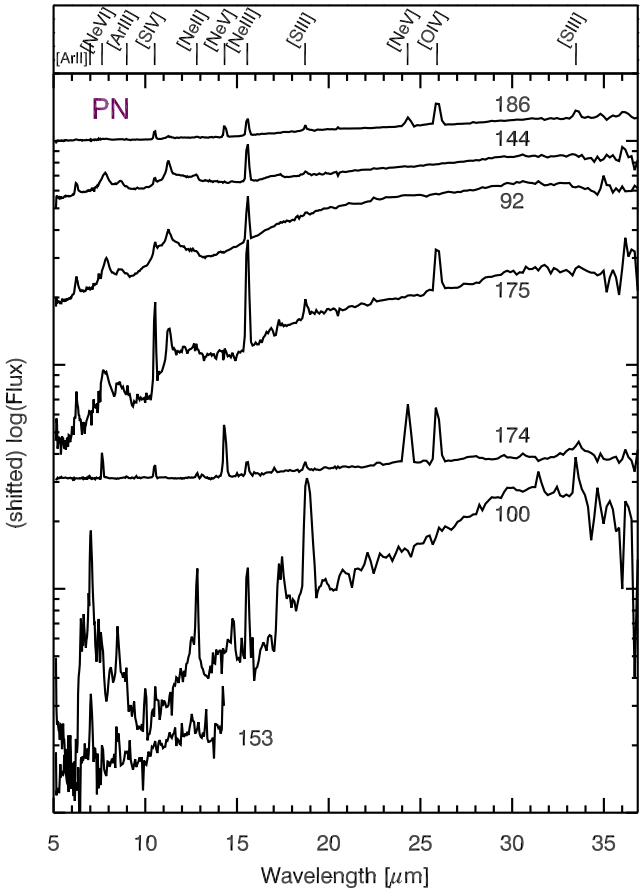

Figure 10. Spectra of the PNe contained in the *SAGE-Spec* sample.

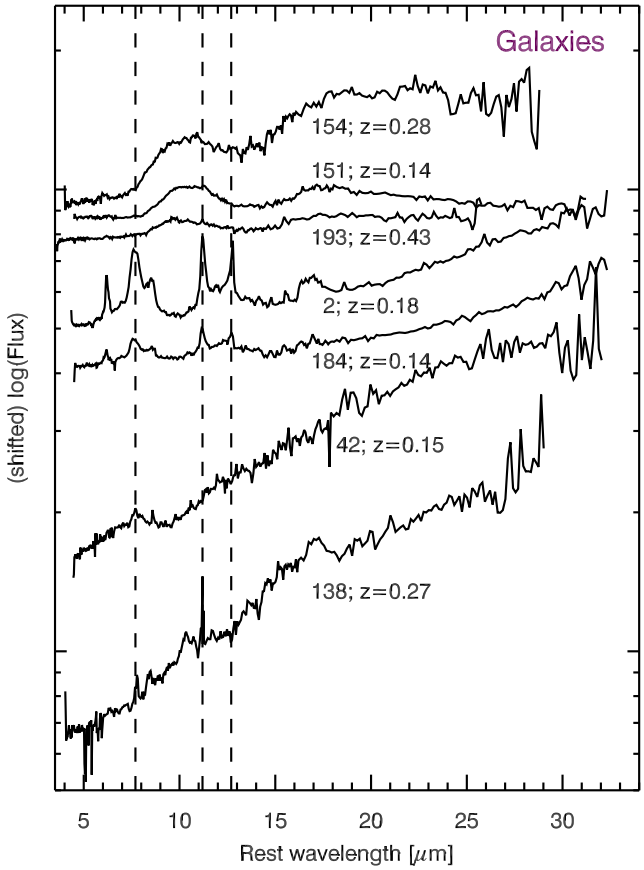

Figure 11. Spectra of the galaxies contained in the *SAGE-Spec* sample. Spectroscopically-determined redshifts are indicated on the figure. Dashed vertical lines indicate the rest-frame positions of narrow PAH features, used to align some of the spectra. Redshift errors for the upper three spectra are on the order of ±0.05; the lower four spectra have narrow features, reducing the error in redshift determination to ±0.01.

3.2.11 Galaxies

All seven galaxy spectra are shown in rest-frame in Fig. 11. Three galaxies show strong silicate features – SSID151, 154 and 193, which are a hallmark of type 1 active galactic nuclei (AGN; cf., Hao et al. 2005; Siebenmorgen et al. 2005; Shi et al. 2006). Two galaxies show strong PAH features (SSID2, 184) and SSID2 clearly shows the [NeV] line at 14.32 μm, which can be indicative of an accreting black hole, since star-forming galaxies rarely show lines with such high ionization potentials. Four of the galaxies (the lower four in Fig. 11) exhibit rising SEDs towards longer wavelengths, again suggesting that these are AGN, similar to those described by Buchanan et al. (2006). It should be mentioned that van Loon et al. (2010) speculate that SSID97 is also a galaxy with z=0.27 or 0.54, based on the presence of a potential oxygen line in a MIPS-SED spectrum. However, the IRS spectrum shows a number of PAH features at the correct rest wavelengths, which leads us to classify SSID97 as `YSO`.

3.2.12 Others

One potential and one subsequently-confirmed (Soszyński et al. 2009a) RCrB stars are found in the sample, SSID26 and 94. Both show red, featureless spectra (Fig. 12), and SSID26 should be further investigated through optical spectra or monitoring of its light curves to confirm RCrB status. The two B supergiants in the sample, SSID50 and 69, show SEDs that plunge to a minimum at ∼8–9 μm. They also show spectra that rise steeply long-ward of 15 μm. SSID17 is a known Wolf-Rayet star, and exhibits an SED which rises steeply at ∼15 μm, levels off, and then decreases. There is an emission line due to [SIII] at 18.7 μm, however this may be sky emission; features in the LL2-wavelength portion of the spectrum are affected by data issues. All these spectra are shown in Fig. 12.

3.2.13 Unidentified objects

The observation of SSID24 was pointed to within 0.″33 of planetary nebula RP 1805, which has a diameter in the Hα image of 5″ (Reid & Parker 2006), however no object is seen in *SAGE-LMC* 8 μm images and no convincing features are seen in the IRS spectrum. We report this as a non-detection. Similarly SSID160 is not visible in *SAGE-LMC* 8 μm images and no features are seen above the noise in the IRS spectrum.

SSID78 is an unusual object in that it presents a rising spectrum toward longer wavelengths which is fea-

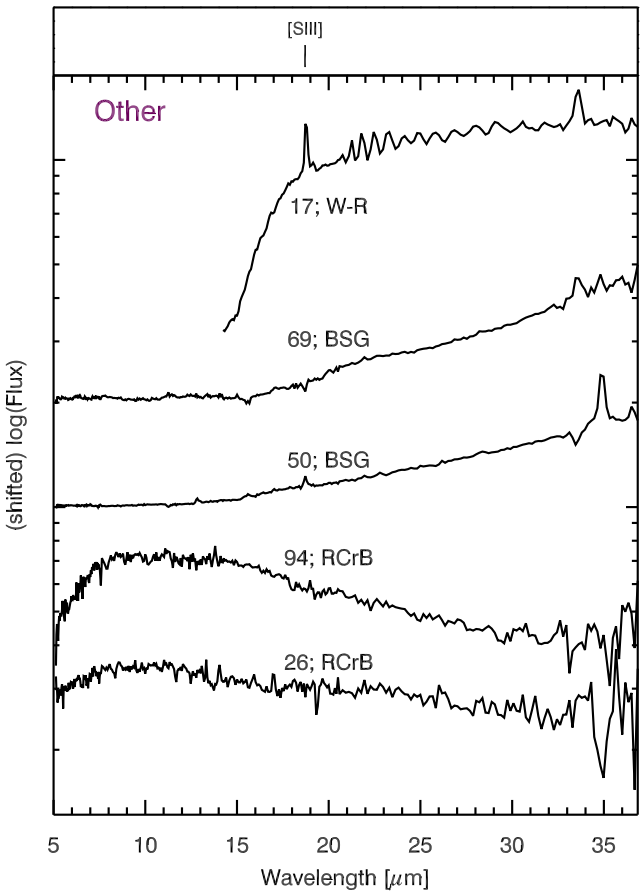

Figure 12. Spectra of the objects in the "Other" group, which contains a Wolf-Rayet star, two B supergiants and two candidate RCrB stars.

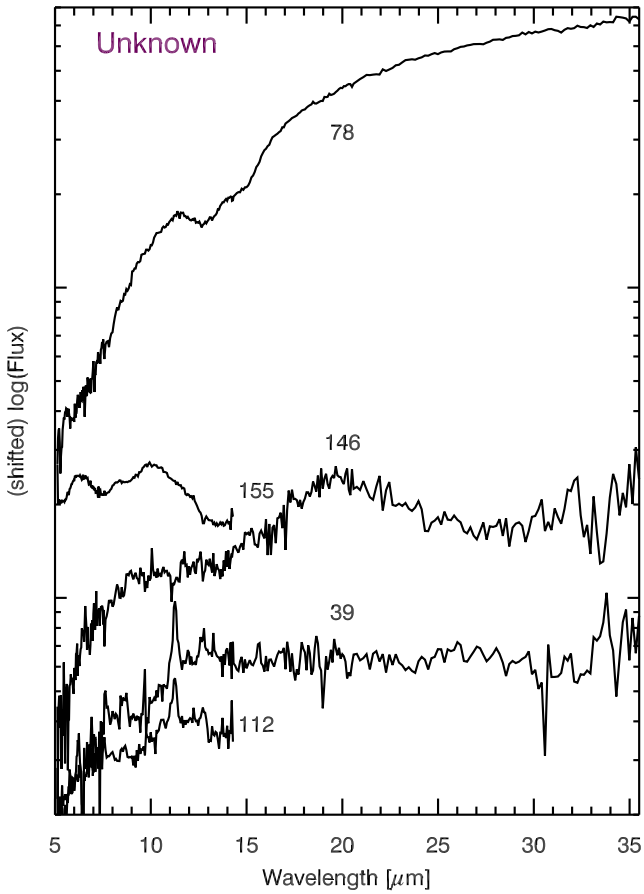

Figure 13. Spectra of unidentified objects.

tureless apart from a dip in the continuum from 11.5–16.0 μm (Fig. 13). de Grijp, Lub & Miley (1987) consider it to be a candidate AGN, and when plotted on Fig.21 it would certainly lie within the "AGN wedge". SSID146 is also an unusual object, in that it shows very broad 20 μm emission and very broad but weak 10 μm emission. Sasaki, Haberl & Pietsch (2000) identifies it as an X-ray source, SHP LMC 256, of unknown physical nature. Its SED is double-peaked, which could be indicative of a post-AGB object, however, it is rather blue. There may be interesting mineralogy, containing iron or magnesium oxides.

SSID39 and SSID112 both present very weak spectra, with no recognisable features apart from a 11.2–12.7 μm PAH complex, which may be due to foreground emission. Both observations were pointed towards PNe, RP 1878 and RP 589 respectively, but no clear emission lines were detected.

SSID155 is optically identified as a carbon star (Kontizas et al. 2001), but shows unusual features, potentially including an absorption at 7.5 μm and either emission at 10 μm or absorption at 9 μm. This could indicate a mixed-chemistry object.

3.2.14 Comparision of results with source selection

At this point it is useful to make a comparison between our original selection of candidates (Kemper et al. 2010, and re-capped here) and our final classification to test the validity of our source selection criteria. The best-selected category were the post-AGB objects (86%), with one C-AGB and one O-AGB creeping into the sample. These were selected from a list of candidates (Wood & Cohen 2001) and the MACHO catalog (Alcock et al. 1998). Also well-selected were non-clustered C-AGBs (78%) and O-AGBs (72%), which were taken from the sample of Srinivasan et al. (2009). Five `STAR`s crept into these two categories, which may in fact be relatively dust-free AGB stars. Categories which yielded poor selections were clustered AGB stars, which only successfully produced 17 AGB stars from 34 (old, intermediate and young AGB stars were chosen from three metallicity bins) but also 12 RSGs; planetary nebulae (5 out of 12, picked from Reid & Parker 2006; Leisy et al. 1997), three of which we classed as `UNK`; and YSO candidates, which only resulted in 26 YSOs from a sample of 88 (selected from Whitney et al. 2008, based on detectability at $\lambda > 14\,\mu$m). The biggest contaminants in the YSO category were 20 C-AGB, 16 O-AGB stars and seven RSGs. This shows the difficulty in selecting good YSO candidates. Somewhat surprisingly, many of the failed YSO candidates were not galaxies, as often expected, but evolved and post-AGB stars. The 13 Colour–Magnitude Diagram (CMD) "fillers" produced 4

C-AGBs, 3 O-AGBs, 3 galaxies, 2 YSOs and one unknown object, possibly an HII region.

4 STELLAR POPULATIONS IN THE LARGE MAGELLANIC CLOUD

A spectral survey such as *SAGE-Spec* can in some way act as a check on the many different classifications based on photometry that have come out of the *SAGE* collaboration (e.g., Blum et al. 2006; Whitney et al. 2008; Srinivasan et al. 2009; Bonanos et al. 2009) and other groups who have studied the LMC (Egan, Van Dyk & Price 2001; Kastner et al. 2008; Buchanan et al. 2009; Matsuura et al. 2009). Whereas photometric surveys can be performed more quickly (in terms of telescope-hours) and spectral surveys in general take more time, classification by photometry can be fraught with inaccuracy, often due to overlapping or co-located classes in colour–magnitude diagrams (e.g., YSOs and galaxies). In Figs. 14–20 we present our versions of the colour–magnitude and colour–colour diagrams presented in the various studies of the LMC performed recently, and discuss the accuracy of their photometric classifications.

The two panels in Fig. 14 show [8.0] versus [J]−[8.0] and [3.6]−[8.0], respectively. The objects from the *SAGE-Spec* sample are over-plotted on a Hess diagram[3] of the entire *SAGE-LMC* sample with the relevant 2MASS/IRSF and IRAC magnitudes. In Figs. 14–18 we also include classifications from the samples of Buchanan et al. (2006), Kastner et al. (2008) and Buchanan et al. (2009), who targeted bright sources with 8 μm MSX detections. These objects were observed in Spitzer Cycles 1–3, and were not part of the *SAGE-Spec* observational sample. Note the large population of objects in the *SAGE-LMC* sample with [8.0]$\gtrsim$11 that are not probed by the *SAGE-Spec* sample; these are mainly background galaxies and YSOs not selected by *SAGE-Spec* due to signal-to-noise constraints. Two objects which stand out in this plot are the two B supergiants, at [8.0]$\approx$12.5 mag. Also we see that of our sample of stellar photospheres the two K giants are distinct from the other M-stars, which cluster at the base of the AGB. The right panel shows reasonably good separation between different groups of objects in the *SAGE-Spec* sample, particularly between C-AGBs ([3.6]−[8.0]$\gtrsim$3) and more evolved carbon-rich and extreme objects. This gap is filled by the brighter Kastner sample, and the conjunction of the two shows the full extent of C-rich (post-)AGB evolution. The distinction between O-AGBs and RSGs can also be seen in this figure, but is clearer in the left panel of Fig. 15, which is a representation of Fig. 3 from Blum et al. (2006). In this arrangement RSGs lie in a sequence slightly bluer (in J-[3.6]) than the O-AGB stars, and so the distinction is not entirely luminosity-based. This colour criterion, then, gives us a very useful tool in making the difficult distinction between RSGs and O-AGBs. In Fig. 15 we can make a cut along [J]=1 and [3.6]=12−2([J]−[3.6]) to select the RSGs from the *SAGE-Spec* sample and the Kastner et al. (2008) sample. This cut also corroborates with the optically-selected RSG sample of Bonanos et al. (2009). This selection is extremely clean – only four non-RSGs are contained within: two potential WR stars, one bright B[e] star (Buchanan et al. 2009) that was formerly classified as a C/O-AGB (Kastner et al. 2008) and one unknown object (Kastner et al. 2008). No contaminants from the *SAGE-Spec* sample are contained in this cut.. The right-hand panel of Fig. 15 shows the colour-cut used by Cioni et al. (2006) to select candidate AGB stars from those detected in the DENIS survey of the LMC (Cioni et al. 2000). The cut is successful over the range it was intended (9.5<[K]<12.6, 0.9<[J]−[K]<2.0), although it may include some red giant branch (RGB) stars since the tip of the RGB is at [K]=12.3 (Nikolaev & Weinberg 2000).

Also in Figs. 14 and 15 we see the large overlap of YSOs with galaxies and extreme and evolved carbon stars. This leads to a great degeneracy in photometric classifications in the region of colour space covered by YSOs, and this is evident particularly in Appendix A with the overlapping and conflicting classifications of Whitney et al. (2008) (YSOs) and Srinivasan et al. (2009) (AGBs), among others, and also in the discrepancy between our original source selection and final classification discussed earlier. It is clear that although our selection was good in that it selected YSOs, it also does not discriminate enough to be uncontaminated.

The next two figures focus in more detail on the O-rich and C-rich evolved objects. Figure 16 shows a clockwise progression in colour space from RSG→O-AGB→O-PAGB→O-PN. These O-rich objects become redder and fainter in [8.0] with age. SSID186, the orange point at [8]$\sim$9.3 mag, may be misclassified since it falls within the colour-space of carbon-rich PNe. Interestingly, the YSOs in the *SAGE-Spec* sample are redder than [3.6]−[8.0]>1.5, and thus only the O-PAGB and O-PN groups are contaminated. The dotted lines in the right-hand panel show the selection criterion for YSOs used by Whitney et al. (2008) in this CMD. The selection of YSOs is very good, although one must be wary of contamination of YSO samples with O-rich post-AGB objects. Figure 17 shows similar colour spaces but for carbon-rich evolved objects. This diagram enables us to separate the VROs and EROs from the remainder of the carbon-rich AGB stars. These seven extreme stars fall red-ward of 2<[4.5]−[8.0].

Figure 18 shows the AGB and RSG stars in [8.0] vs. [3.6]−[8.0] colour–magnitude space (left panel). Such a diagram has been used by various authors (Blum et al. 2006; Srinivasan et al. 2009; Matsuura et al. 2009) to investigate the separation of oxygen-rich and carbon-rich AGB stars. Plotted in the left panel are cuts made by Matsuura et al. (2009) to separate carbon-rich stars out from oxygen-rich (dotted lines). In general, these cuts work well for our sample, with only seven oxygen-rich stars contaminating the carbon-rich sample for [3.6]−[8.0]>0.75. Thus contamination is small, but by rare, extremely interesting objects that would be missed by conservative cuts. Comparison with Fig. 14 shows that this region of the CMD may also contain YSOs, and O-PAGB objects. The right-hand panel of Fig. 18 shows that the fainter evolved stars are missing from the *SAGE-Spec* and Kastner et al. samples. Coverage of this region of colour-space should improve with the addition of data from the IRS archive (Paper II).

To show the distribution of YSOs in colour–magnitude and colour–colour spaces we have constructed Fig. 19 and

[3] Hess diagrams are 2D histograms where the number density is represented by the brightness of each pixel. Darker pixels are more dense.

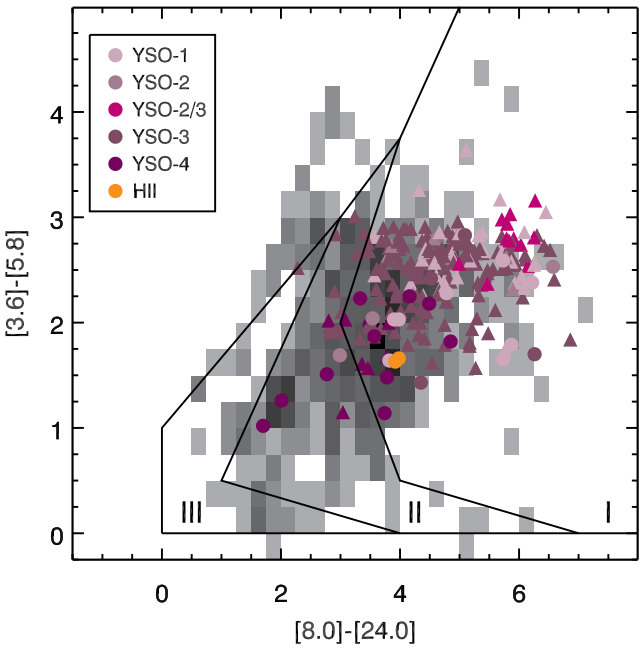

Figure 20. A colour–colour diagram showing the finer grades of classification of YSOs (circles), in comparison to the sample of Seale et al. (2009) (triangles) and the modelling of Robitaille et al. (2006) (solid lines). The areas marked by Roman numerals refer to the different YSO Stages which dominate those regions, as described in the latter work.

20. In Fig. 19 we show the *SAGE-Spec* and Seale et al. (2009) YSO samples plotted on top of the Whitney et al. (2008) sample. We have classified the Seale et al. (2009) YSOs into our groupings, although in some cases it was hard to distinguish between YSO-2 and YSO-3. Surprisingly, there is no clear distinction between groups of YSOs, and no evident gradient is seen either, although on average `YSO-4`s are bluer and fainter than the other classes. It is not clear why this is the case. A similar result is found in Fig. 20, where almost all of the sampled YSOs are classed as Stage I on the colour–colour diagram of Robitaille et al. (2006). The solid lines in Fig. 19 are cuts used by Kirk et al. (2009) to distinguish between YSOs and background galaxies. These cuts are not particularly successful for the LMC, with only one of the *SAGE-Spec* galaxies being isolated from the YSOs in the left-hand panel, and the YSO sample being bisected by the cut in the right-hand panel.

In Fig. 21, we plot the seven galaxies in the *SAGE-Spec* sample in colour–colour space. Stern et al. (2005) were able to show that an empirically-derived wedge-shaped region in this colour space was dominated by luminous AGN. Six of the seven *SAGE-Spec* galaxies reside in this region, while the seventh, SSID2, lies in the region dominated by star-forming galaxies (Gorjian et al. 2008). This is supported by the strong PAH features in the spectrum of SSID2. However, SSID2 seems also to show weak [NeV] emission, indicating that it may have both an AGN and a starburst.

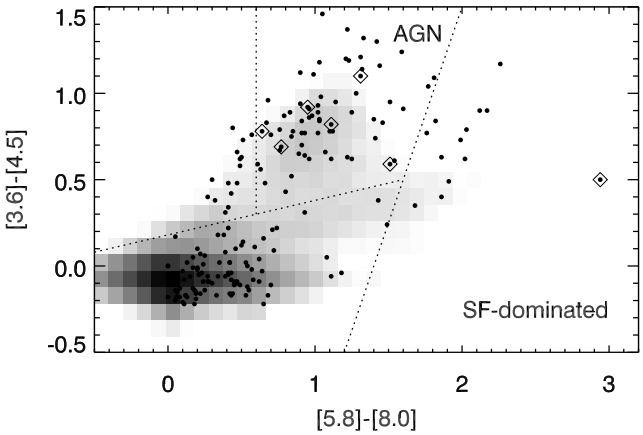

Figure 21. Further classification of galaxies (points surrounded by diamonds), using a colour–colour diagram from Stern et al. (2005) and Gorjian et al. (2008). Six of the seven background galaxies in the *SAGE-Spec* sample are found in the AGN wedge. The seventh, SSID2, is found in the region dominated by star formation. Overplotted on a Hess diagram of the *SAGE-LMC* catalog, with other *SAGE-Spec* objects plotted as black points.

5 APPLICATION TO OTHER SURVEYS

The classification system shown in Fig. 2 is not limited in its application to *Spitzer* data; it can also be applied to JWST, ISO and even IRAS LRS data, allowing for the lower resolution and signal-to-noise ratio of that instrument. One must be careful to allow for differing resolutions, since, for example, at a resolution of 5″ a compact HII region (≈1 pc) may look like a YSO. The scheme can be modified slightly to additionally make use of data from *Herschel* and the AKARI satellite, which will be especially useful in discriminating between classical HII regions and planetary nebulae using the long-wavelength shape of the SED. Similarly, AKARI Infrared Camera data at shorter wavelengths (2.5–5 μm) can be used to provide additional confirmation of YSO status when 3.05 μm H_2O and 4.27 μm CO_2 ice are detected (e.g., Shimonishi et al. 2008), and also encompasses gaseous CO absorption near 5 μm and C_2H_2/HCN bands near 3 μm, which are useful in identifying C-rich AGB stars. The CMDs presented here and Fig.20 will be of use when classifying point sources from the Wide-Field Infrared Survey Explorer (WISE) all-sky survey at 3.3, 4.7, 12 and 23 μm.

The decision tree can also be applied to other external galaxies, or Galactic point sources. The only overt distance factor in the scheme is the cut in bolometric luminosity between O-AGBs and RSGs. This differentiation is difficult to make, and in systems where distances are highly uncertain (i.e., the Galaxy) the luminosity-based selection criterion could be replaced by the [J]=1 and [3.6]=12−2([J]−[3.6]) CMD cut discussed in §4, for instance.

6 SUMMARY

We have classified 197 objects observed as part of the *SAGE-Spec Spitzer* Legacy Program according to their object type using a decision-tree method which discriminates according to spectral features and other ancillary data. Classification using spectra is more robust than that using photometric

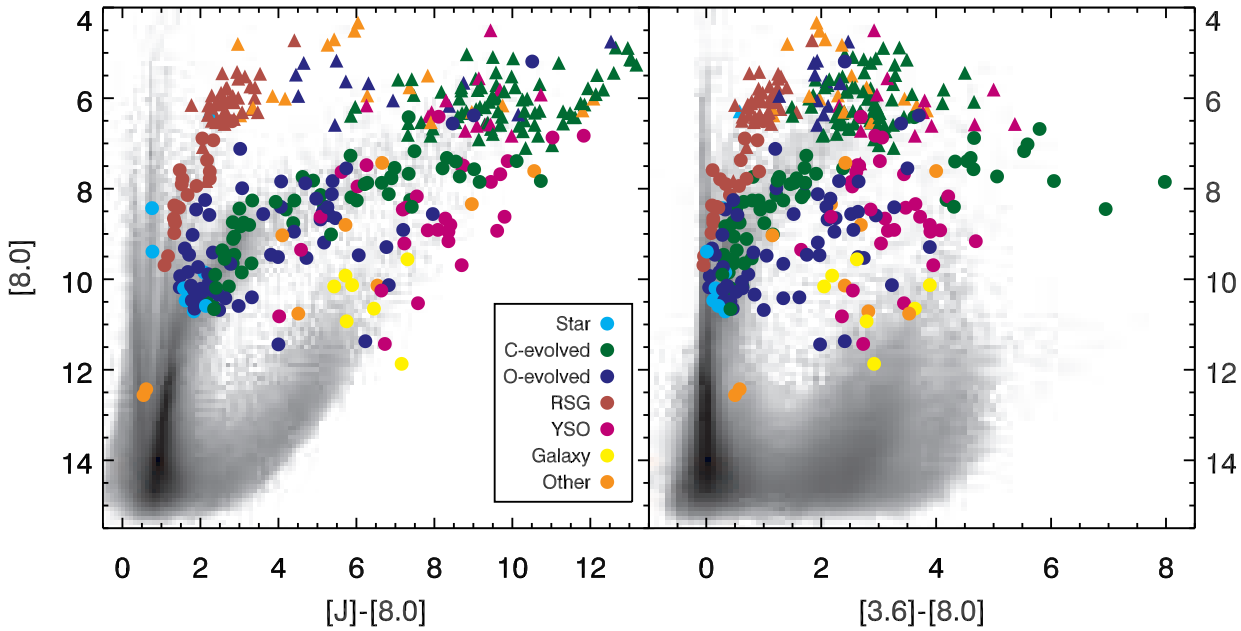

Figure 14. Two plots showing the distribution of all sources in colour–magnitude space. The *SAGE-Spec* sample is shown as filled circles, whilst the brighter Kastner et al. (2008) sample (incorporating the updates of Buchanan et al. 2009) are filled triangles. Here we merge the `O-AGB`, `O-PAGB`, `O-PN`, `C-AGB`, `C-PAGB`, and `C-PN` classifications into broad groups.

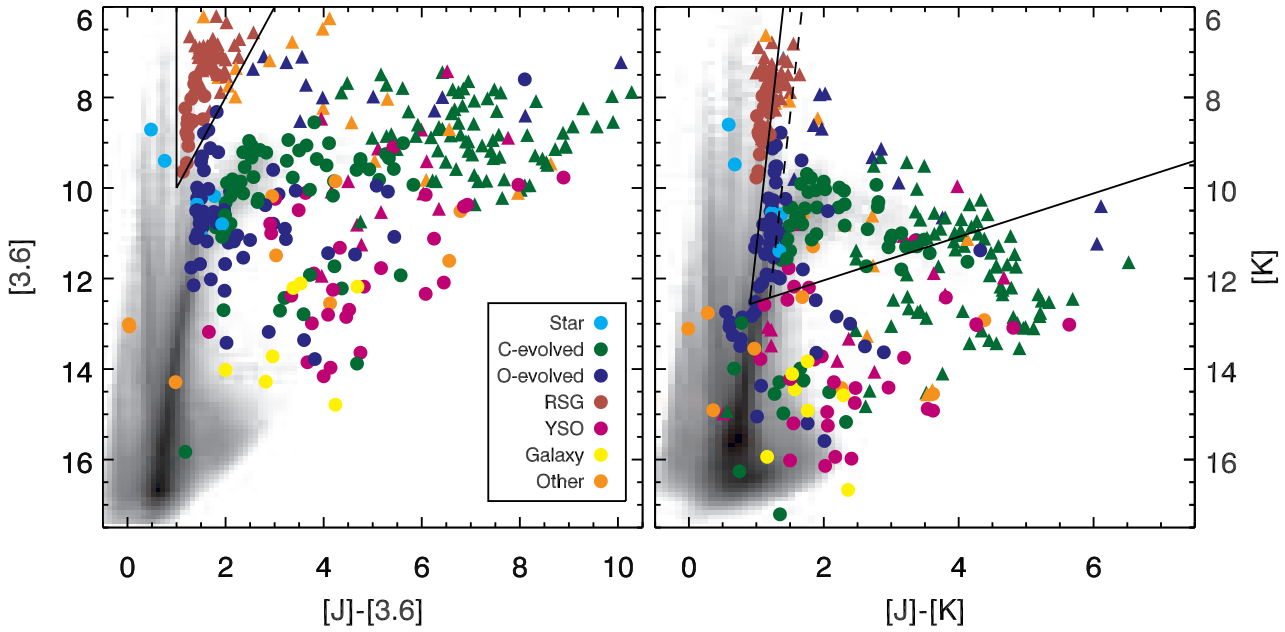

Figure 15. Two further CMDs, with cuts for selecting RSGs and O-AGBs. Symbols are as for Fig. 14. `RSG`s can clearly be distinguished from other oxygen-rich evolved stars in the [3.6] vs. [J]−[3.6] diagram (left panel). In the right panel we use the cuts used by Cioni et al. (2006) to select AGB stars (solid lines) and to distinguish O-AGB from C-AGB (dashed line).

colours and can be used to resolve degeneracies in colour–magnitude space, e.g., between YSOs and galaxies. Our classification is in agreement with, and acts as an extrapolation of, brighter (at 8 μm) sources in the LMC (Kastner et al. 2008; Buchanan et al. 2009), and the combination of both has highlighted the extent of carbon-rich (post-)AGB evolution, for example, in colour–magnitude space. Several colour cuts have been established or confirmed to distinguish between source classes. The *SAGE-Spec* sample will be expanded to include all observations of point sources in the LMC in the *Spitzer* archive, which number approximately 750 (including those of Kastner et al. 2008; Buchanan et al. 2009). Such a large sample will allow us to:

select samples of similar objects for future studies,

obtain a global picture of the mass budget of the LMC through different stellar populations, and their respective contributions to the ISM,

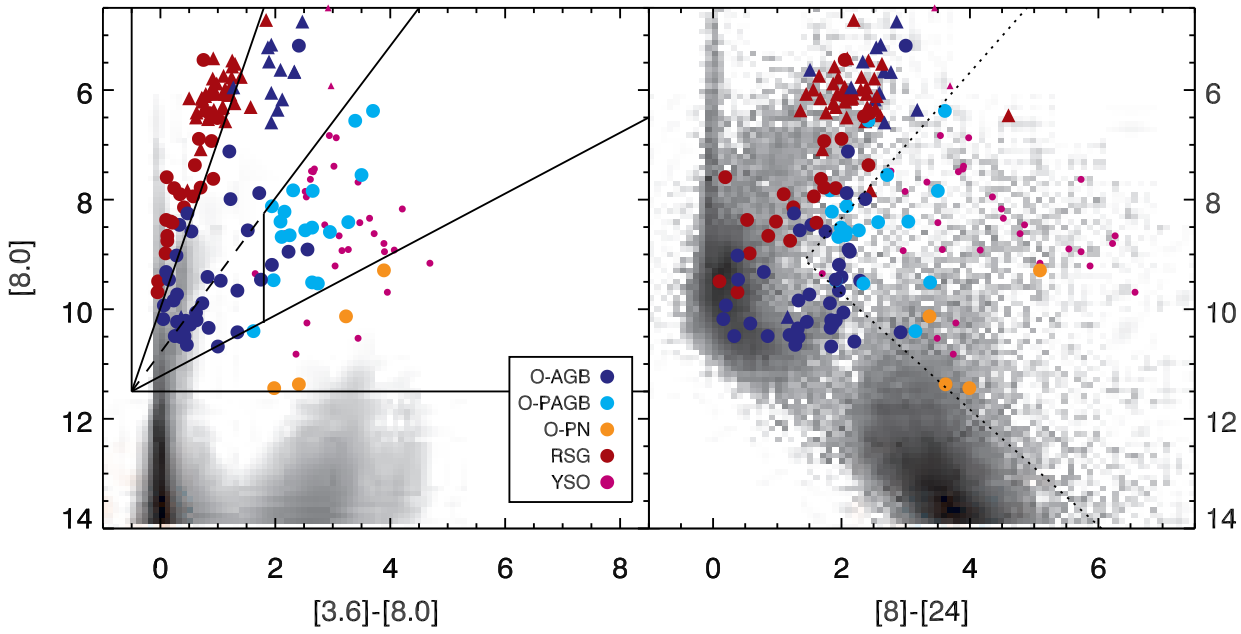

Figure 16. A colour–magnitude diagram showing the classes of O-rich evolved objects. YSOs are shown as small magenta points, since they overlap in colour–magnitude space with the more evolved O-rich objects. Other symbols are as for Fig. 14. The dotted line in the right panel is a cut used by Whitney et al. (2008) to select YSOs. The background shows a Hess diagram of the *SAGE-LMC* sample.

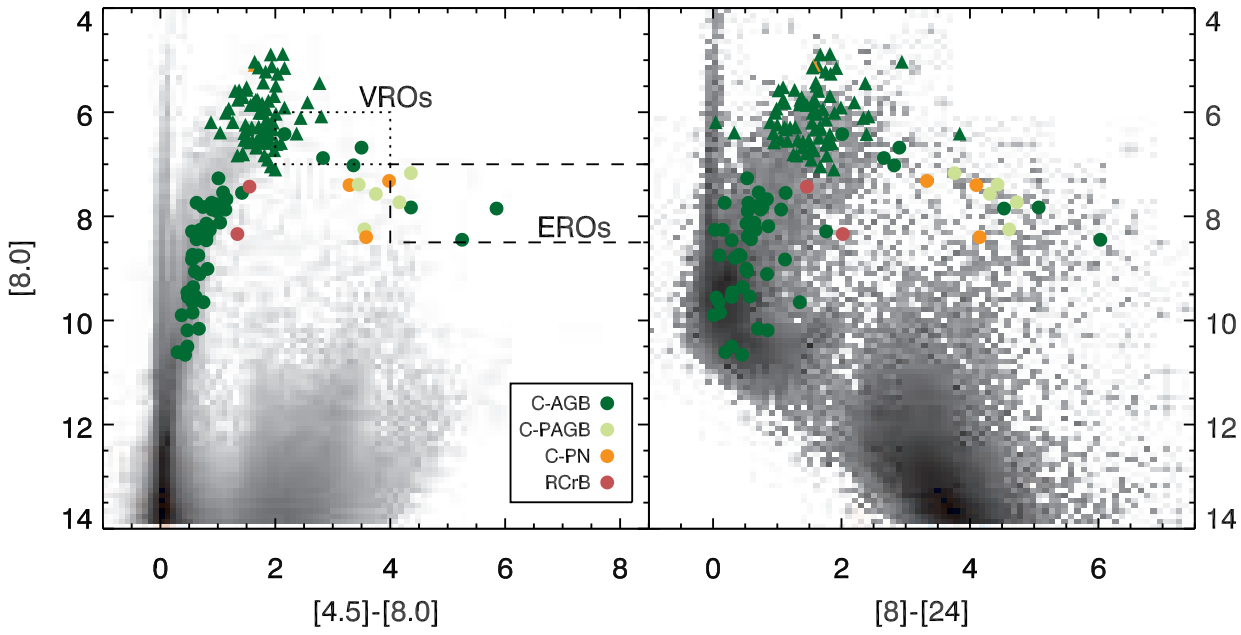

Figure 17. A colour–magnitude diagram showing the classes of C-rich evolved objects and RCrB stars. Symbols are as for Fig. 14. Boxes show the selection of VROs and EROs in the left-hand panel. The background shows a Hess diagram of the *SAGE-LMC* sample.

improve existing colour classifications, and adapt results for use in other galaxies, e.g., the Small Magellanic Cloud, and

use our point-source classifications (a biased sample) as seeds to statistically classify the *SAGE-LMC* sample (an unbiased sample) of ∼6.5 million point sources (Marengo et al., in prep.).

ACKNOWLEDGMENTS

R. Sz. acknowledges support from grant N203 511838 (MNiSW). This paper utilizes public domain data obtained by the MACHO Project, jointly funded by the US Department of Energy through the University of California, Lawrence Livermore National Laboratory under contract No. W-7405-Eng-48, by the National Science Foundation through the Center for Particle Astrophysics of the University of California under cooperative agreement AST-

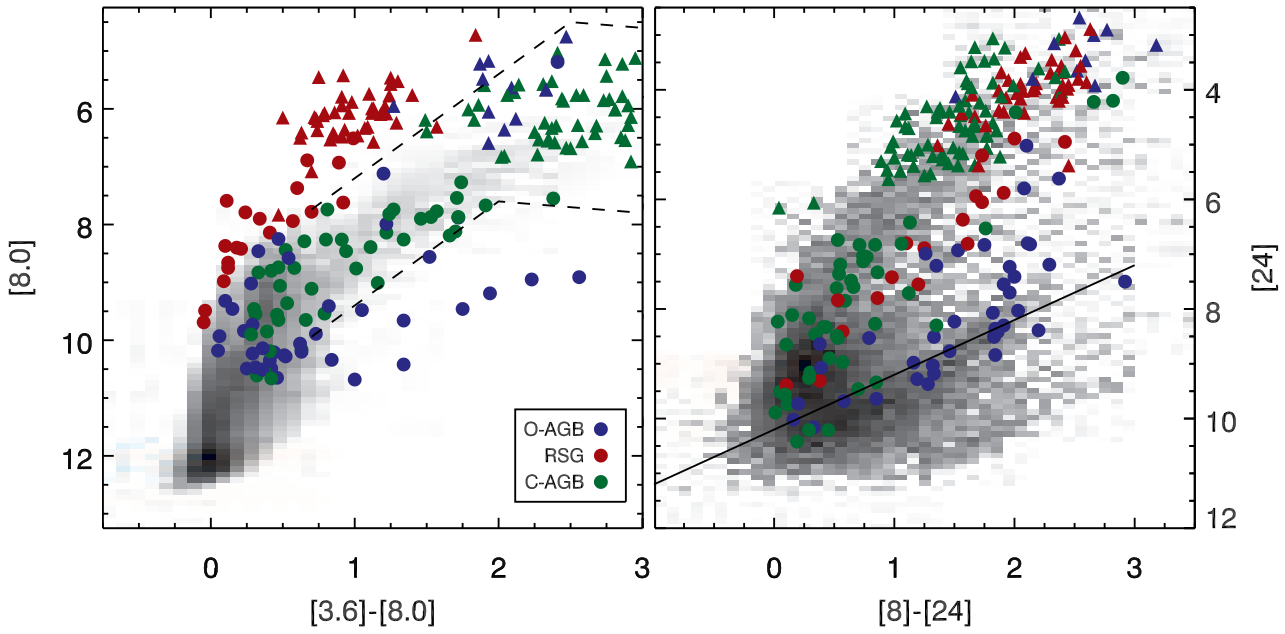

Figure 18. A colour–magnitude diagram showing the distribution of the `O-AGB`, `RSG` and `C-AGB` classes plotted over the evolved star sample of Srinivasan et al. (2009). Symbols are as for Fig. 14. The dashed cuts separate C-AGB and O-AGB stars according to Matsuura et al. (2009). In the right panel the cut differentiates the faint O-AGB stars (below the line; Blum et al. 2006) and the bright O-AGB stars.

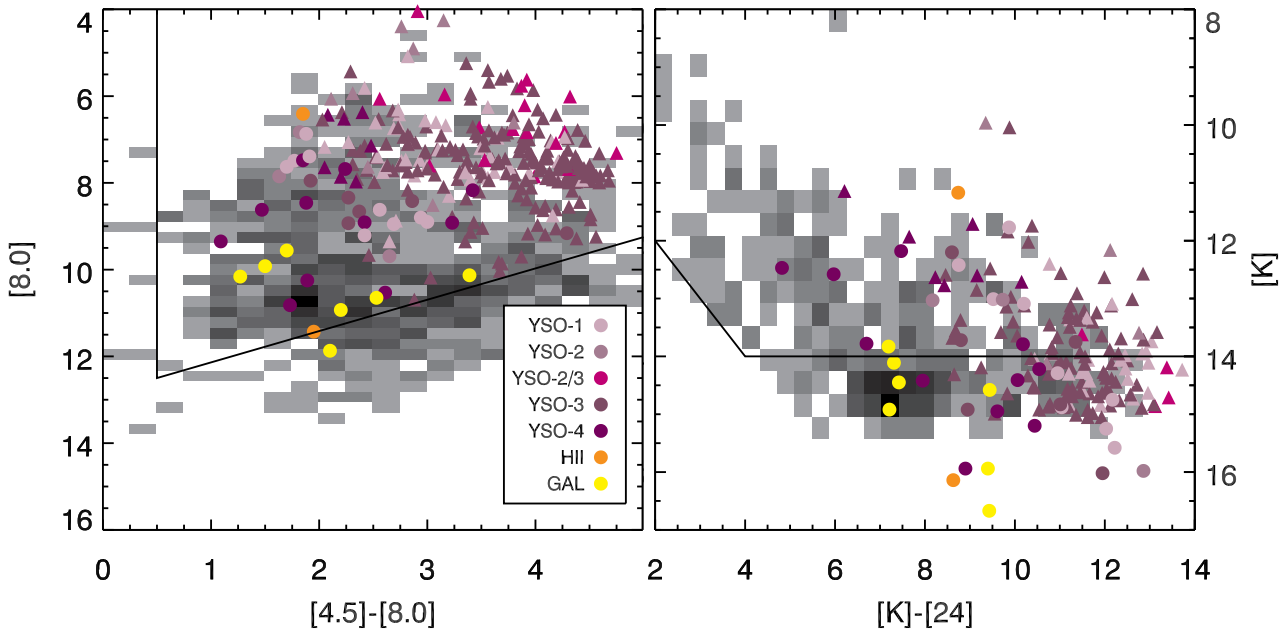

Figure 19. A colour–magnitude diagram showing the distribution of the `YSO`, `HII` and `GAL` classes. In this case, the filled triangles show the YSO sample of Seale et al. (2009), and the YSO sample of Whitney et al. (2008) is plotted as a Hess diagram.

8809616, and by the Mount Stromlo and Siding Spring Observatory, part of the Australian National University. This publication makes use of data products from the Two Micron All Sky Survey, which is a joint project of the University of Massachusetts and the Infrared Processing and Analysis Center/California Institute of Technology, funded by the National Aeronautics and Space Administration and the National Science Foundation. This publication makes use of data products from the Optical Gravitational Lensing Experiment OGLE-III online catalog of variable stars. This research has made use of the VizieR catalog access tool, CDS, Strasbourg, France. This research has made use of the SIMBAD database, operated at CDS, Strasbourg, France. This research has made use of NASA's Astrophysics Data System Bibliographic Services.

REFERENCES

Aaronson M., Mould J., 1985, ApJ, 288, 551
Acke B., Bouwman J., Juhász A., Henning T., van den Ancker M. E., Meeus G., Tielens A. G. G. M., Waters L. B. F. M., 2010, ApJ, 718, 558
Alcock C., et al., 1998, AJ, 115, 1921
Alves D. R., 2004, New Astronomy Review, 48, 659
Andrews A. D., Lindsay E. M., 1964, Irish Astronomical Journal, 6, 241
Becker S. A., Mathews G. J., 1983, ApJ, 270, 155
Bencivenni D., Brocato E., Buonanno R., Castellani V., 1991, AJ, 102, 137
Bernard-Salas J., Peeters E., Sloan G. C., Gutenkunst S., Matsuura M., Tielens A. G. G. M., Zijlstra A. A., Houck J. R., 2009, ApJ, 699, 1541
Bernard-Salas J., Pottasch S. R., Gutenkunst S., Morris P. W., Houck J. R., 2008, ApJ, 672, 274
Bica E. L. D., Schmitt H. R., Dutra C. M., Oliveira H. L., 1999, AJ, 117, 238
Blanco V. M., McCarthy M. F., 1990, AJ, 100, 674
Blum R. D., et al., 2006, AJ, 132, 2034
Bohannan B., Epps H. W., 1974, A&AS, 18, 47
Bolatto A. D., et al., 2007, ApJ, 655, 212
Bonanos A. Z., et al., 2010, AJ, 140, 416
Bonanos A. Z., et al., 2009, AJ, 138, 1003
Boogert A. C. A., et al., 2008, ApJ, 678, 985
Boothroyd A. I., Sackmann I.-J., 1992, ApJ, 393, L21
Boyer M. L., et al., 2010, ApJ, 711, L99
Braun J. M., 2001, Ph.D. Thesis, Bonn University
Breysacher J., Azzopardi M., Testor G., 1999, A&AS, 137, 117
Brocato E., Buonanno R., Castellani V., Walker A. R., 1989, ApJS, 71, 25
Buchanan C. L., Kastner J. H., Hrivnak B. J., Sahai R., 2009, AJ, 138, 1597
Buchanan C. L., Kastner J. H., Forrest W. J., Hrivnak B. J., Sahai R., Egan M., Frank A., Barnbaum C., 2006, AJ, 132, 1890
Cherchneff I., Le Teuff Y. H., Williams P. M., Tielens A. G. G. M., 2000, A&A, 357, 572
Chiar J. E., Peeters E., Tielens A. G. G. M., 2002, ApJ, 579, L91
Churchwell E., 2002, ARA&A, 40, 27
Cioni M.-R. L., Girardi L., Marigo P., Habing H. J., 2006, A&A, 448, 77
Cioni M.-R., et al., 2000, A&AS, 144, 235
Clayton G. C., 2002, Ap&SS, 279, 167
Clayton G. C., 1996, PASP, 108, 225
Cohen M., Walker R. G., Witteborn F. C., 1992, AJ, 104, 2030
Cox A. N., 2000, Allen's Astrophysical Quantities
Cutri R. M., et al., 2003, The IRSA 2MASS All-Sky Point Source Catalog, NASA/IPAC Infrared Science Archive. http://irsa.ipac.caltech.edu/applications/Gator/
de Grijp M. H. K., Lub J., Miley G. K., 1987, A&AS, 70, 95
De Ruyter S., Van Winckel H., Maas T., Lloyd Evans T., Waters L. B. F. M., Dejonghe H., 2006, A&A, 448, 641
Dopita M. A., Meatheringham S. J., 1991, ApJ, 374, L21
Dwek E., 1987, ApJ, 322, 812
Egan M. P., Van Dyk S. D., Price S. D., 2001, AJ, 122, 1844
Elias J. H., Frogel J. A., Humphreys R. M., 1985, ApJS, 57, 91
Engelke C. W., 1992, AJ, 104, 1248
Fazio G. G., et al., 2004, ApJS, 154, 10
Feast M., 1999, IAUS, 190, 542
Feast M. W., Whitelock P. A., 1992, MNRAS, 259, 6
Frantsman I. L., 1988, Ap&SS, 145, 251
Fraser O. J., Hawley S. L., Cook K. H., 2008, AJ, 136, 1242
Fraser O. J., Hawley S. L., Cook K. H., Keller S. C., 2005, AJ, 129, 768
Furlan E., et al., 2008, ApJS, 176, 184
Furlan E., et al., 2006, ApJS, 165, 568
Gehrz R., 1989, Interstellar Dust, IAU Symposium 135, p.445+
Gielen C., et al., 2009, A&A, 508, 1391
Gielen C., Van Winckel H., Min M., Waters L. B. F. M., Lloyd Evans T., 2008, A&A, 490, 725
Gillett F. C., Low F. J., Stein W. A., 1968, ApJ, 154, 677
Goebel J. H., Moseley S. H., 1985, ApJ, 290, L35
Gorjian V., et al., 2008, ApJ, 679, 1040
Gouliermis D., Kontizas M., Kontizas E., Korakitis R., 2003, A&A, 405, 111
Groenewegen M. A. T., Sloan G. C., Soszyński I., Petersen E. A., 2009, A&A, 506, 1277
Groenewegen M. A. T., 2004, A&A, 425, 595
Gruendl R. A., Chu Y.-H., 2009, ApJS, 184, 172
Gruendl R. A., Chu Y.-H., Seale J. P., Matsuura M., Speck A. K., Sloan G. C., Looney L. W., 2008, ApJ, 688, L9
Gustafsson B., Edvardsson B., Eriksson K., Jørgensen U. G., Nordlund Å., Plez B., 2008, A&A, 486, 951
Gustafsson B., Bell R. A., Eriksson K., Nordlund A., 1975, A&A, 42, 407
Hao L., Weedman D. W., Spoon H. W. W., Marshall J. A., Levenson N. A., Elitzur M., Houck J. R., 2007, ApJ, 655, L77
Hao L., et al., 2005, ApJ, 625, L75
Hartwick F. D. A., Cowley A. P., 1988, ApJ, 334, 135
Henize K. G., 1956, ApJS, 2, 315
Heras A. M., et al., 2002, A&A, 394, 539
Herwig F., 2005, ARA&A, 43, 435
Heydari-Malayeri M., Melnick J., 1992, A&A, 258, L13
Heydari-Malayeri M., Melnick J., van Drom E., 1990, A&A, 236, L21
Hodge P. W., 1983, ApJ, 264, 470
Hony S., Waters L. B. F. M., Tielens A. G. G. M., 2002, A&A, 390, 533
Houck J. R., et al., 2004, ApJS, 154, 18
Hrivnak B. J., Volk K., Kwok S., 2009, ApJ, 694, 1147
Hughes S. M. G., 1989, AJ, 97, 1634
Humphreys R. M., 1979, ApJS, 39, 389
Iben I., Jr., Renzini A., 1983, ARA&A, 21, 271
Ishihara D., et al., 2010, A&A, 514, A1
Issersted J., 1979, A&AS, 38, 239
Ita Y., et al., 2004, MNRAS, 353, 705
Jasniewicz G., Thévenin F., 1994, A&A, 282, 717
Jørgensen U. G., Hron J., Loidl R., 2000, A&A, 356, 253
Jura M., 1986, ApJ, 309, 732
Justtanont K., et al., 2000, A&A, 360, 1117
Justtanont K., Cami J., Yamamura I., de Jong T., Waters L. B. F. M., 1998, Ap&SS, 255, 351
Kastner J. H., Thorndike S. L., Romanczyk P. A.,

Buchanan C. L., Hrivnak B. J., Sahai R., Egan M., 2008, AJ, 136, 1221
Kato D., et al., 2007, PASJ, 59, 615
Keller L. D., et al., 2008, ApJ, 684, 411
Keller S. C., Wood P. R., 2006, ApJ, 642, 834
Keller S. C., 1999, AJ, 118, 889
Kemper F., et al., 2010, PASP, 122, 683
Kemper F., Waters L. B. F. M., de Koter A., Tielens A. G. G. M., 2001, A&A, 369, 132
Kirk J. M., et al., 2009, ApJS, 185, 198
Kontizas E., Dapergolas A., Morgan D. H., Kontizas M., 2001, A&A, 369, 932
Kontizas M., Morgan D. H., Kontizas E., Dapergolas A., 1996, A&A, 307, 359
Kraemer K. E., Sloan G. C., Wood P. R., Price S. D., Egan M. P., 2005, ApJ, 631, L147
Kumar B., Sagar R., Melnick J., 2008, MNRAS, 386, 1380
Kwok S., Volk K. M., Hrivnak B. J., 1989, ApJ, 345, L51
Lada C. J., 1987, Star Forming Regions, IAU Symposium 115, 1
Lagadec E., et al., 2007, MNRAS, 376, 1270
Lambert D. L., Rao N. K., Pandey G., Ivans I. I., 2001, ApJ, 555, 925
Leisenring J. M., Kemper F., Sloan G. C., 2008, ApJ, 681, 1557
Leisy P., Dennefeld M., 2006, A&A, 456, 451
Leisy P., Dennefeld M., Alard C., Guibert J., 1997, A&AS, 121, 407
Lindsay E.M., 1974, MNRAS 166, 703
Lindsay E. M., Mullan D. J., 1963, Irish Astronomical Journal, 6, 51
Liu Q., de Grijs R., Deng L. C., Hu Y., Beaulieu S. F., 2009, A&A, 503, 469
Loup C., Delmotte N., Egret D., Cioni M.-R., Genova F., 2003, A&A, 402, 801
Loup C., Zijlstra A.A., Waters L.B.F.M., Groenewegen M.A.T., 1997, A&AS 125, 419
McDonald I., Sloan G. C., Zijlstra A. A., Matsunaga N., Matsuura M., Kraemer K. E., Bernard-Salas J., Markwick A. J., 2010, ApJ, 717, L92
McDonald I., van Loon J. Th., Decin L., Boyer M. L., Dupree A. K., Evans A., Gehrz R. D., Woodward C. E., 2009, MNRAS, 394, 831
Mackey A. D., Gilmore G. F., 2003, MNRAS, 338, 85
Martin P. G., Rogers C., 1987, ApJ, 322, 374
Marx M., Dickey J. M., Mebold U., 1997, A&AS, 126, 325
Massey P., Olsen K. A. G., 2003, AJ, 126, 2867
Massey P., 2002, ApJS, 141, 81
Matsuura M., et al., 2009, MNRAS, 396, 918
Matsuura M., et al., 2006, MNRAS, 371, 415
Matsuura M., et al., 2005, A&A, 434, 691
Matsuura M., et al., 2004, ApJ, 604, 791
Matsuura M., Zijlstra A. A., van Loon J. Th., Yamamura I., Markwick A. J., Woods P. M., Waters L. B. F. M., 2002, ApJ, 580, L133
Meixner M., et al., 2006, AJ, 132, 2268
Merrill K. M., Stein W. A., 1976, PASP, 88, 294
Moffat A. F. J., 1991, A&A, 244, L9
Molster F. J., et al., 1999, A&A, 350, 163
Morgan D. H., 1984, MNRAS, 208, 633
Nikolaev S., Weinberg M. D., 2000, ApJ, 542, 804
Oestreicher M. O., Schmidt-Kaler T., 1999, Astronomische Nachrichten, 320, 385
Oestreicher M. O., Schmidt-Kaler T., 1998, MNRAS, 299, 625
Oliva E., Origlia L., 1998, A&A, 332, 46
Oliveira J. M., et al., 2009, ApJ, 707, 1269
Oliveira J. M., van Loon J. Th., Stanimirović S., Zijlstra A. A., 2006, MNRAS, 372, 1509
Paunzen E., Maitzen H. M., Pintado O. I., Claret A., Iliev I. K., Netopil M., 2006, A&A, 459, 871
Payne-Gaposchkin C. H., 1971, Smithsonian Contributions to Astrophysics, 13
Percy J.R., Hosick J., Leigh N.W.C., 2003, ASPC 292, 159
Poelarends A. J. T., Herwig F., Langer N., & Heger A., 2008, ApJ, 675, 614
Prévot L., et al., 1985, A&AS, 62, 23
Rebeirot E., Martin N., Prévot L., Robin A., Peyrin Y., Mianes P., Rousseau J., 1983, A&AS, 51, 277
Reid W. A., Parker Q. A., 2006, MNRAS, 373, 521
Reyniers M., Van Winckel H., 2007, A&A 463, L1
Rieke G. H., et al., 2004, ApJS, 154, 25
Robitaille T. P., Whitney B. A., Indebetouw R., Wood K., Denzmore P., 2006, ApJS, 167, 256
Rousseau J., Martin N., Prévot L., Rebeirot E., Robin A., Brunet J. P., 1978, A&AS, 31, 243
Sanduleak N., MacConnell D. J., Philip A. G. D., 1978, PASP, 90, 621
Sanduleak N., Philip A. G. D., 1977, Publications of the Warner & Swasey Observatory, 2, 105
Sanduleak N., 1970, Contributions from the Cerro Tololo Inter-American Observatory, 89
Santos J. F. C., Jr., Bica E., Claria J. J., Piatti A. E., Girardi L. A., Dottori H., 1995, MNRAS, 276, 1155
Sargent B. A., Srinivasan S., Meixner M., Kemper F., Tielens A. G. G. M., Speck A. K., Matsuura M., Bernard J.-Ph., Hony S., Gordon K. D., Indebetouw R., Marengo M., Sloan G. C., Woods P. M., 2010, ApJ, 716, 878
Sasaki M., Haberl F., Pietsch W., 2000, A&AS, 143, 391
Schaefer B. E., 2008, AJ, 135, 112
Schaller G., Schaerer D., Meynet G., Maeder A., 1992, A&AS, 96, 269
Seale J. P., Looney L. W., Chu Y.-H., Gruendl R. A., Brandl B., Rosie Chen C.-H., Brandner W., Blake G. A., 2009, ApJ, 699, 150
Shaw R. A., Stanghellini L., Villaver E., Mutchler M., 2006, ApJS, 167, 201
Shaw R. A., Stanghellini L., Mutchler M., Balick B., Blades J. C., 2001, ApJ, 548, 727
Shi Y., et al., 2006, ApJ, 653, 127
Shimonishi T., Onaka T., Kato D., Sakon I., Ita Y., Kawamura A., Kaneda H., 2010, A&A, 514, A12
Shimonishi T., Onaka T., Kato D., Sakon I., Ita Y., Kawamura A., Kaneda H., 2008, ApJ, 686, L99
Siebenmorgen R., Haas M., Krügel E., Schulz B., 2005, A&A, 436, L5
Skiff B. A., 2009, VizieR Online Data Catalog, 1, 2023
Skrutskie M. F., et al., 2006, AJ, 131, 1163
Sloan G. C., Kraemer K. E., Wood P. R., Zijlstra A. A., Bernard-Salas J., Devost D., Houck J. R., 2008, ApJ, 686, 1056
Sloan G. C., Kraemer K. E., Matsuura M., Wood P. R., Price S. D., Egan M. P., 2006, ApJ, 645, 1118

Sloan G. C., Kraemer K. E., Goebel J. H., Price S. D., 2003, ApJ, 594, 483
Sloan G. C., Levan P. D., Little-Marenin I. R., 1996, ApJ, 463, 310
Sloan G. C., Price S. D., 1995, ApJ, 451, 758
Smith V. V., Plez B., Lambert D. L., Lubowich D. A., 1995, ApJ, 441, 735
Soszyński I., et al., 2009a, Acta Astronomica, 59, 335
Soszyński I., et al., 2009b, Acta Astronomica, 59, 239
Soszyński I., et al., 2008, Acta Astronomica, 58, 293
Speck A. K., Corman A. B., Wakeman K., Wheeler C. H., Thompson G., 2009, ApJ, 691, 1202
Speck A. K., Cami J., Markwick-Kemper C., Leisenring J., Szczerba R., Dijkstra C., Van Dyk S., Meixner M., 2006, ApJ, 650, 892
Speck A. K., Barlow M. J., Sylvester R. J., Hofmeister A. M., 2000, A&AS, 146, 437
Srinivasan S., et al., 2010, AJ, submitted
Srinivasan S., et al., 2009, AJ, 137, 4810
Stanghellini L., García-Lario P., García-Hernández D. A., Perea-Calderón J. V., Davies J. E., Manchado A., Villaver E., Shaw R. A., 2007, ApJ, 671, 1669
Stern D., et al., 2005, ApJ, 631, 163
Sylvester R. J., Kemper F., Barlow M. J., de Jong T., Waters L. B. F. M., Tielens A. G. G. M., Omont A., 1999, A&A, 352, 587
Trams N. R., et al., 1999, A&A, 346, 843
Treffers R. Cohen M. 1974, ApJ, 188, 545
Tuthill P. G., Monnier J. D., Danchi W. C., 1999, Nature, 398, 487
van Loon J. Th., et al., 2010, AJ, 139, 68
van Loon J. Th., Cohen M., Oliveira J. M., Matsuura M., McDonald I., Sloan G. C., Wood P. R., Zijlstra A. A., 2008, A&A, 487, 1055
van Loon J. Th., 2006, Stellar Evolution at Low Metallicity: Mass Loss, Explosions, Cosmology, ASPC, 353, 211
van Loon J. Th., et al., 2005, MNRAS, 364, L71
van Loon J. Th., Marshall J. R., Zijlstra A. A., 2005, A&A, 442, 597
van Loon J. Th., Cioni M.-R. L., Zijlstra A. A., Loup C., 2005, A&A, 438, 273
van Loon J. Th., Zijlstra A. A., Kaper L., Gilmore G. F., Loup C., Blommaert J. A. D. L., 2001, A&A, 368, 239
van Loon J. Th., Molster F. J., Van Winckel H., Waters L. B. F. M., 1999, A&A, 350, 120
van Loon J. Th., Zijlstra A. A., Whitelock P. A., Waters L. B. F. M., Loup C., Trams N. R., 1997, A&A, 325, 585
Van Winckel H., et al., 2009, A&A, 505, 1221
Van Winckel H., 2007, Baltic Astronomy, 16, 112
Van Winckel H., 2003, ARA&A, 41, 391
Van Winckel H., Waelkens C., Fernie J. D., Waters L. B. F. M., 1999, A&A, 343, 202
Vijh U. P., et al., 2009, AJ, 137, 3139
Volk K., Cohen M., 1989, AJ, 98, 931
Wagenhuber J., Groenewegen M. A. T., 1998, A&A, 340, 183
Waters L. B. F. M., et al., 1998, Nature, 391, 868
Waters L. B. F. M., Trams N. R., Waelkens C., 1992, A&A, 262, L37
Welch D.L., 1987, ApJ 317, 672
Werner M. W., et al., 2004, ApJS154, 1
Westerlund B. E., Olander N., Hedin B., 1981, A&AS, 43, 267
Westerlund B. E., Olander N., Richer H. B., Crabtree D. R., 1978, A&AS, 31, 61
Westerlund B. E., Smith L. F., 1964, MNRAS, 127, 449
Whitelock P. A., Feast M. W., van Loon J. Th., Zijlstra A. A., 2003, MNRAS, 342, 86
Whitney B. A., et al., 2008, AJ, 136, 18
Will J.-M., Bomans D. J., Tucholke H.-J., de Boer K. S., Grebel E. K., Richtler T., Seggewiss W., Vallenari A., 1995, A&AS, 112, 367
Wolf M. J., Drory N., Gebhardt K., Hill G. J., 2007, ApJ, 655, 179
Wood P. R., Cohen M., 2001, Astrophysics and Space Science Library, 265, 71
Wood P. R., Whiteoak J. B., Hughes S. M. G., Bessell M. S., Gardner F. F., & Hyland A. R., 1992, ApJ, 397, 552
Wood P. R., Bessell M. S., Fox M. W., 1983, ApJ, 272, 99
Woods P. M., Sloan G. C., Gordon K. D., Shiao B., Kemper F. & the *SAGE-Spec*team, 2010, http://data.spitzer.caltech.edu/popular/sage-spec/20100301_enhanced/do
Woolf N. J., Ney E. P., 1969, ApJ, 155, L181
Wright F. W., Hodge P. W., 1971, AJ, 76, 1003
Zaritsky D., Harris J., Thompson I. B., Grebel E. K., 2004, AJ, 128, 1606
Zijlstra A. A., et al., 2006, MNRAS, 370, 1961

APPENDIX A: LITERATURE-BASED CLASSIFICATION SUPPORT FOR *SAGE-Spec* OBJECTS

NGC 1651 SAGE IRS 1 (SSID1). NGC 1651 is an intermediate-aged globular cluster (2×10^9 yr; Mackey & Gilmore 2003), and SAGE IRS 1 is a particular member of that cluster with a K-band magnitude of 11.2 mag (2MASS; Cutri et al. 2003) and a period of 101 days (Soszyński et al. 2009b). Srinivasan et al. (2009) classify this object as an O-rich AGB star. This, and the cluster age, supports our classification of `O-AGB`.

SSTISAGEMC J043727.61−675435.1 (SSID2). This object is classified as a galaxy by Gruendl & Chu (2009) and van Loon et al. (2010), which matches our classification of `GAL`.

SSTISAGEMC J044627.10−684747.0 (SSID3). This object has a period given by MACHO and OGLE-III of ∼400 days (Alcock et al. 1998; Soszyński et al. 2009b). This fits with our classification of `C-AGB`.

SSTISAGEMC J044718.63−694220.6 (SSID4). This object is visibly bright in an uncrowded region, with B−V=1.8 mag and V−R=1.4 mag (Rebeirot et al. 1983). It is classified as a star of spectral type M based on a low-resolution objective prism survey, and has a radial velocity measurement concurrent with being in the LMC (Prévot et al. 1985). This supports our classification of `RSG`.

SSTISAGEMC J044837.76−692337.0 (SSID5). Srinivasan et al. (2009) classify this object as an extreme AGB star, based on *Spitzer* colours. This object is modelled by Whitney et al. (2008), who classify it as a high-probability Stage I YSO (meaning that this YSO is embedded in an infalling envelope; Robitaille et al. 2006). This work supports our classification of `YSO`.

SSTISAGEMC J044934.31−690549.3 (SSID6). This object has recently been identified as LHα 120-S 67 (Skiff 2009) owing to a mistake in the original Henize (1956) co-ordinates. Both authors and Andrews & Lindsay (1964) list this object as a weak emission-line object. Whitney et al. (2008) categorise it as a YSO, but do not put it in their "high probability" class. Vijh et al. (2009) also categorise it as a YSO candidate. However, we classify this object as `O-AGB`.

MSX LMC 1128 (SSID7). This Long Period Variable star (LPV) has a period of 418–445 days (Hughes 1989; Fraser et al. 2005, 2008), and is classified by Egan et al. (2001) as carbon-rich, based on JHK_sA colours from 2MASS and MSX. This supports our classification of `C-AGB`.

SSTISAGEMC J045128.58−695550.1 (SSID8). This variable star has a lengthy period of 884–911 d (Soszyński et al. 2008; Fraser et al. 2005, 2008), which is congruous with it being an evolved `O-AGB`.

IRAS 04518−6852 (SSID9). IRAS 04518-6852 has been identified by van Loon et al. (1997) as C-AGB based on IRAS colours, and as an extreme AGB star by Srinivasan et al. (2009) and Gruendl & Chu (2009), based on *Spitzer* colours. However, Egan et al. (2001) classify this object as an HII region, based on 2MASS and MSX JHK_sA colours. This latter classification would seem to be spurious, since the IRS spectrum shows no indication of atomic emission lines. Hence our classification as `C-AGB`.

SSTISAGEMC J045200.36−691805.6 (SSID10). This is classified as a YSO by Gruendl & Chu (2009) and more specifically, a high-probability Stage I YSO by Whitney et al. (2008), which supports our classification of `YSO`.

SSTISAGEMC J045228.68−685451.3 (SSID11). This object is classified as a YSO (high probability – HP, Stage I) by Whitney et al. (2008) based on an SED fit to photometry points, and by Oliveira et al. (2009) based on modelling of the spectrum. This supports our classification of `YSO`.

KDM 764 (SSID12). KDM 764 is identified as a carbon-rich AGB star from the detection of C_2 in its UK Schmidt Telescope (UKST) spectrum (Kontizas et al. 2001). Srinivasan et al. (2009) also classify this object as C-AGB. The OGLE-III period is given as 445 days (Soszyński et al. 2009b) whereas the MACHO period ranges between 250–873 days (Fraser et al. 2005, 2008). This supports our classification of `C-AGB`.

SSTISAGEMC J045309.39−681710.8 (SSID13). This LPV has a period of 916–1,122 days (Soszyński et al. 2009b; Fraser et al. 2005, 2008) and is classified by OGLE-III (Soszyński et al. 2009b) and Srinivasan et al. (2009) as an oxygen-rich AGB star. Very faint visually, this star has V−R typical of a mid-M Giant (Massey 2002), in agreement with our classification of `O-AGB`.

IRAS F04532−6709 (SSID14). This star is classified as a YSO by Oliveira et al. (2009), based on modelling of the spectrum, and also by Whitney et al. (2008) and Gruendl & Chu (2009), supporting our classification of `YSO`.

SSTISAGEMC J045328.70−660334.4 (SSID15). This object has an extremely long period of 2710 days from MACHO measurements (Alcock et al. 1998). Srinivasan et al. (2009) classify this as `C-AGB`, in agreement with our classification.

GV 60 (SSID16). This object is listed as an M3 star in SIMBAD, which is supported by photometry from Westerlund et al. (1981). It is also included in the RSG catalog of Massey & Olsen (2003), who give $M_{\rm bol}$=−9.39 mag. This would support our classification of `RSG`.

LHα 120-N 82 (SSID17). Alternatively called Brey 3a (Breysacher, Azzopardi & Testor 1999), this object is a known WR star (Heydari-Malayeri, Melnick & van Drom 1990), although its exact spectral type remains controversial (Moffat 1991; Heydari-Malayeri & Melnick 1992). We classify it as `OTHER`.

SSTISAGEMC J045344.24−661146.0 (SSID18). This object is classified as C-AGB by van Loon et al. (1997) and Loup et al. (1997), using IRAS colours and by Gruendl & Chu (2009) using *Spitzer* photometry. This matches our classification of `C-AGB`.

SSTISAGEMC J045422.82−702657.0 (SSID19). This object is a hot foreground star with B−V=1.033, and a stellar type of K5 (Skiff 2009). We classify it as `STAR`.

SSTISAGEMC J045526.69−682508.4 (SSID20). This *SAGE-LMC* source was classified by Whitney et al. (2008) as a high-probability Stage I YSO, and similarly by Gruendl & Chu (2009). It sits within 20″ of the HII region, IRAS 04555-6829. We similarly classify this object as `YSO`.

SSTISAGEMC J045534.07−655701.3 (SSID21). This *SAGE-LMC* source was classified as a YSO by Whitney et al. (2008) with high-probability (Stage I), and with lower confidence by Gruendl & Chu (2009) (who suggest this object could potentially be a PN). No other information in the literature could be found. We agree with Whitney et al. (2008) and Gruendl & Chu (2009), in our classification of `YSO`.

SSTISAGEMC J045623.21−692749.0 (SSID22). This *SAGE-LMC* source was classified by Whitney et al. (2008) as a high-probability YSO. No other information in the literature could be found. We classify it as `O-AGB`.

KDM 1238 (SSID23). KDM 1238 is classified by Kontizas et al. (2001) as C-AGB by a detection of C_2. It has periods which range from 133 days (Soszyński et al. 2009b) to 543 days (Alcock et al. 1998). This information supports our classification of `C-AGB`.

RP 1805 (SSID24). Classified as a PN by Reid & Parker (2006) based on optical spectra, with the comments that it was faint, circular and diffuse. Not detected in our observations, hence classified as `UNK`.

SSTISAGEMC J050032.61−662113.0 (SSID25). Classified as a YSO by Gruendl & Chu (2009), in agreement with our classification (`YSO`).

RP 1631 (SSID26). Classified as a PN by Reid & Parker (2006) based on optical spectra, with the comments that it was bright, circular and small. However, we believe this object to be an RCrB star, and thus classify it as `OTHER`.

MSX LMC 1271 (SSID27). MSX LMC 1271 is likely a member of the compact cluster NGC 1805, which has an age of 8–45 Myr (Wolf et al. 2007; Liu et al. 2009). WFPC2 images from the *Hubble Space Telescope* show a bright star close to the observed co-ordinates. Both these pieces of information are congruous with MSX LMC 1271 being a red supergiant, `RSG`.

SSTISAGEMC J050224.17−660637.4 (SSID28). Whitney et al. (2008) class this object as one of their high-probability YSOs, still in the embedded stages of evo-

lution (Stage I). However, its spectrum has the distinctly double-peaked shape of an oxygen-rich post-AGB object. This object may potentially belong to the young cluster NGC 1805, in which case it would almost certainly be a YSO, but we choose to tentatively classify it as `O-PAGB`.

HV 2281 (SSID29). This variable object is classified as an RV Tau star, based on the MACHO light curve (Alcock et al. 1998). OGLE-III also classifies this object as an RV Tau (Soszyński et al. 2008). We reach an identical conclusion, classifying HV 2281 as `O-PAGB`. Gruendl & Chu (2009), however, class this as a stellar photosphere.

KDM 1656 (SSID30). KDM 1656 is classified by Kontizas et al. (2001) as C-AGB by a detection of C_2, and also by Srinivasan et al. (2009), based on infrared colours. This object has a long period of 1035 days (Alcock et al. 1998). This supports our classification of `C-AGB`.

KDM 1691 (SSID31). Classified by Kontizas et al. (2001) as a carbon star, Westerlund et al. (1978) also detect CN bands in visible and near-infrared photometry and spectra. Srinivasan et al. (2009) group this object with the C-rich AGB stars. MACHO and OGLE-III calculate a period of ∼510 days for this object (Fraser et al. 2005, 2008; Soszyński et al. 2009b). Thus KDM 1691 is classified as `C-AGB`.

LMC-BM 11-19 (SSID32). This object exhibits highly divergent periods of 98 days (Soszyński et al. 2009b) and 894–1082 days (Fraser et al. 2005, 2008), although the OGLE-III data on this object are not particularly good . This object is identified as a carbon star by Blanco & McCarthy (1990) and Loup et al. (2003) based on near-infrared CN bands. Due to the lack of identifiable carbon-rich features in the IRS spectrum, we classify this object as `STAR`.

LMC-BM 12-14 (SSID33). Again, this object has differing periods of 220 days (Soszyński et al. 2009b) and 405–894 days (Fraser et al. 2005, 2008), and is included in the carbon star catalog of Blanco & McCarthy (1990) and Srinivasan et al. (2009). This supports our classification of `C-AGB`.

SSTISAGEMC J050354.55−671848.7 (SSID34). This object was classified as a YSO by Whitney et al. (2008, Stage I), Oliveira et al. (2009) and Gruendl & Chu (2009), fortifying our classification of `YSO`.

NGC 1818 WBT 5 (SSID35). Will et al. (1995) measure the V-band magnitude and calculate the B−V colour (1.745 mag) for this object, which are consistent with it being a late-type star of spectral type ∼M0–M2. Fraser et al. (2005) and Fraser et al. (2008) measure periods of 360–1707 days. Wolf et al. (2007) give a cluster age for NGC 1818 of 14–40 Myr. This supports our classification of `RSG`.

SSTISAGEMC J050407.72−662505.9 (SSID36). Srinivasan et al. (2009) classify this object as a carbon-rich AGB star based on J-K_S infrared colours, and we agree with the classification, `C-AGB`. However, this star is co-located on the sky with globular cluster NGC 1818, a cluster of RSGs. It has a period of ∼840 days (Fraser et al. 2005, 2008).

NGC 1818 WBT 3 (SSID37). Similarly to WBT 5, B−V=1.684 mag (Will et al. 1995) is typical of a late-type star with a spectral type ∼M0. It has a period of 360 days (Fraser et al. 2005, 2008). This would support our classification of `RSG`.

MSX LMC 61 (SSID38). This object is classified by Egan et al. (2001) as an O-AGB star, based on J−K vs. K−A colours, which matches our classification (`O-AGB`). It has a period of 580 days (Fraser et al. 2005, 2008; Soszyński et al. 2009b).

RP 1878 (SSID39). Reid & Parker (2006) list this as a bright, round, small PN, with a diameter of 5.″3 in Hα and a velocity of $v_{\rm helio}$ = 252.3 km s^{-1}. A weak IRS spectrum with no distinctive features leads us to classify this object as `UNK`.

IRAS 05047−6642 (SSID40). This object has a short period of 20 days according to Fraser et al. (2005) and Fraser et al. (2008), and was classified as a high-probability YSO by Whitney et al. (2008). However, Srinivasan et al. (2009) classify it as an extreme AGB star, and Gruendl & Chu (2009) as a stellar photosphere, or a PN. We agree with Whitney et al. (2008), classifying as `YSO`.

SSTISAGEMC J050503.21−692426.5 (SSID41). Little is known about this object, apart from its period (217 d; Soszyński et al. 2009b). We classify it as `C-AGB`.

SSTISAGEMC J050517.08−692157.0 (SSID42). Classified as a potential galaxy or YSO by Gruendl & Chu (2009), we classify this object as `GAL`.

LMC-BM 13-2 (SSID43). Measured to have a period of 206 days by Soszyński et al. (2009b), this `C-AGB` star has CN bands in its near-infrared spectrum (Blanco & McCarthy 1990).

SSTISAGEMC J050558.23−680923.6 (SSID44). This *SAGE-LMC* object was classified as a high-probability YSO by Whitney et al. (2008). We also classify it as `YSO`.

SSTISAGEMC J050607.50−714148.4 (SSID45). Apart from a period of 346 days (Fraser et al. 2005, 2008), little is known about this object. We classify it as `C-AGB`.

KDM 1961 (SSID46). Near-infrared C_2 bands were detected in this star by Kontizas et al. (2001), backing up our classification of `C-AGB`. Srinivasan et al. (2009) agree.

KDM 1966 (SSID47). Similarly to the last object, the Swan C_2 bands were detected in this star by Kontizas et al. (2001), backing up our classification of `C-AGB`. Srinivasan et al. (2009) agree once more.

SSTISAGEMC J050620.12−645458.6 (SSID48). Srinivasan et al. (2009) classify this star as a carbon-rich AGB star, and no other information was found about this object. Our classification of `C-AGB` is in agreement with Srinivasan et al.

SSTISAGEMC J050629.61−685534.9 (SSID49). Apart from a determination of period (154–295 d; Soszyński et al. 2009b; Fraser et al. 2005, 2008; Ita et al. 2004), little is known about this object. Srinivasan et al. (2009) class it as C-AGB, which agrees with our classification, `C-AGB`.

SSTISAGEMC J050639.14−682209.3 (SSID50). Sanduleak (1970) lists this star as having an early-type spectrum, which is refined further by Rousseau et al. (1978) to that of a B4 supergiant. B−V=-0.03 mag and U−B=-0.70 mag (Issersted 1979) are consistent with a B5–B8 supergiant, hence our classification of `OTHER`.

SHV 0507252−690238 (SSID51). This semi-regular variable star has a number of defined periods: 1353 d (Hughes 1989, I-band), 254 d, 431 d, 563 d (Groenewegen 2004, OGLE, 2MASS, DENIS), 507 d (Soszyński et al. 2009b, OGLE-III), and is classified as a C-rich Mira variable by Soszyński et al. (2009b). We classify it as `C-AGB`.

SSTISAGEMC J050713.90−674846.7 (SSID52). This

object is classified by Whitney et al. (2008) as YSO-HP, and by Gruendl & Chu (2009) as a (post-)AGB object. We classify it as `C-PAGB`.

SSTISAGEMC J050752.93−681246.5 (SSID53). Both Vijh et al. (2009) and Srinivasan et al. (2009) include this object in their variable star and evolved star catalogs, respectively. Both classify it as an extreme or obscured AGB star. It has periods of 302–335 days (Soszyński et al. 2009b; Fraser et al. 2005, 2008). We classify it as `C-AGB`.

SSTISAGEMC J050759.35−683925.8 (SSID54). This star has a period of 150–362 days (Soszyński et al. 2009b; Fraser et al. 2005, 2008) and is classified as a semi-regular variable O-AGB by OGLE-III, which supports our classification of `O-AGB`. It has also been classed as a YSO by Whitney et al. (2008), but with a low confidence.

SSTISAGEMC J050826.35−683115.1 (SSID55). This star is classified as an extreme-AGB star by both Vijh et al. (2009) and Srinivasan et al. (2009). We agree, with our classification of `C-AGB`.

SSTISAGEMC J050830.51−692237.4 (SSID56). This is classified as O-AGB by Srinivasan et al. (2009), but has a relatively short period for an AGB star (115 d; Soszyński et al. 2009b). We classify it as `O-PAGB`.

KDM 2187 (SSID57). This object is classified as a C-AGB in the catalog of Kontizas et al. (2001), which was selected by the detection of C_2 bands. We agree with this classification, `C-AGB`.

BMB-BW 180 (SSID58). Classified as an AGB star by the DENIS consortium (Cioni et al. 2000) based on near-infrared colours, this object was also found to be mildly variable, with a period of 70 days (Groenewegen 2004; Ita et al. 2004), which may indicate that it lies on the early AGB. It has a spectral type of M2 (Groenewegen 2004), in line with our classification of `O-AGB`.

NGC 1856 SAGE IRS 1 (SSID59). NGC 1856 is a cluster which has an age of 120–151 Myr (Wolf et al. 2007) and thus is probably composed of relatively massive AGB stars. This object has a positive (I−J) colour from DENIS data, and Whitney et al. (2008) classify this object as a YSO. We classify it as an `O-AGB`.

SSTISAGEMC J051028.27−684431.2 (SSID60). Both Vijh et al. (2009) and Srinivasan et al. (2009) classify this object as an extreme AGB star, based on 2MASS and *Spitzer* colours. It has a period of 465 days (Soszyński et al. 2009b). We classify it as `C-AGB`.

SSTISAGEMC J051059.07−685613.7 (SSID61). This star is an oxygen-rich AGB star according to Srinivasan et al. (2009), which agrees with our classification `O-AGB`.

MSX LMC 209 (SSID62). MSX LMC 209 has a 28-day period according to Soszyński et al. (2009b), and is classified by them as a carbon-rich AGB star. Egan et al. (2001) classify it as a PN, based on colours. It may be associated with the emission-line object LHα 120-S 160 (Henize 1956). We class it as an oxygen-rich protoplanetary nebula, `O-PAGB`.

SSTISAGEMC J051213.54−683922.8 (SSID63). This object is categorised by Srinivasan et al. (2009) as an oxygen-rich AGB star, which matches our classification, `O-AGB`.

SSTISAGEMC J051228.19−690755.8 (SSID64). This object is probably associated with LI-LMC 611 (Loup et al. 1997) and IRAS 05127−6911, but unclassified by these authors. Both Whitney et al. (2008) and Gruendl & Chu (2009) classify it as a YSO candidate, but with low confidence. We classify it as `C-PAGB`.

IRAS 05133−6937 (SSID65). This object is one of the thirteen EROs selected by Gruendl et al. (2008) based on extremely red mid-IR colours. Follow-up observations show that this small sample is composed of extreme carbon-rich AGB stars, confirming our classification (`C-AGB`). This star is also classified by Whitney et al. (2008) and Vijh et al. (2009) as a high-probability YSO, based on its infrared colours.

OGLE 051306.52−690946.4 (SSID66). This star is a long-period variable according to Groenewegen (2004), with a period of 183 days. It has been modelled with a radiative transfer model by Srinivasan et al. (2010), who pay particular attention to the acetylene features in the IRS spectrum, thus supporting our classification of `C-AGB`. Vijh et al. (2009) and Srinivasan et al. (2009) classify it as an extreme AGB star.

SSTISAGEMC J051339.94−663852.5 (SSID67). Classified as O-rich AGB star by Srinivasan et al. (2009), which matches our classification, `O-AGB`.

NGC 1866 Robb B136 (SSID68). Globular cluster NGC 1866 has an age of 100 Myr (Becker & Mathews 1983; Brocato et al. 1989), giving M5 star (Aaronson & Mould 1985) NGC 1866 Robb B136 the age typical of a massive AGB star, and supporting our classification of `O-AGB`. Srinivasan et al. (2009) come to the same conclusion.

BSDL 923 (SSID69). According to Gouliermis et al. (2003) and Bica et al. (1999), this object is a member of the young stellar cluster LMC-N30, suggesting that this is a massive star. We classify it as a B supergiant, hence `OTHER`.

SSTISAGEMC J051347.72−693505.2 (SSID70). This object was classified as a YSO by Whitney et al. (2008, high probability, Stage I), Oliveira et al. (2009) and Gruendl & Chu (2009), strengthening our classification of `YSO`.

SSTISAGEMC J051348.38−670527.0 (SSID71). Whitney et al. (2008) class this as a YSO-HP, Stage I, and Gruendl & Chu (2009) think it to be a probable YSO or galaxy. We classify it as `HII` due to the low-excitation emission lines in the IRS spectrum.

SSTISAGEMC J051412.33−685058.0 (SSID72). Classified as `O-AGB` in agreement with Srinivasan et al. (2009).

HV 915 (SSID73). This object is classified as an RV Tau star, based on the MACHO light curve (MACHO 79.5501.13; Alcock et al. 1998), and Percy, Hosick & Leigh (2003) confirm this (and calculate a period of 48.5 days). Vijh et al. (2009) also class this object as O-rich. Hence our classification of `O-PAGB` is upheld.

SSTISAGEMC J051449.43−671221.4 (SSID74). This object was classified as a YSO by Whitney et al. (2008, high probability, Stage I) and Oliveira et al. (2009), based on the SED and IRS spectrum, respectively. Shimonishi et al. (2008) also classified it as a YSO based on the detection of H_2O and CO_2 ice with AKARI. This object is their ST4, although it must be noted that the association of IRAS 05148-6715 with this object is likely erroneous. Our classification of `YSO` is upheld. Srinivasan et al. (2009) classify this object as an extreme AGB star, based on mid-infrared colours.

SSTISAGEMC J051453.10−691723.5 (SSID75). This

is a possible YSO or naked star according to Gruendl & Chu (2009). We classify it as `O-PAGB`.

SSTISAGEMC J051526.44−675126.9 (SSID76). This object has a period of 107 days according to OGLE-III (Soszyński et al. 2009b) and 441 days according to MACHO (Fraser et al. 2005, 2008). It is classified by the former as an oxygen-rich semi-regular variable star. Due to a lack of evident oxygen-rich features in the IRS spectrum, we classify it as `STAR`.

SSTISAGEMC J051612.42−704930.3 (SSID77). Classified as `O-AGB` by us and by Srinivasan et al. (2009).

IRAS 05170−7156 (SSID78). This object has an unusual IRS spectrum and SED. It is considered to be an AGN candidate according to de Grijp et al. (1987), a YSO-HP, Stage I, according to Whitney et al. (2008) and an extreme AGB star by Srinivasan et al. (2009) and Gruendl & Chu (2009). We classify it as `UNK`.

SSTISAGEMC J051747.18−681842.6 (SSID79). This star is an oxygen-rich AGB star according to Srinivasan et al. (2009), which is in accord with our classification, `O-AGB`.

SSTISAGE1C J051803.28−684950.6 (SSID80). Considered an extreme AGB by Vijh et al. (2009) and Srinivasan et al. (2009), and a carbon-rich AGB star with a period of 349 days by Soszyński et al. (2009b). We classify it as `C-AGB`.

KDM 3196 (SSID81). KDM 3196 is included in the carbon star catalogs of Sanduleak & Philip (1977), Westerlund et al. (1978) and Kontizas et al. (2001). This object may also be a CH star: a metal-poor, carbon-rich giant, found in the halo of the Milky Way, and potentially in the halo of the LMC (Hartwick & Cowley 1988; Feast & Whitelock 1992). We classify it as `STAR` due to the lack of distinguishing features in the IRS spectrum.

HV 5715 (SSID82). This object is a long period variable, with a period of 422 days (Wright & Hodge 1971). It is considered to be an O-AGB by Srinivasan et al. (2009), and its IRS spectrum is modelled by Sargent et al. (2010). This would support our classification of `O-AGB`.

SSTISAGEMC J051832.64−692525.5 (SSID83). Ita et al. (2004) measure a period of 293 days for this object. Srinivasan et al. (2009) consider it to be a carbon-rich AGB star, as do we, `C-AGB`.

IRAS F05192−7008 (SSID84). This object is probably associated with MSX LMC 390 (Egan et al. 2001) and IRAS 05193−7009. It has been classified by Egan et al. (2001) as an HII region and as a star by Gruendl & Chu (2009). We classify it as `C-PAGB`.

HV 2444 (SSID85). This object was regarded as a Type II Cepheid by Welch (1987) and Payne-Gaposchkin (1971), and the OGLE-III catalog further classifies this object as an RV Tau stay with a period of 36 days (Soszyński et al. 2008). This supports our classification of `O-PAGB`.

SSTISAGEMC J051908.46−692314.3 (SSID86). Considered to be a `C-AGB` by both Srinivasan et al. (2009) and us.

2MASS J05191049−6933453 (SSID87). This object is a variable star with a period of 452 days (Ita et al. 2004). We consider it to be `C-AGB`, in agreement with Srinivasan et al. (2009).

2MASS J05194483−6929594 (SSID88). Srinivasan et al. (2009) tentatively classify this object as an oxygen-rich AGB star, but we consider it to be a naked `STAR`.

SSTISAGEMC J052014.24−702931.0 (SSID89). This LPV, with a 686-day period (Soszyński et al. 2009b), is oxygen-rich according to Srinivasan et al. (2009), and we are concordant with that classification, `O-AGB`.

SSTISAGEMC J052023.97−695423.2 (SSID90). This object has a very short period of 0.17 d according to Alcock et al. (1998) and is classed as a high probability YSO by Whitney et al. (2008), in harmony with us, `YSO`.

SSTISAGEMC J052051.83−693407.6 (SSID91). An LPV with a lengthy period of ≈770 days (Soszyński et al. 2009b), this star is considered to be `O-AGB` by us and Srinivasan et al. (2009).

LHα 120−N 125 (SSID92). This object has been recognized as a point-like emission nebula on objective prism photographs of the LMC at Hα wavelengths by Henize (1956), and tentatively classified as a PN by Lindsay & Mullan (1963). The nature of this object has been confirmed by Sanduleak, MacConnell & Philip (1978), who classified it as a medium-excitation PN using very deep blue- and red-sensitive objective prism-plates. This PN is unresolved even on HST images (Shaw et al. 2006). Its chemical composition has been recently determined by Leisy & Dennefeld (2006). Gruendl & Chu (2009) also believe this to be a PN. We agree, and designate it as a carbon-rich PN (`C-PN`).

SSTISAGEMC J052101.66−691417.5 (SSID93). This is a YSO candidate according to Whitney et al. (2008), but an O-AGB according to Srinivasan et al. (2009). We class this object as `O-AGB`.

HV 942 (SSID94). Considered to be an extreme AGB star by Srinivasan et al. (2009), this object was confirmed to be an RCrB star by Soszyński et al. (2009a), in agreement with our classification, `OTHER`.

MACHO 78.6698.38 (SSID95). Identified as an RV Tau star with a period of 25 days by Percy et al. (2003), which agrees with our classification of `O-PAGB`.

SSTISAGEMC J052206.92−715017.7 (SSID96). Our classification of `O-AGB` is concurrent with that of Srinivasan et al. (2009) for this object.

SSTISAGEMC J052222.95−684101.2 (SSID97). This object is considered to be a YSO-HP by Whitney et al. (2008) and Gruendl & Chu (2009). We concur, `YSO`. However, van Loon et al. (2010) speculate that this is a galaxy from the MIPS-SED spectrum.

OGLE 052242.09−691526.2 (SSID98). This LPV has a period of 128 days in the compilation of Groenewegen (2004). Vijh et al. (2009) and Srinivasan et al. (2009) consider it to be an extreme AGB star, whilst we consider it to be `C-AGB`.

SHV 0523185−693932 (SSID99). SHV 0523185−693932 is a variable star with a period on the order of 200 days (Groenewegen 2004). This is typical of a star on the AGB, thus supporting our classification of `O-AGB`.

LHα 120−N 136 (SSID100). This object has been recognized as a point-like emission nebula on objective prism photographs of the LMC at Hα by Henize (1956), but classified as an Hα emission-line object by Lindsay & Mullan (1963) since no other nebular lines were detected on the analyzed plates. The object has been classified as PN by Sanduleak et al. (1978) of very low excitation class (Morgan

1984), which could be a member of SL434 LMC cluster (Kontizas et al. 1996). This PN is resolved and has a round shape on HST images, with radius of $\sim$0.55″ (Shaw et al. 2001). Its chemical composition has been recently determined by Leisy & Dennefeld (2006) and shows an abundance pattern which may suggest low initial abundance of its progenitor. Classified as PN by Gruendl & Chu (2009) using *Spitzer* colours, in accord with our classification, `O-PN`.

IRAS 05240−6809 (SSID101). This object is ST7 in the paper of Shimonishi et al. (2008), and they report an AKARI detection of CO_2 ice in this YSO. Oliveira et al. (2009) and Whitney et al. (2008, high probability YSO) also count this as a YSO, affirming our classification of `YSO`. Srinivasan et al. (2009) classify this as an O-AGB candidate.

IRAS 05246−7137 (SSID102). Ambiguous colours have lead Egan et al. (2001) and van Loon, Marshall & Zijlstra (2005b) to classify this object as an extreme AGB star. However, Whitney et al. (2008), Oliveira et al. (2009) and van Loon et al. (2010) classify this object as a YSO based on fits to the SED, the *Spitzer* IRS spectrum and the *Spitzer* MIPS-SED spectrum, respectively. We also classify this object as `YSO`.

SSTISAGEMC J052405.31−681802.5 (SSID103). Considered an extreme AGB star by Vijh et al. (2009) and Srinivasan et al. (2009), we consider it to be `C-AGB`.

MSX LMC 464 (SSID104). Egan et al. (2001) classify MSX LMC 464 as an OH/IR star, based on colours, whilst Kastner et al. (2008) classify it as a potential HII region based also on colours. Oliveira et al. (2009) consider it in their selection of Class I YSOs, but find no convincing detection of ice in the *Spitzer* IRS spectrum. This conflicts with a previous classification based on photometry by Whitney et al. (2008), who report this object as a high probability YSO at Stage I of evolution. Given the continuum shape and the [SIII] line in the IRS spectrum, we classify this object as `HII`, in agreement with Kastner et al. (2008).

OGLE 052445.53−691605.6 (SSID105). Groenewegen (2004) lists this star as a long-secondary-period variable, with periods of 131 days and 399 days. Srinivasan et al. (2009) classify it as an extreme AGB star, whilst we classify it as `C-AGB`.

LHα 120−S 33 (SSID106). This Hα emitter was detected by Henize (1956), Andrews & Lindsay (1964) and Bohannan & Epps (1974). We class it as `YSO`.

HV 5829 (SSID107). This object was regarded as a Type II Cepheid (Welch 1987), and originally listed in Payne-Gaposchkin (1971). More specifically, OGLE-III (Soszyński et al. 2008) categorises this object as an RV Tau star, which backs up our classification of `O-PAGB`.

SSTISAGEMC J052546.51−661411.5 (SSID108). The SED and ice features in the IRS spectrum of this object were modelled by Whitney et al. (2008) and Oliveira et al. (2009). Shimonishi et al. (2008) also were able to measure H_2O and CO_2 column densities in this YSO (ST3) using AKARI. Srinivasan et al. (2009) count this as an extreme AGB candidate, however we concur with the classification of `YSO`.

SSTISAGEMC J052613.39−684715.0 (SSID109). We classify this object as `YSO`, in agreement with Gruendl & Chu (2009).

OGLE 052620.25−693902.4 (SSID110). This is an LPV with a period in excess of 800 days (e.g., Soszyński et al. 2009b). It is considered to be O-rich by Srinivasan et al. (2009), which is in agreement with our classification of `O-AGB`.

HV 2522 (SSID111). According to Alcock et al. (1998), Payne-Gaposchkin (1971) classified this object as a Type II Cepheid, which would imply that this apparent post-AGB object may be an RV Tauri object. However, without verification we class HV 2522 as `O-PAGB`.

RP 589 (SSID112). Reid & Parker (2006) identify this object as a circular, bright PN, with Hα to the east. They give a diameter of 5.″3 in Hα and a velocity of $v_{\rm helio}$ = 261.1 km s^{-1}. The weak IRS spectrum presents no features to suggest that this object is a PN, so we classify it as `UNK`.

SSTISAGEMC J052707.10−702001.9 (SSID113). Classified as a YSO by Whitney et al. (2008), we classify this object as `O-PAGB`.

SSTISAGEMC J052723.14−712426.3 (SSID114). This object is mentioned by van Loon et al. (2010) as a potential YSO based on the appearance of the *Spitzer* MIPS-SED spectrum. Whitney et al. (2008) and Gruendl & Chu (2009) classify it similarly, with a high confidence, as do we: `YSO`.

LHα 120−N 145 (SSID115). This object has been recognized as a point-like emission nebula on objective prism photographs of the LMC in Hα by Henize (1956), and tentatively classified as PN with strong Hα emission by Lindsay & Mullan (1963). The nature of this object as PN has been confirmed by Sanduleak et al. (1978). This PN is not resolved on HST images (Shaw et al. 2006). This is a peculiar object with extremely high densities and temperature (Dopita & Meatheringham 1991) and may be one of the youngest PN. Its chemical composition has been determined several times with the most recent estimation by Leisy & Dennefeld (2006) showing a low N abundance. Srinivasan et al. (2009) classify this object as an extreme AGB, whilst Gruendl & Chu (2009) choose PN. From the IRS spectrum and SED, we classify this object as a very evolved `O-PAGB`.

HV 2551 (SSID116). This object is likely a red supergiant, with spectral type K5-M0 (Oestreicher & Schmidt-Kaler 1999). It also appears in the catalogs of red supergiant candidates from Westerlund et al. (1981) and Sanduleak & Philip (1977). We classify it as `RSG`.

W61 11−16 (SSID117). This star is given a spectral type of M1 in the catalog of supergiants of Elias, Frogel & Humphreys (1985) and K7 I in the catalog of Massey & Olsen (2003). The latter authors also calculate $M_{\rm bol}$=−8.23 mag, which supports our classification of `RSG`.

SSTISAGEMC J052747.62−714852.8 (SSID118). Whitney et al. (2008) classify this star as a YSO, but with a low confidence. Srinivasan et al. (2009) consider it to be an extreme AGB star. Henize (1956) lists this star as an Hα emitter, which supports our classification of `O-PAGB`.

SHV 0528350−701014 (SSID119). This LPV has a period on the order of 600 days according to Groenewegen (2004), and is a candidate for an obscured AGB star in that paper. Srinivasan et al. (2009), as well, count this object amongst their extreme, or obscured, AGB stars. We concur, with our classification of `C-AGB`.

OGLE 052825.96-694647.4 (SSID120). This star is classified by Kontizas et al. (2001), Srinivasan et al. (2009)

and Groenewegen (2004) as a C-rich AGB star. The latter author notes that it has periods of 135 and 390 days. This supports our classification of `C-AGB`.

IRAS 05298−6957 (SSID121). This is a well-studied oxygen-rich massive ($4\,M_\odot$) AGB star with a high mass-loss rate (van Loon et al. 2010, and references within). Vijh et al. (2009), Srinivasan et al. (2009) and Gruendl & Chu (2009) consider it to be an extreme AGB star. We agree with this classification, `O-AGB`.

HV 5879 (SSID122). Oestreicher & Schmidt-Kaler (1998) derive an effective temperature of 3 675 K for this star from an unpublished optical spectrum, which would indicate a spectral type of ∼M0Iab for a supergiant. Massey & Olsen (2003) give a similar spectral type and effective temperature. They also calculate $M_{\rm bol}$=−8.26 mag. These classifications would suggest that our classification of `RSG` is correct.

SP77 46-50 (SSID123). Sanduleak & Philip (1977) identify this star as spectral type M in their supergiant catalog, and photometry and colours from Massey (2002) and the 2MASS and DENIS databases would seem to confirm our classification of `RSG`. Massey & Olsen (2003) calculate $M_{\rm bol}$=−7.44 mag.

SHV 0530472-690607 (SSID124). This object has a well-defined period of 212 days (Hughes 1989; Soszyński et al. 2009b). We classify it as `O-AGB`.

IRAS 05315−7145 (SSID125). This is an ERO according to Gruendl et al. (2008) and Gruendl & Chu (2009), and was not detected by van Loon et al. (1997) since it is very faint at K-band. We class this object as `C-AGB`.

KDM 4554 (SSID126). Classified as C-AGB by Kontizas et al. (2001) based on the detection of C_2 bands, and an extreme AGB star according to Srinivasan et al. (2009), this star is `C-AGB` in our classification scheme.

NGC 2004 Robb B45 (SSID127). NGC 2004 is a young cluster with an age of 8–10 Myr (Wolf et al. 2007; Hodge 1983). This particular star has a B−V colour which is consistent with an early M spectral type. Bencivenni et al. (1991) classify this object as a red supergiant based upon the assumed V absolute magnitude. This information backs up our classification of `RSG`.

NGC 2004 Wes 18-13 (SSID128). The spectral type given in Elias et al. (1985) is K1Ib, with V=13.053 and B=14.465. The B-V colour is roughly consistent with the spectral type, or one a little later. This affirms our classification of `RSG`.

NGC 2004 Wes 6-14 (SSID129). The spectral type given in Elias et al. (1985) is K0Ib, with V=12.95 and B=14.60. The B-V colour is a bit red for the spectral type, nominally it would match a K5I star. A bolometric magnitude of −8.1 mag is calculated by Massey & Olsen (2003), confirming our classification of `RSG`.

SSTISAGEMC J053128.44−701027.1 (SSID130). This is a YSO candidate according to Whitney et al. (2008), but its ≈400 day period (Fraser et al. 2005, 2008; Soszyński et al. 2009b) would indicate that it is an evolved star. Srinivasan et al. (2009) classify it as C-AGB, but we consider it to be `O-AGB`.

MACHO 82.8405.15 (SSID131). Alcock et al. (1998) identified this object as an RV Tau star based on its MACHO light curve, and this was confirmed by Percy et al. (2003) and given a period of 47 days. Reyniers & Van Winckel (2007) found a depletion pattern which is typically found in RV Tau stars with a binary disc. This fortifies our classification of `O-PAGB`. Gruendl & Chu (2009), however, classify this object as a stellar photosphere.

KDM 4665 (SSID132). Categorised as a carbon-rich AGB star by Kontizas et al. (2001) and Srinivasan et al. (2009), with which we agree, `C-AGB`.

SSTISAGEMC J053206.70−701024.8 (SSID133). This star is assigned a period of ∼120 days in the MACHO and OGLE-III catalogs, and classified as an O-rich AGB star in the latter, as well as in Srinivasan et al. (2009). We classify it as `STAR`, given its lack of mid-infrared dust features.

SSTISAGEMC J053218.64−673145.9 (SSID134). This star may be associated with the nearby young cluster NGC 2011 (see SSID135). No other information could be found on this object, which we classify as `RSG`.

NGC 2011 SAGE IRS 1 (SSID135). NGC 2011 is a young, resolved open cluster for which photometry is given in the catalog of Kumar, Sagar & Melnick (2008) (SAGE IRS 1 is star #4). The age of this cluster is given by Wolf et al. (2007), Hodge (1983) and Santos et al. (1995) as 5–6 Myr. There is a star with V=12.90, B-V=1.97, and V-R=0.56 very close to the *SAGE-Spec* position. The colours are not consistent, the V−R colour should be much larger for the measured B−V (nominally >2 magnitudes). An integrated spectrum of NGC 2011 in the K-band shows a typical M-type supergiant CO band, and from the 2MASS image of the cluster it is clear that this would be dominated by SAGE IRS 1. The only other object of comparable brightness nearby is about 25″ to the south which is too far away to contribute to the near infrared spectrum reported by Oliva & Origlia (1998). Massey & Olsen (2003) calculate $M_{\rm bol}$=−7.74 mag. These facts corroborate with our classification of `RSG`.

KDM 4718 (SSID136). This star was classified as a carbon-rich AGB star by Kontizas et al. (2001) based on the detection of C_2 bands and also by Srinivasan et al. (2009) using Spitzer colours. We too classify this object as `C-AGB`.

RP 774 (SSID137). RP 774 is thought by Reid & Parker (2006) to be a PN based on Hα maps of the LMC. However, it is classified as a YSO by Gruendl & Chu (2009) which agrees with our classification, `YSO`.

SSTISAGEMC J053253.36−660727.8 (SSID138). This is a high-probability YSO according to Whitney et al. (2008) and a background galaxy according to Gruendl & Chu (2009). We agree with Gruendl & Chu (2009), classing this object as `GAL`.

KDM 4774 (SSID139). Categorized as a carbon-rich star, according to Kontizas et al. (2001) and Srinivasan et al. (2009), with which we agree, `C-AGB`.

MSX LMC 736 (SSID140). This object is classified by Egan et al. (2001) as an HII region, based on infrared colours. However, Vijh et al. (2009), Gruendl & Chu (2009) and Srinivasan et al. (2009) categorise this star as an (extreme) AGB star. We classify it as `C-AGB`.

SSTISAGEMC J053318.58−660040.2 (SSID141). Classified as an extreme AGB by Srinivasan et al. (2009), we specify that it is a `C-AGB`.

SSTISAGEMC J053343.27−705921.1 (SSID142). We classify this star as `O-AGB`, in agreement with Srinivasan et al. (2009).

SSTISAGEMC J053343.98−705901.9 (SSID143).

We classify this star as `O-AGB`, in agreement with Srinivasan et al. (2009).

LHα 120−N 151 (SSID144). This object has been recognized as a point-like emission nebula on objective prism photographs of the LMC at Hα by Henize (1956), and tentatively classified as a PN with strong Hα emission by Lindsay & Mullan (1963). The object has been recognized as a PN by Westerlund & Smith (1964) and classified as PN of medium excitation class by Sanduleak et al. (1978). This PN could be a member of the LMC cluster 1086 SL580 (Kontizas et al. 1996). It is resolved and has a round shape on HST images with radius of $\sim 0\farcs33$ (Shaw et al. 2006). Its chemical composition has been determined several times with the most recent estimation by Leisy & Dennefeld (2006). Gruendl & Chu (2009) also classify this object as PN. We, too, classify this object as a PN, designating it carbon-rich, `C-PN`.

SSTISAGEMC J053441.40−692630.6 (SSID145). This object lies very close to planetary nebula RP 793, with which it is confused in the SIMBAD database. However, it is clearly a `C-AGB`, and Soszyński et al. (2009b) agree.

SHP LMC 256 (SSID146). Santos et al. (1995) identify a ROSAT X-ray source near this object ($6''$ away), which may be associated, since it lies within the ROSAT pointing accuracy. This has also been detected by the X-ray Multi-Mirror Mission (XMM/2XMMi), with a spectral energy distribution peaking around 1 keV. The *Spitzer* IRS spectrum is extremely unusual, and hence we classify this object as `UNK`.

HV 2700 (SSID147). SIMBAD gives the spectral type as M2Iab, based on optical spectra in the red (Wood, Bessell, Fox 1983) and blue (Humphreys 1979) parts of the spectrum. This would validate our classification of `RSG`.

SSTISAGEMC J053548.07−703146.6 (SSID148). This LPV has a period of nearly 1 000 days (Fraser et al. 2005, 2008; Soszyński et al. 2009b). Srinivasan et al. (2009) class it as an oxygen-rich AGB star, with which we agree, `O-AGB`.

SSTISAGEMC J053602.36−674517.3 (SSID149). This object is listed as a possible PN by Reid & Parker (2006), but it exhibits no clear emission lines in the IRS spectrum. We classify this object as `YSO`.

IRAS 05370−7019 (SSID150). This object is associated with IRAS 05370−7019 and LI-LMC 1424 and regarded as an unidentified source by (Loup et al. 1997). Gruendl & Chu (2009) consider this object to be a (post-)AGB object, while conversely Whitney et al. (2008) classify this object as a high probability YSO. We agree with Gruendl & Chu (2009), classifying it as `C-PAGB`.

SSTISAGEMC J053634.77−722658.6 (SSID151). This object seems unknown in the literature, and will be the subject of a paper by Hony et al., in prep. We classify it as `GAL`.

SSTISAGEMC J053655.60−681124.5 (SSID152). This star too is relatively unstudied in the literature, but is classified as an oxygen-rich AGB star by Srinivasan et al. (2009) and Soszyński et al. (2009b). We concur, `O-AGB`.

RP 493 (SSID153). Identified by Reid & Parker (2006) as a small, elliptical PN with a high degree of confidence. These authors give a diameter of $4\farcs0$ in Hα and a velocity of $v_{\rm helio} = 326.8\,{\rm km\ s^{-1}}$. We classify this object as `O-PN`.

SSTISAGEMC J053730.59−674041.6 (SSID154). This object is a Stage I YSO candidate according to Whitney et al. (2008), however we classify it as `GAL`.

KDM 5345 (SSID155). This optically-identified carbon-star (Kontizas et al. 2001) exhibits carbon-rich features in its IRS spectrum but also oxygen-rich features. We tentatively suggest that this object is a mixed-chemistry AGB star, and due to this uncertainty only classify it as `UNK`.

OGLE J053930.16−695755.8 (SSID156). This LPV has a period of 291.6 days according to Groenewegen (2004). It is an extreme AGB star according to Srinivasan et al. (2009) and Vijh et al. (2009). We classify it as `C-AGB`.

HV 12631 (SSID157). Alcock et al. (1998) identified this object as an RV Tau star, based on MACHO light curve (MACHO 14.9582.9), and Percy et al. (2003) confirmed this. This star has a period of 31 days. This strengthens our classification of `O-PAGB`. Srinivasan et al. (2009) consider it to be an O-AGB star.

SSTISAGEMC J053942.45−711044.5 (SSID158). This could be the planetary nebula RP618, listed by Reid & Parker (2006) and Whitney et al. (2008) as a possible PN. However, Vijh et al. (2009) and Gruendl & Chu (2009) believe this to be a YSO. We also classify it as a `YSO`.

SSTISAGEMC J053945.40−665809.4 (SSID159). This star has a period of 125 days according to MACHO, and is classified as an oxygen-rich AGB star by Srinivasan et al. (2009). We agree with this classification, `O-AGB`.

SSTISAGEMC J053949.23−693747.0 (SSID160). The IRS spectrum towards this object is very weak, and so we classify it as `UNK`. Gruendl & Chu (2009) classify this object as a probable YSO or star using Spitzer photometry.

MACHO 81.9728.14 (SSID161). This object is classified as a possible RV Tau star, based on MACHO light curve (Alcock et al. 1998). Percy et al. (2003) re-analysed the light curve, and they identified this as only a potential RV Tau star, given the paucity of the MACHO data. They derived a period of 47 days, as did Soszyński et al. (2008), who classified it as an RV Tau star. The IRS spectrum points to the same conclusion, despite contamination by PAH emission, hence our classification of `O-PAGB`.

MSX LMC 949 (SSID162). This object was not classified by Egan et al. (2001) since it is rather faint in JHK_S. It is an extreme AGB star according to Srinivasan et al. (2009) and a (post-)AGB star or star according to Gruendl & Chu (2009). We classify it as `O-PAGB`.

RP 85 (SSID163). Listed by Reid & Parker (2006) as a likely PN, but as a YSO by Gruendl & Chu (2009). Van Loon et al. (2010) suggest that a faint and flat dust continuum with weak emission lines at MIPS-SED wavelengths is strongly suggestive that RP 85 is a PN. We agree with Gruendl & Chu (2009), classifying this object as a `YSO`.

SSTISAGEMC J054059.31−704402.5 (SSID164). SSTISAGEMC J054059.31−704402.5 was successfully modelled by Whitney et al. (2008) and Oliveira et al. (2009) as a YSO, and classified as such by Gruendl & Chu (2009), thus supporting our classification, `YSO`.

MSX LMC 947 (SSID165). Unanimous agreement between Egan et al. (2001), Vijh et al. (2009), Srinivasan et al. (2009) and ourselves that this object is an `O-AGB`. It has a period of ≈700 days (Soszyński et al. 2009b).

SSTISAGEMC J054114.56−713236.0 (SSID166). We

classify this object as O-AGB, as do Srinivasan et al. (2009). It has a period of 583 days according to the MACHO database.

IRAS 05416−6906 (SSID167). This object is variously classed as YSO (Whitney et al. 2008; Vijh et al. 2009), HII region (Egan et al. 2001), and extreme AGB star (Srinivasan et al. 2009). We classify it as C-AGB.

IRAS 05421−7116 (SSID168). IRAS 05421-7116 was successfully modelled by Whitney et al. (2008) and Oliveira et al. (2009) as a Stage I YSO, and classified as such by Gruendl & Chu (2009), thus supporting our classification of YSO.

W61 6-24 (SSID169). A spectral type of M was assigned by Sanduleak & Philip (1977), and with a B−V value of 2.7 magnitudes this object does appear to be of early M-type. This star is also a member of the very young cluster NGC 2100, which has an age of 6–10 Myr (Wolf et al. 2007; Hodge 1983; Santos et al. 1995). Thus our classification of RSG is reinforced.

NGC 2100 Robb 4 (SSID170). This object has V=13.58 and B−V equal to 2.04 (Rebeirot et al. 1983), which implies that it is a late M-type star. The CO band index (in the 2.2 μm window) measured by Elias et al. (1985) matches the values for various early M-type supergiants observed in that paper. Reference is made to HST WFPC2 images of the NGC 2100 cluster to get an estimated V magnitude for the star, from which a V−K value is given by Keller (1999). The JHK values given in that paper do not agree with the 2MASS photometry (potentially due to variability), but the V−K values in either case are relatively large and suggest that the star is of late type. Estimates of cluster age are on the order of 10–30 Myr (Wolf et al. 2007), and the chemistry is thought to be oxygen-rich by van Loon et al. (2005b), upholding our classification of RSG.

2MASS J05420676−6912312 (SSID171). UBV photometry is given in the PhD thesis of Braun (2001). The B−V value of 1.97 implies that the star is of late M-type. The same is true of the J−K value from 2MASS or DENIS, which affirms our classification of RSG.

W61 6-57 (SSID172). This star also has B−V values from the Braun (2001) thesis and infrared data from DENIS and 2MASS. The values B−V = 2.16 and V−K = 1.2 suggest that the star is of late M-type. The K-band CO index from Elias et al. (1985) is consistent with an early M spectral type. A medium optical spectrum was taken of this star, as reported by Jasniewicz & Thévenin (1994). They do not report a spectral type but give fitted values $T_{\rm eff}$ = 4 032 K and log(g) of 1.0 derived from the spectrum. That would seem to match a K-type giant/supergiant rather than an M-type supergiant. However, both types are consistent with our classification of RSG.

WOH G 494 (SSID173). This star is classified as an M giant by Westerlund et al. (1981) and as a carbon-rich AGB star by OGLE-III (although the data quality is far from optimal; Soszyński et al. 2009b). Assigned periods range from 170–333 days (Soszyński et al. 2009b; Fraser et al. 2005, 2008). Srinivasan et al. (2009) classify it as O-AGB, and this agrees with our classification, O-AGB.

LM 2-42 (SSID174). This object has been classified as an Hα emission-line object by Lindsay & Mullan (1963) since no other nebular lines except that of Hα were detected on the analyzed plates. The nature of this object as a PN has been recognized by Sanduleak et al. (1978). This PN could be member of the LMC cluster KMHK 1280/HS 398 (Kontizas et al. 1996). It is compact and elliptical in Hα images (RP 10 Reid & Parker 2006) and is resolved in HST images (Shaw et al. 2006, 0.″61×0.″45). Its chemical composition has been determined several times with the most recent estimation by Leisy & Dennefeld (2006). We classify it as O-PN.

LHα 120-N 178 (SSID175). This object also has been recognized as a point-like emission nebula on objective prism photographs of the LMC at Hα by Henize (1956), and tentatively classified as a PN with strong Hα emission by Lindsay & Mullan (1963). The object has been recognised as a PN by Westerlund & Smith (1964) and classified as a PN of medium excitation class by Sanduleak et al. (1978). It is resolved and has an elliptical shape (0.″51×0.″45) with possible internal structure on HST images (Shaw et al. 2006). Its chemical composition has been determined several times with the most recent estimation by Leisy & Dennefeld (2006). Gruendl & Chu (2009) also classify this object as PN, and we specify carbon chemistry, C-PN.

SSTISAGEMC J054254.38−700807.4 (SSID176). Soszyński et al. (2009b) and Srinivasan et al. (2009) both classify this object as O-AGB, as do we, O-AGB.

SSTISAGE1C J054310.86−672728.0 (SSID177). This object appears very close to the position of IRAS F05432−6728, which has F_{12}=88 and F_{25}=136 mJy, in reasonable agreement with the *Spitzer* IRS spectrum. However, F_{60}=1 916 and F_{100}=3 873 mJy for this object, which would be unusual for an oxygen-rich post-AGB object, and does not fit with the long-wavelength part of the IRS spectrum. AKARI recently detected an object in a nearby position with F_9=75 and F_{18}=133 (Ishihara et al. 2010), also in excellent agreement with the IRS spectrum. Gruendl & Chu (2009) suggest that this object is in the (post-)AGB phase, and that is our conclusion from the IRS spectrum (O-PAGB). SSID177 is probably not related to the faint IRAS source, but potentially to the AKARI source, 0543108-672730.

SSTISAGEMC J054314.12-703835.1 (SSID178). This object is located close to the 130–380 Myr (Frantsman 1988) cluster NGC 2107, but there are no indications that this object is a part of it. The MACHO and OGLE-III catalogs list a period of ∼160 days, and OGLE-III classifies this object as a C-rich AGB star (Soszyński et al. 2009b). However, an SiO feature is clearly visible in the IRS spectrum, which leads us to classify this object as O-AGB. Srinivasan et al. (2009) agree.

KDM 5841 (SSID179). This object shows near-infrared C_2 bands (Kontizas et al. 2001) and has *Spitzer* colours similar to that of a carbon-rich AGB star (Srinivasan et al. 2009), and thus is confirmed as C-AGB.

SSTISAGEMC J054406.01−683753.6 (SSID180). Srinivasan et al. (2009) class this as an O-rich AGB star, and it has periods in the range 239–554 days (Fraser et al. 2005, 2008; Soszyński et al. 2009b). We also classify it as O-AGB.

SSTISAGEMC J054437.87−673657.7 (SSID181). According to Srinivasan et al. (2009) and Vijh et al. (2009) this object is an extreme AGB star. We classify it as C-AGB.

SSTISAGEMC J054440.11−691149.0 (SSID182). We classify this object as O-AGB, in agreement with

Srinivasan et al. (2009) and the 99-day period of Soszyński et al. (2009b).

IRAS 05452−6924 (SSID183). The SED of IRAS 05452-6924 was fitted by Whitney et al. (2008) with a YSO model, and the ice features in this object's IRS spectrum were modelled by Oliveira et al. (2009). Gruendl & Chu (2009) are also in agreement. This confirms our classification of `YSO`.

SSTISAGEMC J054524.23−683041.4 (SSID184). This is a YSO candidate according to Whitney et al. (2008), whilst Gruendl & Chu (2009) classify it as a galaxy. We, too, classify it as `GAL`.

SSTISAGEMC J054546.32−673239.4 (SSID185). This is a YSO candidate according to Whitney et al. (2008), but we classify it as `O-AGB`.

LHα 120−N 170 (SSID186). This object also has been recognized as a point-like emission nebula on objective prism photographs of the LMC at Hα by Henize (1956), and tentatively classified as PN with strong Hα emission by Lindsay & Mullan (1963). The object has been recognized as a PN by Westerlund & Smith (1964) and classified as a PN of high excitation class by Sanduleak et al. (1978). This PN could be a member of LMC cluster KMHK 1364 (Kontizas et al. 1996). It is resolved and has an elliptical shape ($0\farcs62\times0\farcs54$) with internal structure on HST images (Shaw et al. 2006). Its chemical composition has been determined several times with the most recent estimation by Leisy & Dennefeld (2006). Gruendl & Chu (2009) also agree that this object is a PN. This corroborates our classification of `O-PN`.

SSTISAGEMC J054745.79−680734.1 (SSID187). This object has an extremely long period of 2 599 days according to Fraser et al. (2005, 2008). It is a YSO candidate according to Whitney et al. (2008), and this agrees with our classification, `YSO`.

KDM 6247 (SSID188). This object appears in the carbon star catalog of Kontizas et al. (2001), based on the detection of Swan C_2 bands. Sanduleak & Philip (1977) also include it in their catalog of carbon stars. Srinivasan et al. (2009), however, class KDM 6247 as an O-AGB. No distinguishing features are seen in the IRS spectrum, and so we class this object as `STAR`.

NGC 2121 LE 6 (SSID189). This object is a member of the cluster NGC 2121, which has an age of ∼3.2 Gyr (Mackey & Gilmore 2003), and is thought to host carbon stars (van Loon et al. 2005b). An extreme AGB according to Srinivasan et al. (2009), we class it as `C-AGB`.

IRAS 05495−7034 (SSID190). Whitney et al. (2008) consider this object to be a high-probability YSO, whereas Gruendl et al. (2008) class it as an ERO. Our classification is in alignment with Gruendl et al. (2008), `C-AGB`.

KDM 6486 (SSID191). This object is a part of the carbon star catalog of Kontizas et al. (2001), and part of the C-AGB grouping of Srinivasan et al. (2009) which fortifies our classification of `C-AGB`.

HV 2862 (SSID192). This object is known to be a variable star (Lindsay 1974), with a period of 34 days (Fraser et al. 2005, 2008). Soszyński et al. (2008) have classified this star as an RV Tau star, which supports our classification of `O-PAGB`. Gruendl & Chu (2009), however, class this as a star.

SSTISAGEMC J055143.27−684543.0 (SSID193). According to Whitney et al. (2008), this is a high-probability Stage I YSO. However, we disagree and classify this object as `GAL`. There is a radio source located within 3′ (MDM 111; Marx et al. 1997).

PMP 337 (SSID194). This chemically peculiar star is a member of NGC 2136/7, which has an age of 100 Myr (Paunzen et al. 2006). Srinivasan et al. (2009) class this as a C-AGB, and we agree with that classification, `C-AGB`.

PMP 133 (SSID195). This is a chemically peculiar star included in the catalog of Paunzen et al. (2006). As such, this makes it a low- to intermediate-mass star. This agrees with our classification of `STAR`.

IRAS 05537−7015 (SSID196). Mentioned in Loup et al. (1997) as a good candidate for an evolved star, Gruendl & Chu (2009) label this as (post-)AGB. We agree, classifying this object as `C-PAGB`.

SSTISAGEMC J060053.62−680038.8 (SSID197). This star has periods of 281 and 887 days (Fraser et al. 2005, 2008) and is classified as an oxygen-rich AGB star by Srinivasan et al. (2009). We agree, with our classification of `O-AGB`.

This paper has been typeset from a TEX/ LATEX file prepared by the author.

The complete Table 3 follows.

TABLE 3

CLASSIFICATION OF POINT SOURCES TARGETED IN IRS STARING MODE AS PART OF THE *SAGE-Spec* PROGRAM.

SSID	Name[c]	Observed R. A. & Dec. (J2000)	SSTISAGEMC designation[d]	MACHO designation	MACHO[a] period (d)	OGLE-LMC designation	OGLE[b] period (d)	Classification
1	NGC 1651 SAGE IRS 1	$04^h37^m21.15^s$ $-70°34'44.57''$	J043721.15−703444.7	...	...	LPV-00749	101	O-AGB
2	...	$04^h37^m27.69^s$ $-67°54'34.94''$	J043727.61−675435.1	...	...	...	...	GAL
3	...	$04^h46^m27.15^s$ $-68°47'46.83''$	J044627.10−684747.0	45.909.2	386–397	LPV-02759	389	C-AGB
4	...	$04^h47^m18.63^s$ $-69°42'20.53''$	J044718.63−694220.6	...	...	...	...	RSG
5	...	$04^h48^m37.75^s$ $-69°23'36.85''$	J044837.77−692337.0	...	...	...	...	YSO-2
6	...	$04^h49^m34.38^s$ $-69°05'49.17''$	J044934.31−690549.3	...	...	...	...	O-AGB
7	MSX LMC 1128	$04^h50^m40.57^s$ $-68°58'18.76''$	J045040.52−685819.0	45.1632.952	437–445	LPV-04314	441	C-AGB
8	...	$04^h51^m28.58^s$ $-69°55'49.92''$	J045128.58−695550.1	44.1739.170	907–911	LPV-04685	884	O-AGB
9	IRAS 04518−6852	$04^h51^m40.63^s$ $-68°47'34.82''$	J045140.57−684734.6	...	...	...	...	C-AGB
10	...	$04^h52^m00.38^s$ $-69°18'05.53''$	J045200.36−691805.6	...	...	...	...	YSO-2
11	...	$04^h52^m28.66^s$ $-68°54'51.09''$	J045228.68−685451.3	...	...	...	...	YSO-1
12	KDM 764	$04^h52^m32.49^s$ $-67°02'59.30''$	J045232.54−670259.2	48.2024.11	250–873	LPV-05238	445	C-AGB
13	...	$04^h53^m09.54^s$ $-68°17'10.11''$	J045309.39−681710.8	47.2127.16	207–1122	LPV-05538	915	O-AGB
14	IRAS F04532−6709	$04^h53^m11.03^s$ $-67°03'55.96''$	MA J045311.08−670355.6	...	...	...	...	YSO-1
15	...	$04^h53^m28.71^s$ $-66°03'34.76''$	J045328.70−660334.4	54.2160.204	2710	...	...	C-AGB
16	GV 60	$04^h53^m30.86^s$ $-69°17'49.85''$	J045330.88−691749.7	...	...	...	...	RSG
17	LHα 120−N 82	$04^h53^m30.86^s$ $-69°17'49.85''$	2C J045330.15−691749.5	...	...	...	...	OTHER (W-R)
18	...	$04^h53^m44.28^s$ $-66°11'45.76''$	J045344.24−661146.0	...	...	...	...	C-AGB
19	...	$04^h54^m22.88^s$ $-70°26'56.64''$	J045422.82−702657.0	...	...	...	...	STAR
20	...	$04^h55^m26.76^s$ $-68°25'07.93''$	J045526.69−682508.4	...	...	...	...	YSO-3
21	...	$04^h55^m34.06^s$ $-65°57'00.92''$	J045534.07−655701.3	...	...	...	...	YSO-4
22	...	$04^h56^m23.27^s$ $-69°27'48.05''$	J045623.21−692749.0	17.2593.214	undef.	...	...	O-AGB
23	KDM 1238	$04^h58^m55.03^s$ $-69°11'18.21''$	J045855.02−691118.7	18.2960.23	376–543	LPV-09687	133	C-AGB
24	RP 1805	$04^h58^m55.29^s$ $-68°50'36.13''$	—	...	...	...	...	UNK
25	...	$05^h00^m32.59^s$ $-66°21'12.60''$	J050032.61−662113.0	...	...	...	...	YSO-4
26	RP 1631	$05^h00^m34.69^s$ $-70°52'00.34''$	J050034.61−705200.4	...	...	...	...	OTHER (RCrB)
27	MSX LMC 1271	$05^h02^m21.52^s$ $-66°06'37.98''$	J050221.46−660638.3	...	...	...	...	RSG
28		$05^h02^m24.21^s$ $-66°06'37.46''$	J050224.17−660637.4	...	...	...	...	O-PAGB
29	HV 2281	$05^h03^m04.98^s$ $-68°40'24.90''$	J050304.95−684024.7	19.3694.19	32	T2CEP-029	31	O-PAGB (RV Tau)
30	KDM 1656	$05^h03^m16.59^s$ $-65°49'44.79''$	J050316.60−654945.1	55.3736.12	1035	...	...	C-AGB
31	KDM 1691	$05^h03^m36.89^s$ $-68°33'38.71''$	J050336.92−683338.5	19.3817.12	503–512	LPV-14408	519	C-AGB
32	LMC−BM 11−19	$05^h03^m42.54^s$ $-67°59'18.83''$	J050342.57−675919.2	24.3825.2539	894–1082	LPV-14513		STAR
33	LMC−BM 12−14	$05^h03^m53.50^s$ $-70°27'47.53''$	J050353.40−702747.6	23.3788.9	405–894	LPV-14750	220	C-AGB
34	...	$05^h03^m54.60^s$ $-67°18'47.69''$	J050354.55−671848.7	...	...	...	...	YSO-1
35	NGC 1818 WBT 5	$05^h04^m07.38^s$ $-66°26'42.71''$	J050407.42−662643.0	53.3848.14	360–1707	...	...	RSG
36	NGC 1818 WBT 64	$05^h04^m07.73^s$ $-66°25'05.48''$	J050407.72−662505.9	53.3849.19	831–848	...	...	C-AGB
37	NGC 1818 WBT 3	$05^h04^m11.09^s$ $-66°26'16.70''$	J050411.04−662616.8	53.3848.13	360	...	...	RSG
38	MSX LMC 61	$05^h04^m28.91^s$ $-67°41'23.43''$	J050428.91−674123.9	25.3951.67	576–1585	LPV-15419	577	O-AGB

TABLE 3—*Continued*

SSID	Name[c]	Observed R. A. & Dec. (J2000)	SSTISAGEMC designation[d]	MACHO designation	MACHO[a] period (d)	OGLE-LMC designation	OGLE[b] period (d)	Classification
39	RP 1878	$05^h04^m34.17^s$ $-67°52'21.05''$	J050434.20−675221.8	...	...	...	...	UNK
40	IRAS 05047−6642	$05^h04^m51.71^s$ $-66°38'07.41''$	J050451.70−663807.5	53.3966.918	20	...	...	YSO-3
41	...	$05^h05^m03.22^s$ $-69°24'26.51''$	J050503.21−692426.5	...	...	LPV-16169	217	C-AGB
42	...	$05^h05^m17.19^s$ $-69°21'57.12''$	J050517.08−692157.0	...	...	...	...	GAL
43	LMC−BM 13−2	$05^h05^m55.74^s$ $-67°22'09.24''$	J050555.66−672210.0	52.4197.4218	2545	LPV-17258	206	C-AGB
44	...	$05^h05^m58.26^s$ $-68°09'23.79''$	J050558.23−680923.6	19.4186.889	undef.	...	...	YSO-4
45	...	$05^h06^m07.51^s$ $-71°41'48.12''$	J050607.50−714148.4	38.4132.5	346	...	...	C-AGB
46	KDM 1961	$05^h06^m12.61^s$ $-64°55'37.23''$	J050612.59−645537.5	...	...	...	...	C-AGB
47	KDM 1966	$05^h06^m18.95^s$ $-64°56'10.88''$	J050618.98−645610.2	...	...	...	...	C-AGB
48	...	$05^h06^m20.13^s$ $-64°54'58.01''$	J050620.12−645458.6	...	...	...	...	C-AGB
49	...	$05^h06^m29.62^s$ $-68°55'34.54''$	J050629.61−685534.9	1.4174.40	261–267	LPV-17926	154	C-AGB
50	...	$05^h06^m39.24^s$ $-68°22'09.32''$	J050639.14−682209.3	...	...	...	...	OTHER (BSG)
51	SHV 0507252−690238	$05^h07^m09.47^s$ $-68°58'50.18''$	J050707.81−685852.7	1.4294.22	undef.	LPV-18832	507	C-AGB
52	...	$05^h07^m14.00^s$ $-67°48'46.46''$	J050713.90−674846.7	...	...	...	...	C-PAGB
53	...	$05^h07^m53.01^s$ $-68°12'46.38''$	J050752.93−681246.5	19.4427.193	335–335	LPV-19934	302	C-AGB
54	...	$05^h07^m59.36^s$ $-68°39'25.71''$	J050759.35−683925.8	19.4541.306	359–362	LPV-20082	150	O-AGB
55	...	$05^h08^m26.27^s$ $-68°31'15.01''$	J050826.35−683115.1	19.4543.3947	undef.	LPV-20709	400	C-AGB
56	...	$05^h08^m30.62^s$ $-69°22'37.39''$	J050830.51−692237.4	...	...	LPV-20807	115	O-PAGB
57	KDM 2187	$05^h08^m36.42^s$ $-69°43'15.11''$	J050836.39−694315.7	5.4525.42	1229–1361	LPV-20969	758	C-AGB
58	BMB−BW 180	$05^h09^m26.44^s$ $-69°06'56.99''$	J050926.57−690656.3	79.4655.3986	69–69	LPV-22320	68	O-AGB
59	NGC 1856 SAGE IRS 1	$05^h09^m29.54^s$ $-69°07'50.90''$	J050929.53−690750.3	...	...	...	...	O-AGB
60	...	$05^h10^m28.38^s$ $-68°44'31.44''$	J051029.27−684431.2	...	...	LPV-24027	465	C-AGB
61	...	$05^h10^m59.06^s$ $-68°56'13.82''$	J051059.07−685613.7	79.5021.10	175–280	LPV-24921	169	O-AGB
62	MSX LMC 209	$05^h12^m09.19^s$ $-71°06'49.52''$	J051209.02−710649.7	...	...	LPV-26931	28	YSO-4
63	...	$05^h12^m13.57^s$ $-68°39'22.47''$	J051213.54−683922.8	2.5146.30	846–847	LPV-27065	111	O-AGB
64	...	$05^h12^m28.17^s$ $-69°07'56.15''$	J051228.19−690755.8	79.5260.1862	undef.	...	...	C-PAGB
65	IRAS 05133−6937	$05^h13^m01.80^s$ $-69°33'51.21''$	J051301.75−693351.0	...	...	...	...	C-AGB
66	OGLE J051306.52−690946.4	$05^h13^m06.43^s$ $-69°09'46.53''$	J051306.49−690955.3	79.5259.938	undef.	LPV-28579	356	C-AGB
67	...	$05^h13^m39.87^s$ $-66°38'52.70''$	J051339.94−663852.5	58.5418.23	831–843	LPV-29579	742	O-AGB
68	NGC 1866 Robb B136	$05^h13^m41.42^s$ $-65°28'27.91''$	J051341.40−652828.2	59.5436.11	122–122	...	...	O-AGB
69	BSDL 923	$05^h13^m42.83^s$ $-67°24'10.44''$	J051342.63−672409.9	...	...	...	...	OTHER (BSG)
70	...	$05^h13^m47.79^s$ $-69°35'05.06''$	J051347.72−693505.2	...	...	...	...	YSO-1
71	...	$05^h13^m48.33^s$ $-67°05'26.87''$	J051348.38−670527.0	...	...	...	...	HII
72	...	$05^h14^m12.32^s$ $-68°50'58.29''$	J051412.33−685058.0	79.5506.20	694	LPV-30640	795	O-AGB
73	HV 915	$05^h14^m18.15^s$ $-69°12'35.06''$	J051418.09−691234.9	79.5501.13	97	T2CEP-067	48	O-PAGB (RV Tau)
74	...	$05^h14^m49.41^s$ $-67°12'22.24''$	J051449.43−671221.4	...	...	...	...	YSO-1
75	...	$05^h14^m53.12^s$ $-69°17'23.70''$	J051453.10−691723.5	...	...	...	...	O-PAGB
76	...	$05^h15^m26.47^s$ $-67°51'26.91''$	J051526.44−675126.9	16.5763.20	441	LPV-33019	107	STAR

TABLE 3—*Continued*

SSID	Name[c]	Observed R. A. & Dec. (J2000)	SSTISAGEMC designation[d]	MACHO designation	MACHO[a] period (d)	OGLE-LMC designation	OGLE[b] period (d)	Classification
77	...	$05^h16^m12.52^s$ $-70°49'30.18''$	J051612.42−704930.3	13.5840.19	746–776	LPV-34633	768	O-AGB
78	IRAS 05170−7156	$05^h16^m18.69^s$ $-71°53'59.21''$	J051618.69−715359.0	...	...	...	...	UNK
79	...	$05^h17^m47.16^s$ $-68°18'42.64''$	J051747.18−681842.6	...	...	LPV-37798	80	O-AGB
80	...	$05^h18^m03.28^s$ $-68°49'50.29''$	1C J051803.28−684950.6	...	...	LPV-38325	349	C-AGB
81	KDM 3196	$05^h18^m07.94^s$ $-71°51'53.66''$	J051807.93−715153.7	37.6066.16	867–1198	LPV-38462	118	STAR
82	HV 5715	$05^h18^m11.05^s$ $-67°26'48.92''$	J051811.08−672648.5	49.6132.10	416–886	...	...	O-AGB
83	...	$05^h18^m32.63^s$ $-69°25'25.59''$	J051832.64−692525.5	78.6224.39	256–269	LPV-39261	171	C-AGB
84	IRAS F05192−7008	$05^h18^m45.27^s$ $-70°05'34.70''$	J051845.23−700534.5	78.6214.72	undef.	LPV-39671	39	C-PAGB
85	HV 2444	$05^h18^m45.46^s$ $-69°03'21.65''$	J051845.47−690321.8	...	...	T2CEP-091	36	O-PAGB (RV Tau)
86	...	$05^h19^m08.52^s$ $-69°23'14.44''$	J051908.46−692314.3	80.6345.4422	351–398	LPV-40384	188	C-AGB
87	2MASS J05191049−6933453	$05^h19^m10.63^s$ $-69°33'46.51''$	J051910.49−693345.3	78.6342.4688	undef.	LPV-40465	481	C-AGB
88	2MASS J05194483−6929594	$05^h19^m44.87^s$ $-69°29'59.84''$	J051944.81−692959.4	78.6343.28	115–1081	LPV-41591	107	STAR
89	...	$05^h20^m14.31^s$ $-70°29'31.33''$	J052014.24−702931.0	6.6450.20	423–624	LPV-42635	686	O-AGB
90	...	$05^h20^m23.97^s$ $-69°54'23.08''$	J052023.97−695423.2	78.6458.125	undef.	...	...	YSO-4
91	...	$05^h20^m51.86^s$ $-69°34'08.04''$	J052051.83−693407.6	78.6584.36	732–770	LPV-43982	779	O-AGB
92	LHα 120−N 125	$05^h20^m52.44^s$ $-70°09'35.60''$	J052052.42−700935.5	...	...	...	...	C-PN
93	...	$05^h21^m01.71^s$ $-69°14'17.07''$	J052101.66−691417.5	80.6589.15	130–217	LPV-44309	92	O-AGB
94	HV 942	$05^h21^m47.99^s$ $-70°09'57.22''$	J052147.95−700957.0	6.6696.60	946	...	...	OTHER (RCrB)
95	MACHO 78.6698.38	$05^h21^m49.40^s$ $-70°04'35.26''$	J052149.11−700434.2	78.6698.38	25	T2CEP-104	25	O-PAGB (RV Tau)
96	...	$05^h22^m06.91^s$ $-71°50'17.89''$	J052206.92−715017.7	...	...	LPV-46603	81	O-AGB
97	...	$05^h22^m22.98^s$ $-68°41'00.72''$	J052222.95−684101.2	...	...	...	...	YSO-3
98	OGLE 052242.09−691526.2	$05^h22^m42.01^s$ $-69°15'26.04''$	J052241.93−691526.2	80.6831.630	411	LPV-47888	417	C-AGB
99	SHV 0523185−693932	$05^h22^m54.96^s$ $-69°36'52.34''$	J052254.97−693651.7	78.6947.2742	209–209	LPV-48376	208	O-AGB
100	LHα 120−N 136	$05^h23^m31.25^s$ $-69°04'04.56''$	J052331.11−690404.6	...	...	...	...	O-PN
101	IRAS 05240−6809	$05^h23^m51.14^s$ $-68°07'12.37''$	J052351.13−680712.2	...	...	...	...	YSO-1
102	IRAS 05246−7137	$05^h23^m53.95^s$ $-71°34'43.97''$	J052353.92−713443.9	...	...	...	...	YSO-2
103	...	$05^h24^m05.25^s$ $-68°18'01.99''$	J052405.31−681802.5	4.7087.2529	304–387	LPV-50988	330	C-AGB
104	MSX LMC 464	$05^h24^m13.30^s$ $-68°29'58.98''$	J052413.36−682958.8	3.7084.121	596–1100	...	...	HII
105	OGLE J052445.53−691605.6	$05^h24^m45.36^s$ $-69°16'05.53''$	J052445.38−691605.3	80.7194.86	399–401	LPV-52434	403	C-AGB
106	LHα 120−S 33	$05^h24^m57.86^s$ $-67°24'58.43''$	J052457.85−672458.3	...	...	...	...	YSO-4
107	HV 5829	$05^h25^m19.52^s$ $-70°54'09.84''$	J052519.48−705410.0	...	...	T2CEP-119	34	O-PAGB (RV Tau)
108	...	$05^h25^m46.52^s$ $-66°14'11.30''$	J052546.51−661411.5	...	...	...	...	YSO-1
109	...	$05^h26^m13.35^s$ $-68°47'15.24''$	J052613.39−684715.0	...	...	...	...	YSO-4
110	OGLE J052620.25−693902.4	$05^h26^m20.15^s$ $-69°39'02.59''$	J052620.10−693902.1	77.7430.51	820	LPV-55565	810	O-AGB
111	HV 2522	$05^h26^m27.19^s$ $-66°42'58.66''$	J052627.23−664258.7	62.7474.1378	undefined	...	...	O-PAGB
112	RP 589	$05^h26^m37.58^s$ $-70°29'07.18''$	J052637.81−702906.7	...	...	...	...	UNK
113	...	$05^h27^m07.14^s$ $-70°20'02.12''$	J052707.10−702001.9	7.7541.31	undefined	...	...	O-PAGB
114	...	$05^h27^m23.24^s$ $-71°24'25.41''$	J052723.14−712426.3	...	...	...	...	YSO-3

TABLE 3—*Continued*

SSID	Name[c]	Observed R. A. & Dec. (J2000)	SSTISAGEMC designation[d]	MACHO designation	MACHO[a] period (d)	OGLE-LMC designation	OGLE[b] period (d)	Classification
115	LHα 120−N 145	$05^h27^m35.64^s$ $-69°08'56.22''$	J052735.63−690856.3	...	...	...	...	O-PAGB
116	HV 2551	$05^h27^m38.76^s$ $-69°28'45.57''$	J052738.58−692843.9	...	...	...	...	RSG
117	W61 11−16	$05^h27^m39.62^s$ $-69°09'01.57''$	J052739.63−690901.4	...	...	...	...	RSG
118	...	$05^h27^m47.60^s$ $-71°48'52.75''$	J052747.62−714852.8	...	...	...	...	O-PAGB
119	SHV 0528350−701014	$05^h28^m05.91^s$ $-70°07'54.03''$	J052805.91−700753.4	...	...	LPV-59143	476	C-AGB
120	OGLE J052825.96−694647.4	$05^h28^m25.86^s$ $-69°46'47.45''$	J052825.81−694647.3	...	...	LPV-59817	133	C-AGB
121	IRAS 05298−6957	$05^h29^m24.61^s$ $-69°55'14.19''$	J052924.85−695519.2	...	...	...	...	O-AGB
122	HV 5879	$05^h29^m54.80^s$ $-69°04'15.73''$	J052954.73−690415.7	82.8044.1115	122–1566	...	...	RSG
123	SP77 46−50	$05^h30^m04.67^s$ $-68°47'29.08''$	J053004.56−684728.8	...	...	...	...	RSG
124	SHV 0530472−690607	$05^h30^m27.56^s$ $-69°03'59.04''$	J053027.49−690358.3	82.8165.1133	212–212	LPV-63816	214	O-AGB
125	IRAS 05315−7145	$05^h30^m44.72^s$ $-71°42'59.62''$	J053044.10−714300.6	...	...	...	...	C-AGB
126	KDM 4554	$05^h30^m45.03^s$ $-68°21'29.11''$	J053044.55−682119.2	8.8176.2019	467–612	LPV-64345	426	C-AGB
127	NGC 2004 Robb B45	$05^h30^m46.74^s$ $-67°16'56.92''$	J053046.81−671657.2	61.8192.23	381	...	...	RSG
128	NGC 2004 Wes 18−13	$05^h30^m48.40^s$ $-67°16'45.88''$	J053048.42−671645.8	...	...	...	...	RSG
129	NGC 2004 Wes 6−14	$05^h30^m52.25^s$ $-67°17'34.22''$	J053052.28−671734.4	...	...	...	...	RSG
130	...	$05^h31^m28.43^s$ $-70°10'27.65''$	J053128.44−701027.1	7.8269.63	401–405	LPV-65660	393	O-AGB
131	MACHO 82.8405.15	$05^h31^m51.01^s$ $-69°11'46.56''$	J053150.98−691146.4	82.8405.15	93	T2CEP-147	47	O-PAGB (RV Tau)
132	KDM 4665	$05^h31^m58.96^s$ $-72°44'36.35''$	J053158.92−724436.0	35.8352.3	118–212	...	...	C-AGB
133	...	$05^h32^m06.64^s$ $-70°10'25.34''$	J053206.70−701024.8	7.8390.36	115–206	LPV-66766	124	STAR
134	...	$05^h32^m18.66^s$ $-67°31'46.16''$	J053218.64−673145.9	...	...	...	...	RSG
135	NGC 2011 SAGE IRS 1	$05^h32^m19.31^s$ $-67°31'20.34''$	J053219.33−673120.5	...	...	...	...	RSG
136	KDM 4718	$05^h32^m26.52^s$ $-73°10'06.99''$	J053226.51−731006.8	...	...	...	...	C-AGB
137	RP 774	$05^h32^m39.71^s$ $-69°30'49.25''$	J053239.68−693049.4	81.8521.506	undef.	...	...	YSO-4
138	...	$05^h32^m53.35^s$ $-66°07'27.17''$	J053253.36−660727.8	64.8572.519	undef.	...	...	GAL
139	KDM 4774	$05^h32^m54.98^s$ $-67°36'47.10''$	J053254.99−673647.2	...	...	...	...	C-AGB
140	MSX LMC 736	$05^h33^m06.86^s$ $-70°30'34.22''$	J053306.86−703033.9	...	...	...	...	C-AGB
141	...	$05^h33^m18.61^s$ $-66°00'39.91''$	J053318.58−660040.2	64.8695.450	undef.	...	...	C-AGB
142	...	$05^h33^m43.18^s$ $-70°59'21.16''$	J053343.27−705921.1	14.8620.13	151–182	LPV-69535	106	O-AGB
143	...	$05^h33^m44.00^s$ $-70°59'01.14''$	J053343.98−705901.9	14.8620.21	146–1080	LPV-69554	148	O-AGB
144	LHα 120−N 151	$05^h33^m46.97^s$ $-68°36'44.08''$	J053346.97−683644.2	...	...	...	...	C-PN
145	...	$05^h34^m41.46^s$ $-69°26'30.74''$	J053441.40−692630.6	...	...	LPV-71117	503	C-AGB
146	SHP LMC 256	$05^h34^m44.20^s$ $-67°37'50.82''$	J053444.17−673750.1	...	...	...	...	UNK
147	HV 2700	$05^h35^m19.01^s$ $-67°02'19.50''$	J053518.91−670219.5	...	...	...	...	RSG
148	...	$05^h35^m48.02^s$ $-70°31'46.92''$	J053548.07−703146.6	11.8990.10	965–981	LPV-72897	953	O-AGB
149	...	$05^h36^m02.42^s$ $-67°45'17.41''$	J053602.36−674517.3	8.9032.176	1137	...	...	YSO-4
150	IRAS 05370−7019	$05^h36^m32.48^s$ $-70°17'38.81''$	J053632.56−701738.4	...	...	...	...	C-PAGB
151	...	$05^h36^m34.82^s$ $-72°26'58.67''$	J053634.77−722658.6	...	...	...	...	GAL
152	...	$05^h36^m55.68^s$ $-68°11'24.31''$	J053655.60−681124.6	8.9146.17	752–810	LPV-74445	748	O-AGB

TABLE 3—*Continued*

SSID	Name[c]	Observed R. A. & Dec. (J2000)	SSTISAGEMC designation[d]	MACHO designation	MACHO[a] period (d)	OGLE-LMC designation	OGLE[b] period (d)	Classification
153	RP 493	$05^h37^m10.12^s$ $-71°23'14.06''$	J053710.26−712314.3	...	...	...	...	O-PN
154	...	$05^h37^m30.63^s$ $-67°40'41.19''$	J053730.59−674041.6	...	...	...	...	GAL
155	KDM 5345	$05^h38^m23.66^s$ $-66°09'00.91''$	J053823.58−660900.3	66.9419.10	112	...	...	UNK
156	OGLE J053930.16−695755.8	$05^h39^m29.94^s$ $-69°57'56.27''$	J053930.06−695800.9	81.9603.512	405	LPV-77631	399	C-AGB
157	HV 12631	$05^h39^m33.17^s$ $-71°21'55.45''$	J053932.92−712200.6	14.9582.9	31	T2CEP-169	31	O-PAGB (RV Tau)
158	...	$05^h39^m42.37^s$ $-71°10'45.03''$	J053942.45−711044.5	...	...	...	...	YSO-3
159	...	$05^h39^m45.46^s$ $-66°58'09.75''$	J053945.40−665809.4	67.9648.7	125–126	...	...	O-AGB
160	...	$05^h39^m49.22^s$ $-69°37'47.03''$	J053949.23−693747.0	...	...	...	...	UNK
161	MACHO 81.9728.14	$05^h40^m00.47^s$ $-69°42'14.85''$	J054000.52−694214.6	81.9728.14	47	T2CEP-174	47	O-PAGB (RV Tau)
162	MSX LMC 949	$05^h40^m14.78^s$ $-69°28'49.33''$	J054014.83−692849.1	76.9732.1316	403–566	...	...	O-PAGB
163	RP 85	$05^h40^m33.51^s$ $-70°32'41.06''$	J054033.54−703240.8	...	...	...	...	YSO-4
164	...	$05^h40^m59.28^s$ $-70°44'02.82''$	J054059.31−704402.5	...	...	...	...	YSO-3
165	MSX LMC 947	$05^h41^m02.04^s$ $-70°43'10.55''$	J054103.55−704307.6	11.9834.92	694–703	LPV-79341	709	O-AGB
166	...	$05^h41^m14.58^s$ $-71°32'36.01''$	J054114.56−713236.0	15.9822.4	583	...	...	O-AGB
167	IRAS 05416−6906	$05^h41^m20.69^s$ $-69°04'44.46''$	J054121.18−690438.7	...	...	...	...	C-AGB
168	IRAS 05421−7116	$05^h41^m25.08^s$ $-71°15'32.74''$	J054125.09−711532.6	...	...	...	...	YSO-1
169	W61 6−24	$05^h41^m57.43^s$ $-69°12'18.61''$	J054157.40−691218.1	...	...	...	...	RSG
170	NGC 2100 Robb 4	$05^h42^m03.91^s$ $-69°13'07.64''$	J054206.15−691307.7	...	...	...	...	RSG
171	2MASS J05420676−6912312	$05^h42^m06.76^s$ $-69°12'31.35''$	J054206.76−691231.1	...	...	...	...	RSG
172	W61 6−57	$05^h42^m09.98^s$ $-69°13'28.76''$	J054209.95−691328.7	...	...	...	...	RSG
173	WOH G 494	$05^h42^m30.51^s$ $-69°48'57.47''$	J054230.55−694857.3	76.10090.12	183–333	LPV-80890	170	O-AGB
174	LM 2−42	$05^h42^m33.35^s$ $-70°29'24.18''$	J054233.17−702924.1	...	...	...	...	O-PN
175	LHα 120−N 178	$05^h42^m36.63^s$ $-70°09'32.50''$	J054236.65−700932.0	...	...	...	...	C-PN
176	...	$05^h42^m54.62^s$ $-70°08'07.74''$	J054254.38−700807.4	76.10206.25	166–274	LPV-81294	278	O-AGB
177	...	$05^h43^m10.87^s$ $-67°27'28.42''$	J054310.86−672728.0	...	...	...	...	O-PAGB
178	...	$05^h43^m14.23^s$ $-70°38'35.12''$	J054314.12−703835.1	12.10198.12	156–467	LPV-81615	162	O-AGB
179	KDM 5841	$05^h43^m28.77^s$ $-69°42'43.88''$	J054328.84−694243.7	76.10212.28	417–918	LPV-81866	191	C-AGB
180	...	$05^h44^m06.10^s$ $-68°37'53.68''$	J054406.01−683753.6	33.10349.11	470–554	LPV-82411	239	O-AGB
181	...	$05^h44^m37.92^s$ $-67°36'58.17''$	J054437.87−673657.7	68.10486.408	undef.	...	...	C-AGB
182	...	$05^h44^m40.08^s$ $-69°11'49.11''$	J054440.11−691149.0	...	...	LPV-82889	99	O-AGB
183	IRAS 05452−6924	$05^h44^m50.23^s$ $-69°23'04.72''$	J054450.23−692304.2	...	...	...	...	YSO-1
184	...	$05^h45^m24.23^s$ $-68°30'41.61''$	J054524.23−683041.4	...	...	...	...	GAL
185	...	$05^h45^m46.35^s$ $-67°32'39.16''$	J054546.32−673239.4	68.10608.258	484–491	...	...	O-AGB
186	LHα 120−N 170	$05^h47^m04.62^s$ $-69°27'34.24''$	J054704.54−692733.9	31.10821.779	undef.	LPV-84717	362	O-PN
187	...	$05^h47^m45.80^s$ $-68°07'34.26''$	J054745.79−680734.1	32.10962.261	2599	...	...	YSO-4
188	KDM 6247	$05^h47^m57.25^s$ $-68°14'56.90''$	J054757.37−681457.0	...	...	...	...	STAR
189	NGC 2121 LE 6	$05^h48^m16.84^s$ $-71°28'39.64''$	J054816.79−712839.3	28.11033.2559	387–387	LPV-85475	385	C-AGB
190	IRAS 05495−7034	$05^h49^m00.12^s$ $-70°33'22.51''$	J054900.01−703322.5	...	...	...	...	C-AGB

TABLE 3—*Continued*

SSID	Name[c]	Observed R. A. & Dec. (J2000)	SSTISAGEMC designation[d]	MACHO designation	MACHO[a] period (d)	OGLE-LMC designation	OGLE[b] period (d)	Classification
191	KDM 6486	$05^h50^m36.62^s$ $-68°28'52.27''$	J055036.69−682852.4	32.11441.5	336–643	LPV-86831	663	C-AGB
192	HV 2862	$05^h51^m22.58^s$ $-69°53'51.05''$	J055122.52−695351.4	30.11540.16	34	T2CEP-191	34	O-PAGB (RV Tau)
193	...	$05^h51^m43.25^s$ $-68°45'42.79''$	J055143.27−684543.0	72.11557.1055	642	...	...	GAL
194	PMP 337	$05^h52^m51.07^s$ $-69°28'39.09''$	J055251.05−692839.6	31.11789.29	269–1015	LPV-87711	151	C-AGB
195	PMP 133	$05^h52^m52.51^s$ $-69°30'35.54''$	J055252.50−693035.6	31.11788.10	25	...	...	STAR
196	IRAS 05537−7015	$05^h53^m12.04^s$ $-70°15'22.71''$	J055311.98−701522.5	...	...	...	...	C-PAGB
197	...	$06^h00^m53.60^s$ $-68°00'39.08''$	J060053.62−680038.8	74.13142.12	281–887	...	...	O-AGB